ABSTRACT

Title of dissertation: SYNTHESIS AND CHARACTERIZATION OF LOW FLAMMABILITY POLYMER/LAYERED SILICATE NANOCOMPOSITES

Xin Zhang, Doctor of Philosophy, 2009

Dissertation directed by: Professor Robert M. Briber
Department of Materials Science
and Engineering

There has been significant interest in the applications of polymer nanocomposites in a variety of areas. Polymer/layered silicate nanocomposites have been of interest because of relatively low raw material cost and improved materials properties such as higher Young's modulus, higher thermal deformation temperature, lower small molecule permeability, lower density (compared to metals and traditional glass fiber reinforced composites) as well as low flammability. The relationships between the flammability and the dispersion of the layered silicate platelets inside the polymer matrix is just being established. The complete set of factors that affect the flammability of polymer/layered nanocomposites are not fully identified.

In this thesis polymer/layered silicate nanocomposites with different degrees of platelet dispersion were synthesized. The structure of the nanocomposites was characterized by X-ray diffraction (XRD), small angle X-ray scattering (SAXS), and transmission electron microscopy (TEM). The flammability of these nanocomposites

was characterized by TGA, cone calorimetry and gasification. By coupling the structural and flammability data it has been concluded that forming a nanometer scale dispersed structure significantly improves the flammability but the details of the degree of dispersion are not critical. The improvement in the flammability arises from the formation of a residue or char layer at the surface of the nanocomposite. This residue layer acts as a radiation shield and as a physical barrier preventing the polymer degradation products from escaping and acting as fuel. It is observed that the stability of the residue layer formed during combustion has major impact on the flammability.

This thesis also describes work to improve the flammability of the polymer/layered silicate nanocomposites by enhancing char/residue formation in order to improve the residue layer stability.

SYNTHESIS AND CHARACTERIZATION OF LOW FLAMMABILITY POLYMER/LAYERED SILICATE NANOCOMPOSITES

by

Xin Zhang

Dissertation submitted to the Faculty of the Graduate School of the
University of Maryland, College Park in partial fulfillment
of the requirements for the degree of
Doctor of Philosophy
2009

Advisory Committee:
Professor Robert M. Briber, Chair/Advisor
Professor Takashi Kashiwagi
Professor Peter Kofinas
Professor Lourdes Salamanca-Riba
Professor James Quinterie

Dedication

To my wife.

Acknowledgments

I would like to express my sincere thanks to my advisor, Dr. Robert M. Briber, who has given me the opportunity to work in his group, for his advice, encouragement, and support on research and also support during my hard time of my life. A lot of appreciation also goes to Dr. Takashi Kashiwagi, who also contributed a lot of work in this research. I would also thank all committee members, Dr. Lourdes Salamanca-Riba, Dr. James Quintiere, and Dr. Peter Kofinas for all the time and efforts put on my thesis. I would like to thank Dr. Stephen Henderson for all the help on the small angle X-ray scattering and machine shop work.

Special thanks go to Dr. Bani Cipriano and Dr. Srinivasa Raghavan's group for all the works we have done together.

A lot of thanks go to all members of Dr. Briber's group and Dr. Kofinas' group. A lot of thanks go to my friends, Dr. Xiang Wang, Dr. Li Ling, Dr. Zhengkun Ma, Dr. Kehai Zhang, Dr. Lang Chen, Dr. Jason Hattrick-Simpers, Dr. Liyang Dai and Dr.Jianhua Li for all the helps they gave to me.

Finally, I would like to thank my family for all the support, especially to my wife, Lei Zheng, whose love supported me through the hardest days in my life, to my grandmother who supported her two sons to college by weaving, later one became a diplomat and the other one became a professor.

Contents

List of Tables vii

List of Figures viii

List of Abbreviations xiii

1 Introduction 1
- 1.1 Polymer Nanocomposites . . . 1
  - 1.1.1 Nanocomposites with 0-Dimensional Fillers . . . 2
  - 1.1.2 Nanocomposites with 1-Dimensional Fillers . . . 3
  - 1.1.3 Nanocomposites with 2-Dimensional Filler . . . 4
- 1.2 Clay and Organoclay . . . 8
- 1.3 Silane Coupling Agent . . . 10
- 1.4 Flammability of Polymers . . . 12
  - 1.4.1 Combustion and Pyrolysis of Polymers . . . 12
    - 1.4.1.1 So Called "Self-Extinguishing" Polymers . . . 17
    - 1.4.1.2 Flame Retardant Additives . . . 18
  - 1.4.2 Flammability Measurements . . . 20
- 1.5 Flammability of Polymer Nanocomposites . . . 21

2 Experimental 23
- 2.1 Research Outline . . . 23
- 2.2 Materials . . . 23
  - 2.2.1 Resin Polymer . . . 23
  - 2.2.2 Additives . . . 24
    - 2.2.2.1 Cloisite 30B . . . 24
    - 2.2.2.2 Cloisite 15A . . . 24
    - 2.2.2.3 Somasif MAE120 . . . 25
    - 2.2.2.4 Synthesis of PMMA Grafted Layered Silicate . . . 25
- 2.3 Synthesis of Layered Silicate/Polymer Nanocomposite . . . 27
  - 2.3.1 *In-situ* Polymerization . . . 27
  - 2.3.2 Solution Mixing . . . 28
  - 2.3.3 Synthesis of Nanocomposites with PMMA Grafted Clay . . . 28
- 2.4 Structural Characterization of Nanocomposites . . . 28
  - 2.4.1 X-ray Diffraction . . . 30
  - 2.4.2 Small Angle Scattering . . . 31
  - 2.4.3 Transmission Electronic Microscopy . . . 33
- 2.5 Flammability Measurement . . . 34
  - 2.5.1 Thermogravimetric Analysis . . . 34
    - 2.5.1.1 Degradation Kinetics . . . 35
  - 2.5.2 Cone Calorimetry . . . 37
  - 2.5.3 Gasification . . . 39
- 2.6 Rheology Measurement . . . 40

3 Results and Discussion 41
3.1 X-ray Diffraction from Clays . . . 41
3.2 *In-situ* Polymerization Samples . . . 41
3.2.1 Dispersion of Clay in MMA Monomer . . . 41
3.2.2 Polymerization of the Nanocomposites . . . 43
3.2.3 Structure of *in-situ* Polymerized Samples . . . 45
3.2.3.1 X-ray Diffraction . . . 45
3.2.3.2 Transmission Electron Microscopy . . . 45
3.2.4 Flammability measurement of *in-situ* Polymerized Samples . . . 47
3.2.5 Summary of *in-situ* Polymerized Nanocomposites . . . 52
3.3 Solution Mixing Nanocomposite Structure . . . 52
3.3.1 Transmission Electron Microscopy . . . 52
3.3.2 X-ray Diffraction . . . 63
3.3.2.1 X-ray Diffraction from Nanocomposites . . . 63
3.3.3 Small Angle X-ray Scattering . . . 65
3.4 Discussion on the Dispersion of Layered Silicate in Polymer . . . 68
3.5 Flammability Tests . . . 71
3.5.1 Thermogravimetric Analysis of Nanocomposites Made by the Solution Mixing Method . . . 71
3.5.1.1 Clay Samples . . . 71
3.5.1.2 Nanocomposite Samples . . . 73
3.5.2 Gasification Experiments . . . 103
3.5.3 Cone Calorimetry . . . 107
3.5.4 Effect of Clay Dispersion . . . 115
3.5.4.1 Solvent Introduced Dispersion Change . . . 115
3.5.4.2 PMMA Grafted Clay Introduced Dispersion Change 119
3.5.5 Residue Layer . . . 120
3.6 Rheology Measurements . . . 125
3.7 Glass Transition Measurement . . . 125
3.7.1 Differential Scanning Calorimetry . . . 125
3.8 Discussion on the Flammability of Nanocomposites . . . 131
3.8.1 Mechanism of Low Flammability Nanocomposites . . . 131
3.8.1.1 Structure Integrity . . . 133
3.8.2 Effect of Heat Conductivity on the Fire Safety . . . 133

4 Phosphorus Containing Nanocomposite 136
4.1 Introduction . . . 136
4.2 Char Forming Compound . . . 137
4.3 Synthesis . . . 138
4.3.1 Adding phosphorus to Cloisite 30B Clay . . . 138
4.4 Structure Characterization with TEM . . . 138
4.5 Flammability Test . . . 139
4.5.1 Gasification . . . 139
4.5.2 Cone Calorimetry . . . 139
4.6 Residue Characterization . . . 144

4.7 Discussion . . . 148
4.7.1 Char Formation . . . 148
4.7.2 Position of the phosphorus Compound During Combustion . . 149

5 Conclusions 150

6 Future Work 154
6.1 Introduction . . . 154
6.2 Proposed Experiment . . . 156
6.2.1 Material Selection . . . 156
6.2.2 Organic Modification of Nanoparticles and Nanocomposite Synthesis . . . 157
6.2.3 Structure Characterization . . . 160
6.2.4 Flammability Characterization . . . 160

Bibliography 161

List of Tables

2.1 Solution Precipitated Samples 29

2.2 Relationship Between the Heat Flux and Fire Scale 39

3.1 Silicate Stack Thickness Based on Scherrer Equation 65

3.2 Kinetic Parameters Derived from Pure Polymer TGA Data 98

3.3 Kinetic Parameters Derived from Cloisite 15A Low Molecular Weight Nanocomposite TGA Data 99

3.4 Kinetic Parameters Derived from Cloisite 30B Low Molecular Weight Nanocomposite TGA Data 100

3.5 Kinetic Parameters Derived from MAE120 Low Molecular Weight Nanocomposite TGA Data 101

3.6 Kinetic Parameters Derived from PMMA Grafted Clay Low Molecular Weight Nanocomposite TGA Data 102

3.7 Kinetic Parameters Derived from TGA Data of High Molecular Weight Samples 103

3.8 Results from Gasification Experiments for Samples with 5wt.% Filler 111

3.9 Results from Cone Calorimetry Experiments 114

3.10 Glass Transition Temperatures from DSC 127

4.1 EDX Analysis of the Residue from Cloisite 30B Nanocomposites Containing phosphorus Silane 148

6.1 Commercially Available Calcium Phosphates 158

6.2 Commercially Available Inorganic Phosphates 159

List of Figures

1.1 Intercalated Structure 7

1.2 Exfoliated Structure 7

1.3 Hydrous Silanization Process 11

1.4 Anhydrous Silanization Process 12

1.5 Three Types of Flow During Combustion 13

1.6 PMMA Degradation Mechanism 15

1.7 PS Degradation Mechanism 15

2.1 Structure of Surfactant Used in Cloisite 30B Clay 24

2.2 Structure of Surfactant Used in Cloisite 15A Clay 25

2.3 Silane A174 Structure 26

2.4 Short PMMA Chain Grafted on Clay 27

2.5 Shape Factor 37

2.6 Ozawa Method for Calculating Degradation Kinetic Parameters . . . 38

2.7 Schematic of Gasification Apparatus 40

3.1 XRD Data from Cloisite 15A Clay with a Peak at 2.27 nm, Cloisite 30B Clay with a Peak at 1.67 nm and Peaks from Somasif MAE120 Synthetic Mica (2.76 nm, 1.96 nm, 1.38 nm and 1.18 nm) 42

3.2 XRD Data from *in-situ* Polymerized Nanocomposites with Peaks Labeled. 46

3.3 TEM of *in-situ* Polymerized Cloisite 15A Nanocomposites 48

3.4 TEM of *in-situ* Polymerized Cloisite 30B Nanocomposites 48

3.5 TEM of *in-situ* Polymerized MAE120 Nanocomposites 49

3.6 TEM of *in-situ* Polymerized MAE120 Nanocomposites Showing Clay Stacks Being Spread Apart 50

3.7 Gasification Data from *in-situ* Polymerized Nanocomposites 51

3.8 Clay Stack Count from the Cloisite 15A/PMMA Nanocomposites . . 54

3.9 Clay Stack Count from the Cloisite 30B/PMMA Nanocomposites . . 55

3.10 Clay Stack Count from the MAE120/PMMA Nanocomposites 56

3.11 Clay Stack Count from the PMMA Grafted Clay/PMMA Nanocomposites 57

3.12 Intercalated Structure Produced with Cloisite 15A Clay 58

3.13 Exfoliated Structure Produced with Cloisite 30B Clay 59

3.14 Intercalated Structure Produced with MAE120 Clay 60

3.15 Exfoliated Structure from Nanocomposite with PMMA Grafted Clay 61

3.16 Exfoliated Structure from Nanocomposite with PMMA Grafted Clay 62

3.17 XRD Data from Precipitated Nanocomposites 64

3.18 Small Angle X-ray Scattering from Nanocomposites 66

3.19 Fitting of PMMA Grafted Sample with Average Stack Model 67

3.20 Fitting of Cloisite 30B Sample with Average Stack Model 68

3.21 Fitting of PMMA Grafted Sample with Multiple Stack Summation Model 69

3.22 Fitting of Cloisite 30B Sample with Multiple Stack Summation Model 69

3.23 Fitting of Cloisite 15A Sample with Multiple Stack Summation Model 70

3.24 TGA Data from Various Clay Samples 72

3.25 TGA Data from Pure PMMA Samples 74

3.26 Derivative of TGA Data from Pure PMMA Samples 75

3.27 TGA Data from Cloisite 30B/PMMA Low Molecular Weight Nanocomposite Samples 76

3.28 TGA Data from Cloisite 30B/PMMA Low Molecular Weight Nanocomposite Samples 77

3.29 TGA Data from Cloisite 15A/PMMA Low Molecular Weight Nanocomposite Samples . . . 78

3.30 TGA Data from Cloisite 15A/PMMA Low Molecular Weight Nanocomposite Samples . . . 79

3.31 TGA Data from MAE120/PMMA Low Molecular Weight Nanocomposite Samples . . . 80

3.32 TGA Data from MAE120/PMMA Low Molecular Weight Nanocomposite Samples . . . 81

3.33 TGA Data from Grafted Clay/PMMA Low Molecular Weight Nanocomposite Samples . . . 82

3.34 TGA Data from Grafted Clay/PMMA Low Molecular Weight Nanocomposite Samples . . . 83

3.35 TGA Data from Pure PMMA High Molecular Weight Samples . . . 84

3.36 TGA Data from Pure PMMA High Molecular Weight Samples . . . 85

3.37 TGA Data from Cloisite 30B/PMMA High Molecular Weight Nanocomposite Samples . . . 86

3.38 TGA Data from Cloisite 30B/PMMA High Molecular Weight Nanocomposite Samples . . . 87

3.39 TGA Data from Cloisite 15A/PMMA High Molecular Weight Nanocomposite Samples . . . 88

3.40 TGA Data from Cloisite 15A/PMMA High Molecular Weight Nanocomposite Samples . . . 89

3.41 TGA Data from MAE120/PMMA High Molecular Weight Nanocomposite Samples . . . 90

3.42 TGA Data from MAE120/PMMA High Molecular Weight Nanocomposite Samples . . . 91

3.43 TGA Data from Grafted Clay/PMMA High Molecular Weight Nanocomposite Samples . . . 93

3.44 TGA Data from Grafted Clay/PMMA High Molecular Weight Nanocomposite Samples . . . 94

3.45 Kissinger Analysis of Low Molecular Weight PMMA and Nanocomposite Degradation Kinetics . . . 97

3.46 Mass Loss Rate Curve from Gasification Experiments 104

3.47 Residue After Gasification Experiments 105

3.48 Effect of Bubbles on Thin Residue Layer 107

3.49 Effect of Bubbles on Thick Residue Layer 108

3.50 Effect of Disk Warping on the Flammability 108

3.51 Video images captured during the gasification of a high molecular weight sample, showing stacks in thin residue (5s, 10s), swelling (28s), and large cracks formed during swelling (28s, 30s). 109

3.52 Video images captured during the gasification of a low molecular weight sample, showing cracks in thin residue (5s), island like structure formed because of bubbles pushing residue (15s), swelling (25s), and large cracks formed during swelling (25s, 30s). 110

3.53 Heat Release Rate Curve from Cone Calorimetry Experiments 112

3.54 Residue After Cone Calorimetry Experiment 113

3.55 Mass Loss Rate Curve from Gasification Experiment of Samples Cast from Chloroform Compared to Samples from THF 116

3.56 Intercalated/Microcomposite Structure Formed when Cloisite 15A/PMMA Sample Cast from Chloroform 117

3.57 Intercalated Structure Produced from MAE120/PMMA Cast from Chloroform. 118

3.58 Mass Loss Rate Data from Nanocomposites with PMMA Grafted Clay 120

3.59 Heat Release Rate from Cone Calorimetry Experiment of Nanocomposite Samples with PMMA Chain Grafted Clay in Comparison with Nanocomposite Samples with Cloisite 30B Clay and Samples of Pure PMMA Polymer 121

3.60 XRD Data from the Residues 122

3.61 SEM Observation of Cross Section of a Residue from Gasification Experiment 124

3.62 Viscosity of Different Nanocomposites 126

4.1 Structure of Diethylphosphatoethyltriethoxysilane 138

4.2 TEM of phosphorus Containing Cloisite 30B Clay/PMMA Nanocomposites . . . 140

4.3 TEM of phosphorus Containing Cloisite 30B Clay/PMMA Nanocomposites . . . 141

4.4 Gasification of phosphorus Containing Cloisite 30B Clay/PMMA Nanocomposites . . . 142

4.5 Cone Data of phosphorus Containing Clay/PMMA Nanocomposites . 143

4.6 Mass Loss During Cone Experiments of phosphorus Containing Clay/PMMA Nanocomposites . . . 145

4.7 Residue from 10wt% of Cloisite 30B/5wt% phosphorus Containing Silane . . . 146

4.8 Residue from 10wt% of Cloisite 30B/5wt% phosphorus Containing Silane . . . 147

List of Abbreviations

AIBN	Azobisisobutyronitrile
AFM	Atomic Force Microscope
CEC	Cation Exchange Capacity
DMA	Dynamic Mechanical Analysis
DMF	Dimethylformamide
DMSO	Dimethylsulfoxide
DSC	Differential Scanning Calorimetry
EDX	Energy Dispersive X-ray Analysis
GSD	Gaussian Standard Deviation
HRR	Heat Release Rate
IC	Integrated Circuit
MLR	Mass Loss Rate
MMA	Methylmathacrylate
NMR	Nuclear Magnetic Resonance
PAN	Polyacrylonitrile
PC	Polycarbonate
PCB	Printed Circuit Board
PE	Polyethylene
PEO	Polyethylene Oxide
PHRR	Peak Heat Release Rate
PMA	Polymethylacrylate
PMLR	Peak Mass Loss Rate
PMMA	Poly (Methyl Methacrylate)
POSS	Polyhedral Oligomeric Silsesquioxane
PP	Polypropylene
PS	Polystyrene
PVC	Polyvinyl Chloride
SAS	Small Angle Scattering
SANS	Small Angle Neutron Scattering
SAXS	Small Angle X-ray Scattering
SEM	Scanning Electron Microscopy
SLD	Scattering Length Density
TEM	Transmission Electron Microscopy
TGA	Thermogravimetic Analysis
TSCA	Toxic Substances Control Act
THF	Tetrahydrofuran
TPO	Thermal Plastic Olefin
UL	Underwriters Laboratories
UV	Ultra Violet
XRD	X-ray Diffraction

Chapter 1

Introduction

1.1 Polymer Nanocomposites

Most polymers, especially those used for structural applications, often contain large amounts of filler. Fillers are used to increase the modulus, increase the thermal or electric conduction, increase wear resistance, increase stability against weathering, UV, increase flame retardancy, increase processability, decrease thermal expansion or just reduce the cost of the material. Common inorganic fillers include mica, calcite, clay, glass fibers, glass beads and carbon black. Organic fillers are commonly termed additives.

Polymer nanocomposites are polymers containing nanometer size fillers. The fillers can be inorganic or organic, but small organic molecules like lubricants, flame retardant additives or dyes are generally not classified as fillers for nanocomposites.

Compared to traditional polymer based composite materials, polymer nanocomposites have a number of advantages. For mechanical properties, nanocomposites have been shown to achieve the modulus of traditional composites at a lower concentration, which also results in a lower density of the final product and potentially lower cost.

Due to the large surface area of the fillers, there is a significant amount of interfacial area introduced into the composites, which in turn could be large enough

to affect the conformation of the polymer molecules. Also due to the size of the filler and depending on the dispersion, it can be hard to classify the nanocomposites as a traditional two phase mixtures [1].

The nanoparticles used in polymer nanocomposites can be either 0-dimensional, 1-dimensional or 2-dimensional.

1.1.1 Nanocomposites with 0-Dimensional Fillers

0-dimensional fillers are particles where all three dimensions in the nanometer scale. The overall shape of the filler is a generally equi-axed particle and can be termed 0-dimensional.

Different 0-dimensional nanoparticles have been used to make nanocomposites for industrial applications, for example, nanometer scale silica gel and polyhedral oligomeric silsesquioxane (POSS).

Nanometer scale silica gel has long been used as a filler for polymer based IC packaging materials to control the viscosity of the raw material, to increase the modulus and decrease the cure shrinkage [2].

Surface modified silica gel has also been used as flame retardant material in the printed circuit board (PCB) materials like the new Hitachi Chemical RO resin. The amount of silica gel can be as much as 80 wt% in this type of resin. Due to the surface modification on the silica gel, the processability is still good [1].

POSS molecules are a group of well studied nanoscale particles that can be used in nanocomposites [3]. A POSS molecule is essentially a cage made of silicon

and oxygen with organic groups attached to the silicon atoms via covalent bonding [4]. Different organic groups have been used with POSS, even different monomers have been successfully attached to the POSS molecules. As a result, it is possible to directly polymerize the POSS molecule on polymer chains [5].

CdSe nanoparticle based 0-dimensional nanocomposites have been developed for their light emitting properties [6]. Zinc oxide nanoparticles have also been used as a UV stabilizing component. [7] Metal, ceramic and salt 0-dimensional nanoparticles have also been used as fillers in various applications such as electromagnetic wave shielding, magnetic memory, super capacitors and etc. [8, 9]

Direct mixing in solution, melt or *in-situ* polymerization are the typical methods used to make nanocomposites with 0-dimensional fillers. Nanocomposites with 0-dimensional fillers can also be synthesized by block copolymer templating and sol-gel processes [10, 11, 12].

1.1.2 Nanocomposites with 1-Dimensional Fillers

1-dimensional fillers have two dimensions at the nanometer scale. The overall shape of the filler is a 1-dimensional wire such as a nano-fiber, nano-wire or nano-tube [13, 14, 15]. The most studied systems are carbon nanotubes, which include multi-walled carbon nanotube and single walled carbon nanotubes [16].

The carbon nanotube polymer nanocomposites combine the properties of the matrix polymer and the carbon nanotube. Generally properties of high thermal conduction, graphite grade electrical conductivity are found, while the processabil-

ity of the polymer matrix is retained. Changes in the rheology upon addition of nanotubes to the polymer has been reported [17]. The nanotubes can also be filled with different salts or metals to alter the magnetic, optical or electrical properties of the final material [18].

The mechanical properties of carbon nanotube/polymer nanocomposites are strongly affected by the interface between the carbon nanotube and the polymer. The surface of carbon nanotubes is hydrophobic and as a result, non-polar polymers like polypropylene (PP) trend to be more compatible with the nanotubes [19, 20] while polar polymers like PMMA or nylon are less compatible. Consequently the mechanical properties of nanocomposites which are made with polar polymers can be worse than the pure polymer. To prevent this, a range of surface modification methods have been developed in an attempt to make the carbon nanotubes more compatible with polar polymers [18, 21].

Methods to prepare carbon nanotube/polymer nanocomposite include *in-situ* polymerization [22], solution casting and melt compounding.

Nanotubes made with materials other than carbon have also been reported [23, 24, 25]. Clay also exists in a tube form naturally [26] and these nanotubes have potential applications in polymer nanocomposites [27].

1.1.3 Nanocomposites with 2-Dimensional Filler

2-dimensional fillers have only one dimension at the nanometer scale, with the overall shape of the filler being a 2-dimensional disk or platelet. Examples include

single layers of clay, graphite [28], and layered double hydroxide [29, 30, 31, 32, 33]. Clay/polymer nanocomposites are the most important class of nanocomposites with 2D fillers. There is considerable interest on using modified clay mixed with polymers dating back to the 1980s and even earlier [34, 35]. Toyota Central Research Laboratory first synthesized clay/Nylon 6 nanocomposites which exhibited a relatively high modulus and heat distortion temperature [36, 37, 38]. It has also been proved that the reenforce effect is due to the clay particles added and not the change in the crystalline phase of PA6 [39]. This nanocomposite achieved significant commercial success. This nanocomposite has been used to make timing belt covers, engine covers and other under-the-hood car components by Toyota and Mitsubishi [36]. In 2004, clay/PP nanocomposites were used in the 2004 Acura TL head rest and Chevrolet Impala body side mount. In 2005 the Hummer H2 SUT had clay/TPO (thermoplastic olefin) nanocomposites as trim, center bridge, sail panels and box rail protectors [40, 41, 42].

2-Dimensional filler nanocomposites, especially layered silicate/polymer nanocomposites, are the most important class of nanocomposites. The reasons are that the raw materials (clay and mica) are readily available and relatively cheap, the synthesis process is simple and the modulus of nanocomposites is readily increased compared to the polymer and many different polymer can be used to synthesize nanocomposites [43, 44, 45, 46, 47, 48, 49, 50, 51, 52, 53, 54, 55, 56, 57, 58, 59, 60]. Other advantages include lowered small molecule permeability which leads to the potential of using it as a food packaging materials, fuel tanks [61, 41, 62, 63] and low dielectric materials [64].

Clay minerals have long been mixed with polymeric materials. Kaolinite has been used to replace asbestos in thermoset polymers. Kaolinite can also improve flow, shrinkage and water resistance of thermoset polymers. In thermoplastic materials, the clay can be used to lower the viscosity, and improve the mechanical properties of polymers such as polyesters and nylons. Clay has also been used to replace carbon black in rubber. Montmorillonite clays are preferred as filler in painting applications as they are easily modified by ion exchange to be compatible with different paints [65].

Based on the dispersion of the silicate in the polymer matrix, layered silicate/polymer nanocomposites can be classified with two different structures, exfoliated and intercalated [43, 45, 66].

An intercalated structure is where polymer enters the spaces between silicate layers, termed the gallery space, but the disruption is not large enough to lose the overall stack structure of the silicate (schematic shown in figure 1.1) [67]. When unmodified clay with +2 charged cations is dispersed in water, water enters the gallery space of the clay but the stack structure is preserved due to the strong interaction between neighboring clay platelets via the divalent cations [68].

Exfoliated means that the layered silicate has lost the original stack structure and single layers of the silicate are dispersed in the polymer matrix (schematically shown in figure 1.2). When clay with +1 charged cations is dispersed in water, it usually forms an exfoliated structure, where there is essentially no interaction between two neighboring platelets (there are only weak interactions via hydrogen bonding between water molecule network) [68].

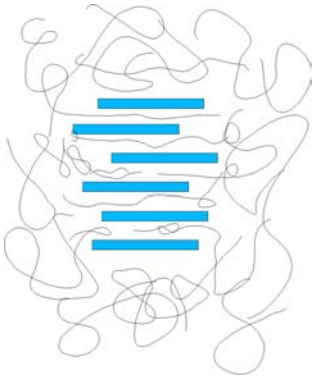

Figure 1.1: Intercalated Structure

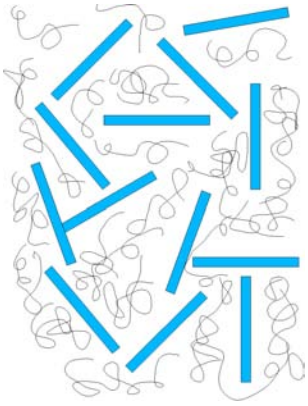

Figure 1.2: Exfoliated Structure

Based on the orientation of the silicate platelets, the exfoliated structure can be classified into different sub-structures. The silicate platelets can either be randomly dispersed or aligned. When isotropic properties are required, a totally random exfoliated structure is preferred. However, if enhanced properties are required in particular direction, an oriented exfoliated or intercalated structure may work better.

The silicate particles can also potentially touch each other via edge-to-edge or edge-to-center interactions, which allows for more complexity in the structure of the dispersed layered silicate. Structures with these interactions usually appear in silicate/small molecules mixture and are not common in polymer nanocomposites.

1.2 Clay and Organoclay

Clay has long been used as a filler for polymers, generally to enhance the modulus and wear properties. It has also been used to lower the viscosity.

Most clay minerals exist in a layered form, but may also exist as needles (halloysite, sepiolite) or as spheres (halloysite). The layered silicates contain silicon-oxygen layers which are composed of tetrahedral blocks and aluminum-oxygen-hydroxy layers which are composed of octahedral shaped blocks [69].

The ratio between tetrahedral layers and octahedral layers can be 1:1 (kaolinate), 2:1(mica type clay minerals, including montmorillonite) or 2:1:1 (chlorite) [70]. Some of the aluminum atoms at octahedral positions can be replaced by +2 iron or magnesium atoms, and some of the silicon atoms at tetrahedral positions can be replaced by aluminum atoms. So the clay platelet being negatively charged. To compensate this negative charge, some cations are attracted to the clay platelets. Lithium, sodium, potassium, ammonium, calcium are the cations commonly found in clay platelets.

The clay platelets are stacked together to lower the total surface energy. The stacking leads to at least two different interesting properties of clay. The first one is swelling of clay in water, and the second is the large inner surface area (the total surface of the clay platelets including area inside the clay stack).

The oxygen layer on the surface of clay is organophilic, but clay is commonly described as hydrophilic, which comes from two sources. The first rises from cations that are attracted to the clay platelets and trapped in the gallery space.

These cations attract water molecules and shield the oxygen layer from free water molecules. The second reason is that hydroxyl groups are exposed at the edge of the clay platelets, which can form hydrogen bonding with water.

When the cations adsorb water, the gallery space expands. In the case of monovalent cations like Na+ or K+, the gallery space can expand infinitely (eventually exfoliating), while the case of Ca+2 may lead to a 45-145% volume increase [68]. Divalent Ca+2 behaves differently from monovalent Na+ is because the divalent cation is attracted to platelets on both sides of the gallery space, while the Na+ is only attracted to only one side.

The average distance between cations in the case of Na+ clay is around 0.7 to 0.8 nm [71, 72]. The oxygen layer on the surface of the clay is considered to be organophilic [73] or have the ability to form very weak hydrogen bonding with species with hydroxyl groups. Small organic molecules like glycerol or alcohols readily adsorb to the inner surface of clay [74, 75, 76].

Another important property of clay is that the cations are exchangeable. By replacing the inorganic cations with organic cations, the clay can be made more hydrophobic. The inorganic - organic ion exchange reaction is commonly done with a sodium - ammonium cationic surfactant exchange reaction in water solution to produce a clay with an organic surfactant surface. When the clay is exposed to surfactant molecules in water, the surfactant will be "sucked" into the clay. The exchange of the organic surfactant is both enthalpically and entropically favored. By leaving the water and entering the gallery space, the surfactant molecules increase the system entropy by releasing adsorbed water molecules from the surfactant tail,

and decrease the system enthalpy through charge interaction and the van de Waals interactions between the surfactant molecule and oxygen layer of the clay [77].

The unit of cation exchange capacity (CEC) is meq/100g, which stands for millil-equivalents per 100 gram of clay, which is the same as 10^{-5} mole of charge per gram of clay. The CEC of montmorillonite is around 100, that of mica ranges from 20 to 40, while the kaolinite has a value of 10 or lower. The exact number depends on the geographical origin of the clay and the pH value of the clay solution [78].

The organically modified clay, also called organoclay, has been widely used as an absorbent of oil or organic [79]. Early attempts to make polymer organoclay composites can be traced back to the 1950's [80], although those composites were not termed nanocomposites.

Clays behaves differently from salts, acids or bases. For example, clay surface shows strong or moderate acidity, but the clay solution doesn't show acidity [81]. Such acidity has been attributed to the low flammability of polymer/layered silicate nanocomposites [82].

1.3 Silane Coupling Agent

Silane coupling agents are usually alkoxysilanes, which means the silane contains Si-O-CH_3 groups or Si-O-CH_2-CH_3 groups. Alkoxysilanes can loose the methoxy (-O-CH_3) or ethoxy (-O-CH_2-CH_3) groups and form silanol (Si-OH) groups or Si-O-X type covalent bonding, where X is Si or other metals. Silane coupling agents have been used to promote wetting between polymers and inorganic materials like mica,

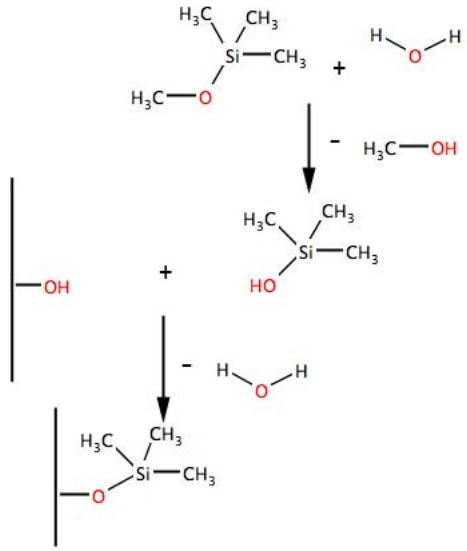

Figure 1.3: Hydrous Silanization Process

glass, silica, alumina, copper, tin, talc, steel, etc. The silane coupling agent also can bond to the polymer via covalent, hydrogen bonds or van de Waals interaction [83].

Silane coupling agents can bond to inorganic material via covalent bonds or hydrogen bonding [84]. The covalent bonding between the inorganic material and silane coupling agent is formed by condensation. When there is water involved in the reaction, the silane coupling agents firstly form silanols, then the silanols form covalent bonding with hydroxyl groups on the surface of inorganic materials via dehydration. The process of hydrous silanization is shown in figure 1.3. When there is no water involved in the reaction, silane can form covalent bonding with hydroxyl groups on the surface of inorganic materials via condensation without forming silanol. The process of anhydrous silanization is shown in figure 1.4.

In this research silane coupling agent was used to attach short polymer chains to the surface of silicate. Attaching short polymer chains to the surface of clay has

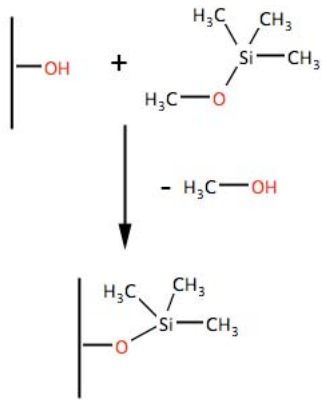

Figure 1.4: Anhydrous Silanization Process

been achieved by making ammonium salt containing short polymer chains [85] and grafting PDMS on to the surface of clay in solution [86]. The advantage of silane over the ammonium salt containing short polymer chain is that silane containing polymer chains are more stable. The advantage of silane over PDMS approach is that silane can be adopted to work with different polymers.

1.4 Flammability of Polymers

1.4.1 Combustion and Pyrolysis of Polymers

Three factors are required for any kinds of combustion. They are an oxidizing agent, fuel, and an ignition source. When a high temperature ignition source is applied to a polymer, the polymer begins to decompose. During decomposition, molecules of monomer or oligomers are given off. In most cases these small molecules

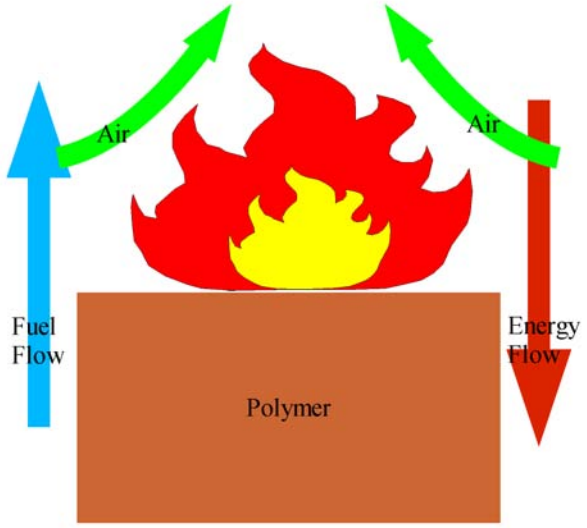

Figure 1.5: Three Types of Flow During Combustion

are a flammable fuel. Then fuel is mixed with oxygen in the air. Generally a specific fuel concentration is required for combustion. If the fuel/oxygen ratio is either too high or too low, combustion will not occur. At last the fuel molecules in air combust. In this step, energy is released and some of this thermal energy is radiated back to the condensed polymer phase and further facilitates the decomposition.

There are also two mass flows and one energy flow that must be maintained to sustain the combustion. The first mass flow is the fuel flow from the condensed phase to the combustion zone in the gas phase, the second mass flow is the flow of air to provide oxygen, and the energy flow is the radiation from the combustion zone in the gaseous phase to the decomposition zone in the condensed phase. These flows are shown schematically in figure 1.5.

The polymer decomposition is an important step in the combustion process. There are two different major paths for polymer decomposition without char forma-

tion. Polymers of the first type yield monomer. Polymers falling into this decomposition path include PMMA, polyoxymethylene, poly-α-methylstyrene and Teflon. This type of polymer degradation is also called "unzipping". The second decomposition path yields monomer, dimer, trimer and etc. Polymers falling into this second decomposition type include polystyrene (PS), polymethylacrylate (PMA), polypropylene (PP), polyethylene (PE). This type of polymer degradation is also termed the "unbutton" [87]. The degradation mechanisms are shown in figure 1.6 for "unzipping" and figure 1.7 for "unbutton".

The α hydrogen plays an important role in the degradation of polymers. If the α hydrogens of polystyrene are replaced by deuterium, the number of monomers in the thermal degradation product increases greatly. If the α hydrogens of polystyrene are replaced by methyl group, the degradation product will be only monomer. In the unbuttoning degradation mechanism, the free radical abstracts the α hydrogen of other polymer chain or α hydrogen on the same polymer chain, and then the free radical cleaves the backbone and creates one double bond. The "unbuttoning" reaction mechanism is also called bite back. By bite back, the polymer may be cut into either monomer, dimer, trimer or etc. For polymers without α hydrogens, the free radical can not bite back, thus those polymers generally degrade by unzipping.

Unzipping and unbuttoning type polymers have different properties during thermal degradation. The unzipping type polymer maintains relatively high molecular weight at the beginning of the thermal degradation, properties related with molecular weight like viscosity, modulus also remain relative stable. But the degradation product is highly volatile and easily enters the gaseous phase. The molecular

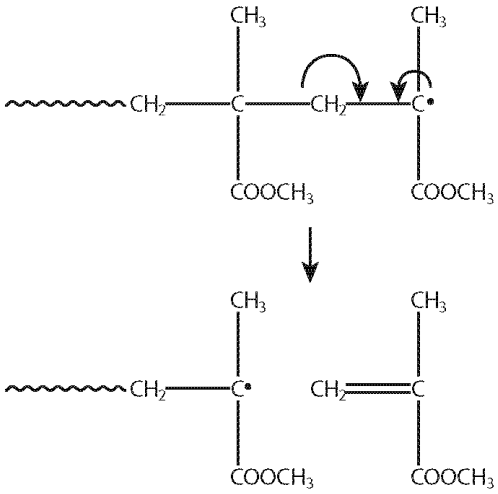

Figure 1.6: PMMA Degradation Mechanism

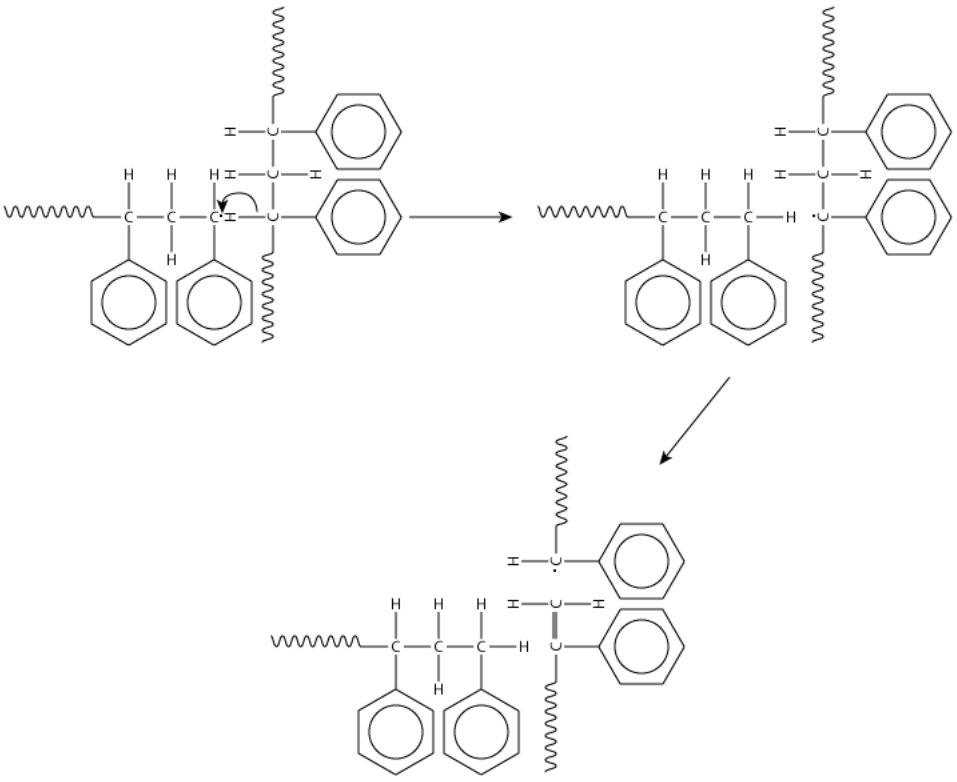

Figure 1.7: PS Degradation Mechanism

weight of an unbutton type polymer drop dramatically at the beginning of the polymer degradation, and consequently properties like viscosity and modulus change dramatically. However, a large amount of the degradation products are large molecules that remain in the condensed phase and burn slowly.

Defects in the polymer chains also play an important role in the degradation of polymers. Head-to-head defects are generally unstable sites which degrade at lower temperature than the random scission temperature of the main chain. There are only a small amount of head-to-head defects in PMMA chains made by free radical polymerization. On the other hand, there are a relatively larger amount of head-to-head defects in PS chains made by free radical polymerization.

Unsaturated bonds also have an effect on polymer stability. The carbons connected with double bonds are in SP^3 bonded. The carbons connected to C-C single bonds are in SP^2 bonded. In bonds adjacent to a C=C double bond, the single bonds are made by one electron in SP^2 status and one electron in SP^3 status. As a result, the single bonds neighboring a double bond are weakened and relatively easy to break.

There are several properties that are readily quantified to describe the combustion hazard of polymers [88]. They are:

(1) Ignition time, which is a measure of the time required to ignite the polymer.

(2) Flame spread speed, which is a measure of the velocity at which the flame travel on the surface of the polymer.

(3) Fire penetration, which is a measure of how quickly a controlled fire (heat source) can penetrate through a material.

(4) Extinction, which is a measure of how easily a burning material can be extinguished or if it exhibits self-extinction.

(5) Smoke evolution, which is a quantitative measure of the amount of smoke released by a material during combustion.

(6) Toxic gas evolution, which is an important factor in determining the combustion hazard of a particular material.

1.4.1.1 So Called "Self-Extinguishing" Polymers

The "self-extinguishing" polymer is a claim made by the plastic industry. There are no real "self-extinguishing" polymers, there are many polymers with very low flammability, for example polycarbonate, polyvinyl chloride, some nylons and many thermoset polymers. In 1973, the US Federal Trade Commission filed a complaint against the use of the term "self-extinguishing" [89, 90].

All these polymers have chemical groups which limit combustion through char formation and specific chemistry.

Polyvinyl chloride (PVC) is in the class of self extinguishing polymers. PVC loses hydrogen chloride from its backbone during the first step of degradation. The hydrogen chloride scavenges free radicals in both the condensed phase and gaseous phases. The PVC back bone without hydrogen chloride groups is essentially polyene. The polyene wraps around itself and forms char at higher temperature. The stability and mechanical properties of pure PVC is very poor so PVC products on the market generally have large amounts of additives. Many PVC products actually

have increased flammability because of the additives.

Polycarbonate (PC) has phenyl rings in its backbone, and during thermal degradation the phenyl rings form char.

1.4.1.2 Flame Retardant Additives

Different methods have been developed to reduce the flammability of polymers. The most effective method developed so far is to add flammability retardant additives. Flammability retardants reduce the flammability of the polymer by either physical or chemical processes. Physical processes include cooling, forming a protective layer or diluting the concentration of flammable small molecules and oxygen. Chemical processes include reaction in the gas or condensed phase [91].

Three major classes of additives have been widely used with polymers. The first class is halogen based additives. The second class is phosphorus based additives. The third class is $Al(OH)_3$ or $Mg(OH)_2$ based additives. Other less prominent flame retardants include antimony oxide, nitrogen compounds based flame retardants and intumenscent flame retardants.

Halogen based additives quench free radicals formed during the polymer decomposition process and stop the oxidation of fuel molecules in the gas phase.

Halogen based flame retardants are often used together with antimony oxide to decrease flammability. Antimony oxide evaporates during combustion and absorbs energy. One problem is that antimony oxide vapor is poisonous.

Addition of halogen based additives is an effective way to reduce the flamma-

bility of polymers, but many flame retardants release corrosive or harmful products during combustion, some halogen compounds may be carcinogenic. Some flame retardants may release dioxin or other poisonous byproducts during smoldering. Because of these reasons, some of these compounds have been outlawed in many countries (particularly in Europe). In the United States, halogen based additives are currently being phased out. The only major producer in the United States, Great Lakes Chemical Corporation (now Chemtura Corporation), has stopped manufacturing most halogen based flame retardants [92, 93, 94, 95, 96, 97, 98]. States like Oregon and California have taken very restrict regulation against the halogen based flame retardants.

Phosphorus based flame retardant additives include red phosphorus, phosphate and phosphorus compounds. Phosphorus based flame retardant additives have been successfully used in polymeric materials such as flame retardant polyurethane foam for building construction, polyimide and epoxy [99, 100, 101]. After the banning of halogen based flame retardants, phosphorus based flame retardants have been used in electronic applications like printed wire board and integrated circuit packaging materials [102, 1].

In 1786, King Louis XVIII commissioned Gay-Lussac to search for methods that could protect fabrics in the theaters. Around 1820, Gay-Lussac reported that a mixture of ammonium phosphate and ammonium chloride was the most effective [65]. These products are still on the market under variant trade names like Fire-Trol, FR CROS, ANTIBLAZE ML.

Recently it has been reported that phosphorus based flame retardant addi-

tives can leach out from the polymer matrix and cause shorts in copper wiring in integrated circuits [103].

$Al(OH)_3$ or $Mg(OH)_2$ based flame retardants can form a protective layer on the surface of the polymer, which can partially stop the transfer of energy from the gas phase to the condensed phase. During the combustion process, the $Al(OH)_3$ or $Mg(OH)_2$ based flame retardants decompose and release water, which absorbs a large amount of energy. The water vapor also dilutes the oxygen in the air. Without enough energy to break the polymer and enough oxygen, the combustion process cannot be sustained. The degradation products of $Mg(OH)_2$ also suppress smoke. One common drawback of the $Al(OH)_3$ or $Mg(OH)_2$ based flame retardants is that high concentrations (around 65%) are required to effectively reduce the flammability. As a result, the mechanical properties of polymers with $Al(OH)_3$ or $Mg(OH)_2$ based flame retardants are often significantly degraded.

A successful flame retardant can not only prevent the ignition, but also prevent the flame spreading and penetration.

1.4.2 Flammability Measurements

To measure whether a retardant is effective, a quantitative standard is needed to measure the flammability of the polymer.

There are several measurement systems used in the United States in the building and construction, aerospace, automobile and home electronics industries. One of the most important methods is Underwriters Laboratories UL-94 specification,

which is used to measure the flammability of materials used in home electronics.

UL-94 tests the tendency of polymer to extinguish or the flame to spread the flame after the polymer has been successfully ignited. There are three different series of UL-94. The first series is designed to test the materials used in consumer electronic products, building structural parts or enclosures. The second series are designed to test foam materials. The third series are designed to measure the flammability of thin film materials.

The other area of polymer flammability is the ability to resist ignition, especially electrical-related ignition. There are three kinds of electrical-related ignition, hot wire, high current arc and high voltage arc. UL-764A is a test designed to study the ignition resistance of polymers.

1.5 Flammability of Polymer Nanocomposites

Most polymer based nanocomposites show reduced flammability compared to their pure matrix polymers, including 0-dimensional, 1-dimensional and 2-dimensional fillers [104, 105, 106, 107, 108, 109, 110, 111, 112, 113].

Because there is no significant change in the combustion products of nanocomposites compared with pure matrix polymer, it is believed that the reduced flammability of nanocomposites arise from physical reasons, particularly the shielding effect of the protective char layer formed on the surface of the residue.

Compared with other flammability retardants, nanocomposites reduce the fire risk while improving the mechanical properties without adding harmful chemical

additives. However, the use of a nanofiller alone has not yet produced a nanocomposite which has low enough flammability to eliminate the need for flame retardant additives.

Chapter 2

Experimental

2.1 Research Outline

Poly(methyl methacrylate) based polymer nanocomposites were synthesized, and their flammability and structure were examined. This work focused on the effect of molecular weight, clay distribution and clay aspect ratio on the flammability of the PMMA nanocomposites.

2.2 Materials

2.2.1 Resin Polymer

PMMA was selected as the matrix polymer in this study for two reasons. The first reason is that PMMA decomposes via unzipping, and consequently the molecular weight of the polymer and the change of melt viscosity during the combustion process is less dramatic than the polymers that degrade to oligomers. The second reason is that PMMA is a widely used plastic with high transparency, good mechanical properties and good UV resistance and hence studying the flammability of PMMA based nanocomposites has important industrial and commercial value.

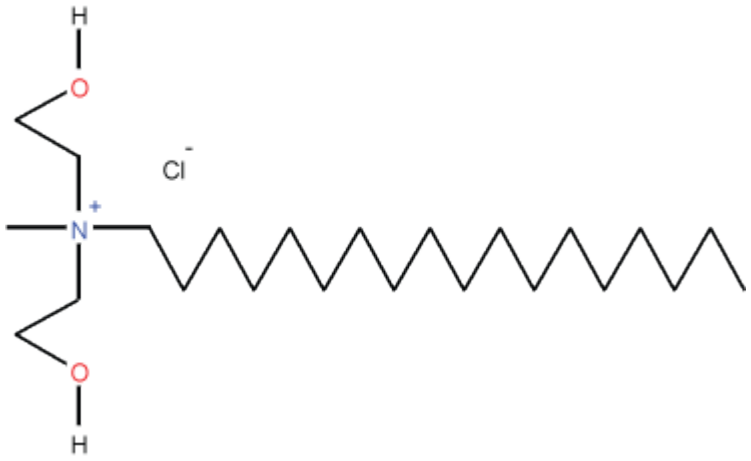

Figure 2.1: Structure of Surfactant Used in Cloisite 30B Clay

2.2.2 Additives

2.2.2.1 Cloisite 30B

Cloisite 30B organically modified clay was purchased from Southern Clay Products Inc. It is an organically modified montmorillonite with literature lateral dimensions of 100 nm to more than 1000 nm [114]. The organic modifier is methyl, tallow, bis-2-hydroxyethyl, quaternary ammonium. The tallow contains 65% C18, 30% C16 and 5% C14. The structure of the surfactant is shown in figure 2.1 [115]. Cloisite 30B clay forms a transparent dispersion in dimethylformamide (DMF) and dimethylsulfoxide (DMSO).

2.2.2.2 Cloisite 15A

Cloisite 15A was purchased from Southern Clay Products Inc. It is an organically modified montmorillonite with literature lateral dimensions of 100 nm to more than 1000 nm[114]. The organic modifier is dimethyl, dehydrogenated tallow,

Figure 2.2: Structure of Surfactant Used in Cloisite 15A Clay

quaternary ammonium. The tallow contains 65% C18, 30% C16 and 5% C14. The structure of the surfactant of Cloisite 15A is shown in figure 2.2 [116]. Cloisite 15A clay forms a transparent dispersion in styrene monomer and chloroform.

2.2.2.3 Somasif MAE120

The Somasif series of synthetic micas were provided by Unicoop Japan. Fluorine is used to replace the hydroxyl groups on the mica. In the case of MAE120, an organic modifier was used to replace the sodium cations, making the synthetic mica hydrophobic.

The MAE120 synthetic mica disperses well in benzene, xylene, chloroform and dichloromethane [117]. The lateral dimension of platelet was measured by AFM as 1-3 um.

2.2.2.4 Synthesis of PMMA Grafted Layered Silicate

Short PMMA chains were grafted to the surface of Cloisite 30B clay by silane chemistry.

Methyl methacrylate (MMA) monomer, 3-(Trimethoxysilyl)propyl methacry-

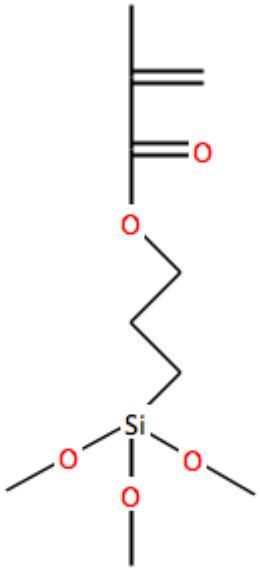

Figure 2.3: Silane A174 Structure

late (silane A174, figure 2.3), Azobisisobutyronitrile (AIBN), and water were dissolved in DMF with mole ratio of 10:1:1:1. Cloisite 30B clay and Silane A174 at a weight ratio of 2:1 was also dispersed in DMF with help of a sonicator. Then the two solutions were mixed, stirred, bubbled with nitrogen and sealed. The solution was then kept at $60°C$ for 3 hours. The mixture was then kept at $100°C$ in vacuum for 1 hour to remove water and complete the reaction.

Silane A174 can polymerize with MMA monomer and form a copolymer of silane and MMA. The silane in the copolymer can bond to hydroxyl groups on the surface of clay via covalent bonding as shown in figure 2.4.

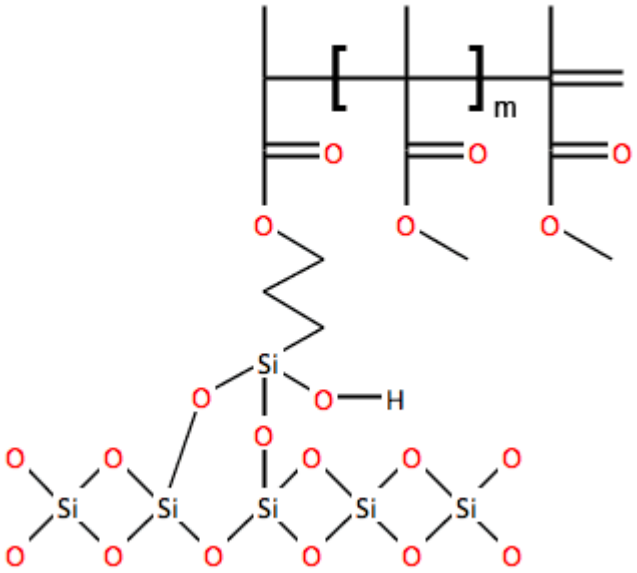

Figure 2.4: Short PMMA Chain Grafted on Clay

2.3 Synthesis of Layered Silicate/Polymer Nanocomposite

2.3.1 *In-situ* Polymerization

In-situ polymerization is a method where the layered silicate is mixed with monomer and initiator, then the polymerization reaction is initiated by either heating or UV. PMMA/Layered silicate nanocomposites with high transparency can be made by this method. However, due to the batch nature of the synthesis, the molecular weight repeatability is not very good.

In these experiments, methyl methacrylate monomer was mixed with organically modified clays by sonicating in a flask for 6+ hours. AIBN initiator was added, and the mixture was then heated and sonicated at 60°C until the viscosity started to increase. The viscous mixture was poured into a glass mold and kept in a nitrogen environment at 60°C for 24 hours to cure. The nanocomposite sheets were then

milled into disks with diameter of 75 mm and thickness of 8 mm, a size appropriate for gasification and cone calorimetry experiment.

2.3.2 Solution Mixing

In this method, layered silicate was first dispersed in THF. Then the polymer was added to this solvent mixture. After mixing, the nanocomposite was precipitated in water. In general, the solvent must be a common solvent for both the organic clay and the polymer, and the precipitation agent must be a non-solvent for both the organic clay and the polymer.

A list of samples is presented in table 2.1.

2.3.3 Synthesis of Nanocomposites with PMMA Grafted Clay

Nanocomposites with PMMA grafted clay were also synthesized by solution mixing.

2.4 Structural Characterization of Nanocomposites

Three common methods for structural characterization of nanocomposites are: direct imaging, including TEM (transmission electron microscopy), SEM (scanning electron microscopy), optical microscopy and AFM (atomic force microscopy); scattering, including XRD (X-ray diffraction) and SAS (small angle scattering), and spectroscopy including rheology, dielectric analysis and NMR (nuclear magnetic resonance).

Table 2.1: Solution Precipitated Samples

Sample Number	Matrix Mw (kDa)	Clay Type	Clay Concentration (wt%)	Solvent
1	25	Cloisite 15A	5	THF
2	350	Cloisite 15A	5	THF
3	25	Cloisite 30B	5	THF
4	350	Cloisite 30B	5	THF
5	25	MAE 120	5	THF
6	350	MAE120	5	THF
7	350	Cloisite 30B	10	THF
8	350	Cloisite 15A	5	Chloroform
9	350	MAE 120	5	Chloroform

In general, there are three important factors that need to be identified in the structural characterization of nanocomposites. These are the degree of dispersion, the degree of orientation and the distance between clay platelets.

The particle distribution at the micrometer scale can be measured using transmission optical microscopy and TEM at low magnification. The degree of dispersion can be quantified by measuring the percentage of single platelets, double platelets, triple platelets etc. This can be achieved via high magnification TEM, but difficulties include sample preparation and the low contrast of the platelets in the polymer matrix.

The percentage of clay particles containing different numbers of platelets can be described by an average number of platelets per stack. The overall dispersion of clay particles can be described by a number average and a weight average distribution of clay particles.

Distance between clay particles can be measured by TEM. XRD is can also be used when the distance between clay particles is relative small, while SAS is applicable when the distance between clay particles is on the scale of nanometers.

2.4.1 X-ray Diffraction

X-ray diffraction (XRD) is a useful method to distinguish an intercalated structure from a traditional microcomposite structure. If the clay platelets are in stacks, the XRD spectrum exhibits diffraction peaks indicating the distance between the clay platelets.

The diffraction peak can disappear due to either the formation of a fully exfoliated structure or significant deformation of the clay platelet stacks [109].

The XRD experiments were conducted using a four-circle Bruker D8 Discover XRD system equipped with a single Gobel mirror and a scintillation counter at NIST.

2.4.2 Small Angle Scattering

Small angle scattering is a powerful tool for measuring the nanometer scale structure.

Scattering from disk has been developed by Kratky and Porod in 1948 as

$$I_s(q) = \Delta\rho^2\mu^2 \int_0^{\pi/2} \{\frac{sin[qHcos(\phi)]}{qHcos(\phi)}\}^2 \{\frac{2J_1[qRsin(\phi)]}{qRsin(\phi)}\}^2 sin(\phi)d\phi \qquad (2.1)$$

Where J_1 is a first order Bessel function. $\Delta\rho$ is the scattering length density difference between the disk and the matrix. μ is the volume of the disk. ϕ is the angle between the clay and $\vec{q}$.

The structure factor of a stack clay platelets can be expressed as

$$S(q,n) = 1 + \frac{2}{n}\sum_{k=1}^{n}(N-k)\cos(kDq\cos\varphi)\exp[-k(q\cos\varphi)^2\delta_D^2/2] \qquad (2.2)$$

where φ is the angle between q and the axis of the tactoid (ie. stack of clay platelets), n corresponds to the total number of platelets in the stack, and D and δ_D represent the next neighbor center-to-center distance and the Gaussian standard deviation (GSD), respectively. D and δ_D can be deduced from the SAXS data plot.

It is safe to assume that the surfactant region and pure polymer region have similar electron densities which results in no contrast from the surfactant. Then the scattering intensity from a tactoid of clay with N clay platelets can be expressed as

$$I(q) = (\Delta\rho)^2 \phi V P(q) S(q, N) \tag{2.3}$$

where the $\Delta\rho$ is the difference between the SLD of clay and PMMA. However, the X-ray SLD of organically modified clay is affected by the organic modifier and clay, because the nominal composition and density of organoclay are not known, the X-ray SLD of organoclay cannot be calculated easily.

In the nanocomposites, the clay exists in stacks of different thickness as well as single layers. The interaction between all clay particles can be described by the correlation function of the clay particles. Two simple methods to solve this problem have been proposed. The first one is to deduce the average clay stack thickness from the linear region of the log-log plot. The second one is to add the intensity from stacks with different thicknesses together.

$$I(q) = \sum_N (\Delta\rho)^2 \phi_N V P(q) S(q, N) \tag{2.4}$$

where

$$\phi = \sum_N \phi_N \tag{2.5}$$

Both methods have their drawbacks. For the average thickness method the meaning of average value is unclear, it is not clear whether it represents an arithmetic mean, weighted mean, median or mode of the clay distribution. Also bimodal distributions cannot be described by single average. For the multiple stack thickness summation

method, different distributions of stack thickness may fit one set of scattering data. Thus, it is useful to couple the scattering data with TEM to determine distribution of clay stacks. However, because of the limited observation area in TEM, it is difficult to obtain enough data. Also it is assumed that the distance between the clay stacks is large and the interaction between different clay stacks is negligible.

A third model has been recently proposed by Hermes [118]. In this model, clay stacks were treated as single particles. However, this model does not appear to provide any improvement in the analysis of the scattering data than the first two methods, but does increase the computation difficulty.

2.4.3 Transmission Electronic Microscopy

TEM can provide direct image information of the clay platelet dispersion. TEM is particularly useful in identifying exfoliated structures [119].

Bright field microscopy is the most widely used method to observe the nanocomposite structure.

There are several difficulties in measuring clay distribution by TEM. The first one is sample preparation. For this work, ultramicrotoming was used to prepare thin sections for TEM. During the microtoming process, the sections can be compressed and the effect on the original structure is unknown. The second difficulty is the observation of single clay platelets in the polymer matrix due to intrinsically low contrast. TEM benefits from being coupled with XRD to characterize dispersion of the clay.

Transmission electron microscopy samples were prepared using a Leica UC-6 ultramicrotome with a Diatome diamond knife at room temperature. The thickness of samples was estimated to be less than 100 nm. Samples were examined with a JEOL JEM-2100 TEM at 200kV coupled with a Gatan CCD camera.

2.5 Flammability Measurement

The flammability of polymer products can be measured at different mass scales, i.e. milligrams, grams or kilograms. Thermogravimetric analysis (TGA) experiments can estimate the thermal degradation at the milligram level, while cone calorimetry and gasification measures the flammability for sample size of tens of grams. Unfortunately it is not always clear that these experiments correlate well with the flammability in real world cases, such as a fully furnished house or building, due to the complex nature of real world combustion situations.

2.5.1 Thermogravimetric Analysis

TGA measures the change of mass as a function of time or temperature. TGA uses a sample size on the order of tens of milligrams. Because of the small sample volume, the temperature gradient and degradation product diffusion can generally be ignored. TGA can be used to measure the temperatures at which the degradation starts and ends. TGA data can also be used to calculate the degradation kinetics.

However, the TGA experiments must be carried out carefully for samples that produce protective residue layers like nanocomposites. The protective layers can

influence in the transport process and affect the measurements [120].

TGA experiments were conducted using a TA Q-500 equipment at different heating speeds from room temperature to 450°C.

2.5.1.1 Degradation Kinetics

The reaction kinetics of homogeneous system is described as

$$\frac{d[X]}{dt} = A \exp^{-\frac{E}{RT}} f([X]) \tag{2.6}$$

where E is the activation energy, T is temperature, R is the universal gas constant, A is the pre-exponential factor, $[X]$ is concentration of the reactant, and t is time.

However, equation 2.6 cannot be directly used on polymeric materials. A typical polymer sample is considered to be a heterogeneous system because of the difference in the distribution of the molecular weight and other parameters. Polymer nanocomposites and composites should also be considered a heterogeneous system. The reaction kinetics of heterogeneous system is described below.

The amount of polymer converted into monomer (or degree of conversion) is expressed as

$$\alpha = \frac{m_s - m}{m_s} \tag{2.7}$$

where α is the degree of the conversion, m_s is the initial mass, and m is the current mass.

The reaction kinetics are described by

$$\frac{d\alpha}{dt} = A \exp^{-E/RT} f(\alpha) h(\alpha, T) \tag{2.8}$$

$h(\alpha, T)$ is normally considered to be equal to 1 in most cases for ease of discussion. $f(\alpha)$ can take many different forms, one commonly presumed form is

$$f(\alpha) = (1 - \alpha)^n \tag{2.9}$$

where n is the reaction order, then the equation can be expressed as

$$\frac{d\alpha}{dt} = A \exp^{-E/RT}(1 - \alpha)^n \tag{2.10}$$

The relationship between temperature and time can be expressed as

$$T = t\phi + T_0 \tag{2.11}$$

where ϕ is the heating rate, and T_0 is the initial temperature.

There are several methods to analyze the thermal degradation kinetic parameters. The Kissinger equation is one of the most widely used methods. The Kissinger equation is expressed as

$$\ln(\phi/T_m^2) = \ln(nRAW_m^{n-1}/E) - E/RT_m \tag{2.12}$$

where T_m is the temperature at the maximum rate of mass loss expressed in K, R is the universal gas constant, W_m is the weight of sample at the maximum rate of weight loss, and n is the apparent order of the reaction. The reaction order can be derived from the shape factor or shape index s. The shape factor, as illustrated in figure 2.5, is expressed as

$$s = -a/b \tag{2.13}$$

where b is the "down hill" slope and a is the "up hill" slope. The relationship between reaction order and shape factor is

$$n = 1.26\sqrt{s} \tag{2.14}$$

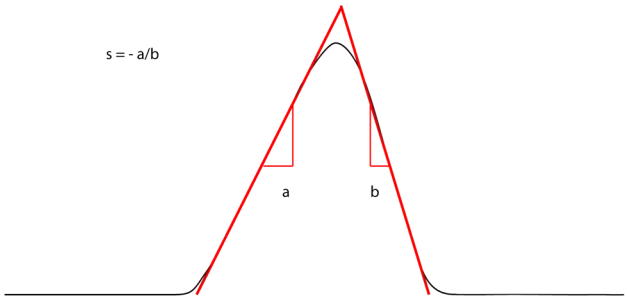

Figure 2.5: Shape Factor

Using the Kissinger method, the activation energy can be derived by plotting $\ln(\phi/T_m^2)$ vs. T_m at different heating rates. The reaction order n can be derived from the shape factor, the pre-exponential factor can be derived from the intersection of $\ln(\phi/T_m^2)$ vs. T_m.

A second method that can be used to derive the degradation kinetics is the Ozawa method. At the same degree of conversion, the temperature, heating rate and activation energy have a relationship described as

$$\frac{d(\log \phi_i)}{d(1/T_i)} \approx 0.4567(E/R) \tag{2.15}$$

where ϕ_i is the heating speed, T_i is the temperatures at the selected conversion rate at different heating rates, E is the activation energy, and R is the universal gas constant. The activation energy can be calculated by plot $\log \phi_i$ vs. $1/T_i$. The change of T_i in respect to ϕ_i is illustrated in figure 2.6.

2.5.2 Cone Calorimetry

Cone calorimetry measures the mass loss and heat release during the combustion process and uses sample sizes on the order of tens of grams. It is the most

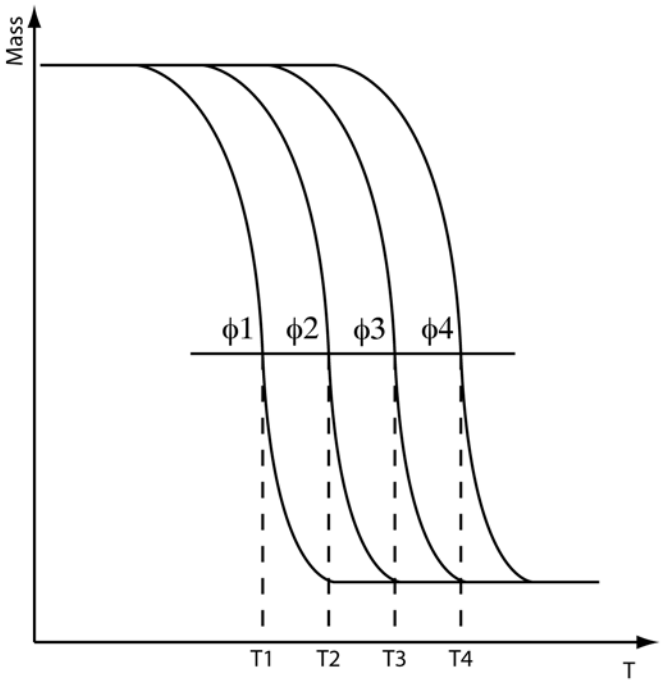

Figure 2.6: Ozawa Method for Calculating Degradation Kinetic Parameters

widely used bench scale experiment of polymer flammability. Data acquired from cone calorimetry reveals the behavior of polymers exposed to a fully developed flame. In cone calorimetry experiments, the polymer is in a closed environment with a constant radiant heat source, which supplies energy from the top and heats the sample continuously during the experiment. After ignition, the loss of mass and the release of heat energy are monitored continuously. The combustion products and oxygen consumption can also be monitored by analyzing the exhaust.

The energy flux applied in a cone calorimeter can be controlled to simulate different fire conditions. A heat flux of $50 kW/m^2$ is reasonable to simulate a full scale fire in a room. A list of heat fluxes at different fire situations are given at table 2.2.

Table 2.2: Relationship Between the Heat Flux and Fire Scale

Flux (kW/m^2)	Scale
25	Small fire
35	Fire before flash over
50	Fire after flash over, aircraft fire
75	Conflagration
100	Petroleum fire

A model based on DSC and TGA measurements has been developed to predict the behavior of thin polymer samples, where the thermal conductivity is not an important factor [146, 147]. This model was designed to produce an easier method to predict the flammability of a polymer using (relatively) common TGA and DSC equipment without the requirement of running cone calorimetry experiments.

2.5.3 Gasification

Gasification is an experiment similar to cone calorimetry where the samples are exposed to a radiation heat source in a nitrogen environment. This simulated combustion during a gasification experiment does not produce exactly the same data as cone calorimetry, but the overall shape of the mass loss curve will be similar. More importantly, there will be no smoke or flame generated at the surface of sample which allows for direct observation of the sample surface. To study the combustion process of nanocomposite materials which may generate a residue layer, gasification

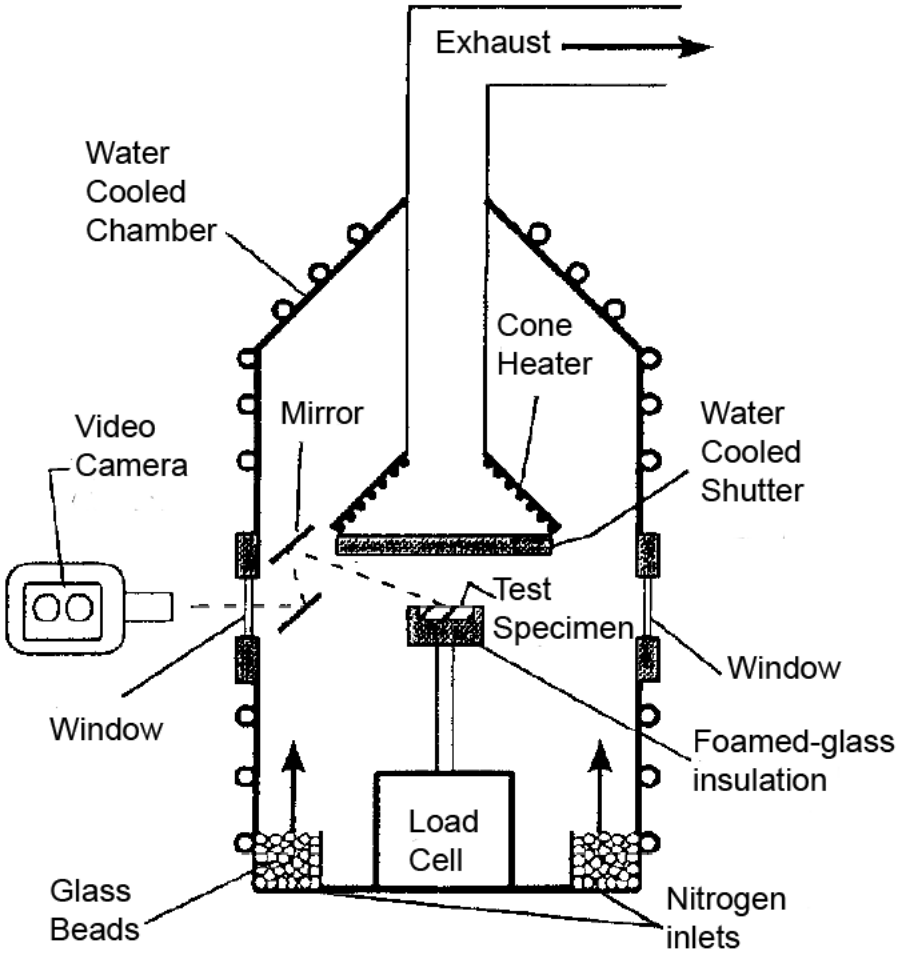

Figure 2.7: Schematic of Gasification Apparatus

experiment can provide information about the formation of this layer. A schematic of the gasification equipment built by NIST is shown in figure 2.7 [121].

2.6 Rheology Measurement

Rheology measurements were conducted on a TA RAD III rheometer at 200 °C. The frequency sweep tests were conducted in the linear region of the stress-strain curves.

Chapter 3

Results and Discussion

3.1 X-ray Diffraction from Clays

The clay XRD data are shown in figure 3.1. The MAE120 sample showed diffraction peaks at 2.76 nm, 1.96 nm, 1.38 nm and 1.18 nm. The XRD data shows that the MAE120 mica has platelets which have a well ordered structure. One explanation is that the mica stacks never became fully exfoliated during the organic modification. The Cloisite 15A sample showed a peak at 2.27 nm. The Cloisite 30B showed a broad peak at 1.67 nm. The montmorillonite clay from which the Cloisite 15A and Cloisite 30B were made has been known to have random distribution of crystal orientations except for the [001] direction, so the (001) diffraction peak has higher intensity than the other planes [122].

3.2 *In-situ* Polymerization Samples

3.2.1 Dispersion of Clay in MMA Monomer

Cloisite 15A, Cloisite 30B and MAE120 clay showed different behavior when dispersed in MMA monomer.

The Cloisite 30B organically modified clay forms gel like mixture at 5 wt% of clay dispersed in MMA monomer. The gel like Cloisite 30B dispersion does not flow,

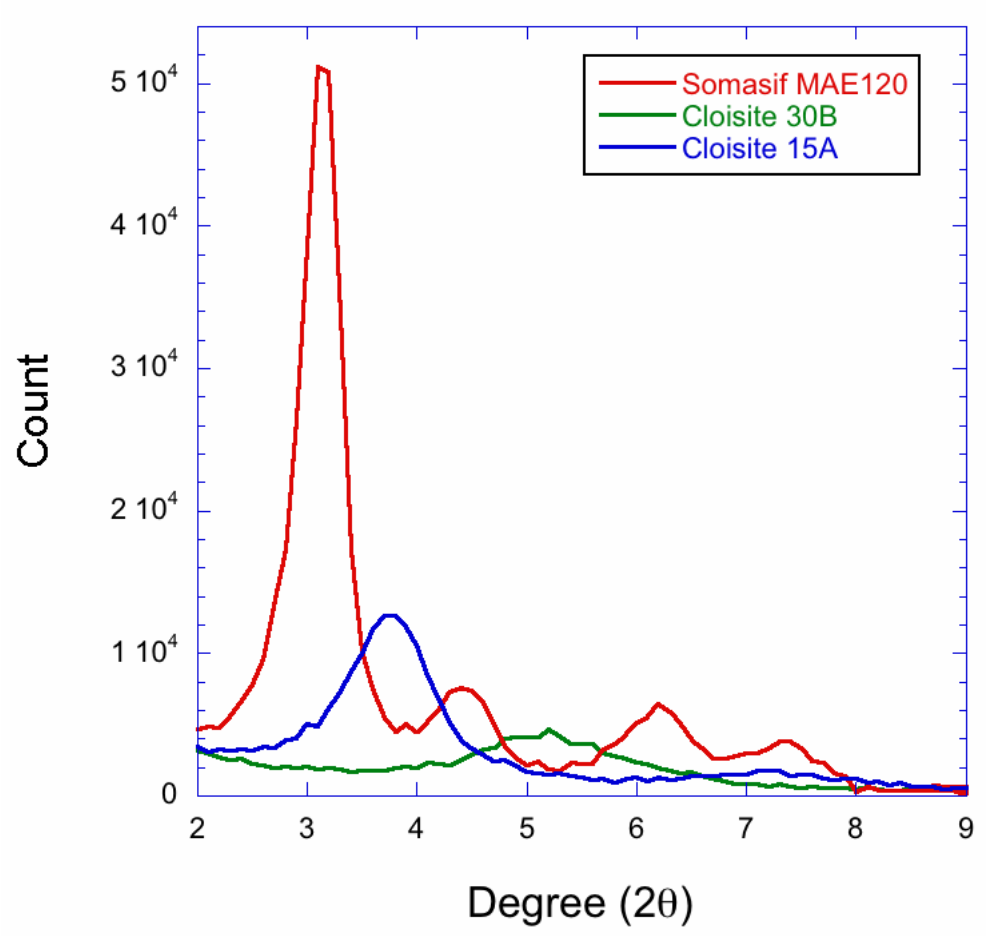

Figure 3.1: XRD Data from Cloisite 15A Clay with a Peak at 2.27 nm, Cloisite 30B Clay with a Peak at 1.67 nm and Peaks from Somasif MAE120 Synthetic Mica (2.76 nm, 1.96 nm, 1.38 nm and 1.18 nm)

when the container is held upside down. But it does flow when a force is applied.

A dispersion of 5 wt% Cloisite 15A organically modified clay in MMA is a viscous liquid, and the clay settles out of the dispersion after 24 hours.

The dispersion of MAE120 organically modified mica is a low viscosity liquid and the mica settles out of the dispersion within minutes after the stirring is stopped.

During the PMMA polymerization, the monomer is usually partially polymerized to a viscous mixture before casting. During the curing of the MMA, the viscosity of the partially polymerized monomer can prevent the Cloisite 15A and MAE120 clay particles from precipitating out.

3.2.2 Polymerization of the Nanocomposites

During the polymerization of the nanocomposites, there are several difficulties associated with the properties and structures of the nanocomposites.

First, because of the interaction between the clay platelets and the monomer, the viscosity of the clay dispersion is much higher than that of the pure monomer. As a result, during the polymerization, the heat dissipation by convection is suppressed and autoacceleration of the polymerization reaction is difficult to control. If autoacceleration occurs, the temperature increases rapidly. If the temperature exceeds the boiling point of the monomer, a large amount of bubbles will be produced.

Second, the clay platelets limit the diffusion of monomer in the solidified polymer. This leads to two different events at different stages of the polymerization. The first event is at the end of the free radical polymerization, the viscosity is large

and the active chain ends have limited motion. Under these conditions, the polymer chains grow by monomers diffusing to the active chain ends. But the monomer diffusion is hindered by the clay platelets and a relatively large amount of monomer remains in the final sample. The second event happens after the polymerization is finished. Bulk free radical polymerization usually leaves some unreacted monomer which is usually removed by heating the sample. However, the clay platelets prevent the monomer from diffusing out of the nanocomposite. These two events lead to the same result, a relatively large amount of monomer remains in the *in-situ* polymerized nanocomposite samples, and the concentration is related with the dispersion of clay. Monomers are more flammable than polymers and have a shorter ignition time. Thus the monomer inside the *in-situ* polymerized samples affects the flammability experiment.

Finally, it is difficult to control molecular weight properly. Due to the batch nature of the synthesis, the molecular weight of sample with the same recipe will be different for different batches. During the polymerization, different parts of the reaction mixture may experience different temperatures, resulting in different molecular weights. It is also difficult to make low molecular weight samples by this polymerization method. Low molecular weight samples can be produced by using either a very high concentration of initiator or chain transfer agent. Both methods have drawbacks. High initiator concentration increases the reaction speed and likelihood of autoacceleration. A high concentration of chain transfer agent can produce low molecular weight polymer repeatedly but the thiol chain transfer agents have terrible smell which limits their use. Halogen chain transfer agents are flame

retardants and obscures the effect of molecular weight on flammability.

3.2.3 Structure of *in-situ* Polymerized Samples

3.2.3.1 X-ray Diffraction

The XRD data of samples made by *in-situ* polymerization are shown in 3.2. All samples showed very weak diffraction peaks.

Nanocomposite with Cloisite 30B clay showed peaks at 3.4 nm and 1.7 nm. Nanocomposite with Cloisite 15A clay showed peaks at 3.5 nm and 1.77 nm. Nanocomposites made with MAE120 synthetic mica showed peaks at 2.1 nm and 1.36 nm. Comparing the data to that from the clay samples, the nanocomposites made by this *in-situ* polymerization method showed that an intercalated structure had formed.

3.2.3.2 Transmission Electron Microscopy

A TEM micrograph of an *in-situ* polymerized Cloisite 30B nanocomposite is shown in figure 3.4, a TEM micrograph of an *in-situ* polymerized Cloisite 15A nanocomposite is shown in figure 3.3. Two TEM micrographs of an *in-situ* polymerized Somasif MAE120 nanocomposite are shown, one is at relatively high magnification (figure 3.5) and one is at relatively low magnification (figure 3.6). The low magnification Somasif MAE120 micrograph shows how a clay stack can be spread apart during the *in-situ* polymerization.

All TEM micrographs show thin stacks of clay platelets with Cloisite 30B nanocomposites showing more single layers. It can be concluded that Cloisite 30B,

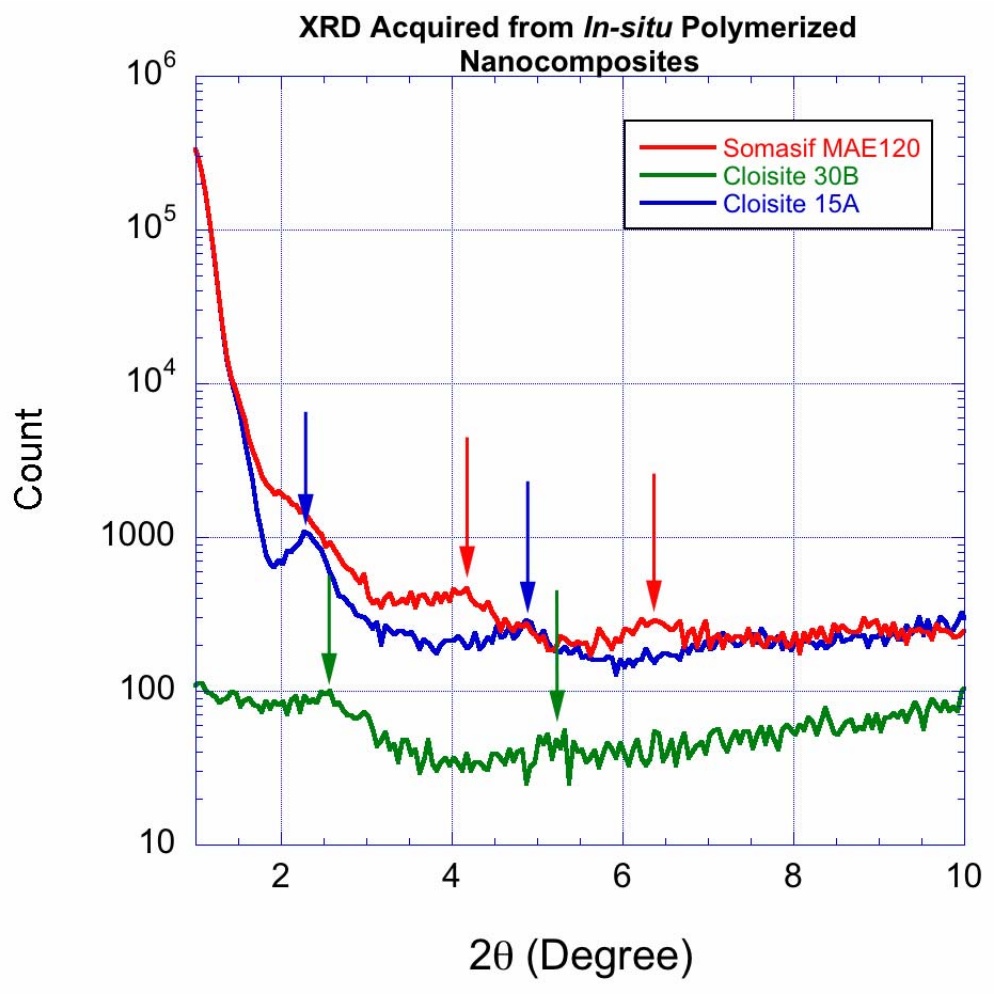

Figure 3.2: XRD Data from *in-situ* Polymerized Nanocomposites with Peaks Labeled.

Cloisite 15A and Somasif MAE120 nanocomposites have an intercalated structure with Cloisite 30B nanocomposite showing the largest degree of exfoliation.

The XRD data also shows that an intercalated structure exists for all three types of nanocomposites synthesized by this *in-situ* polymerization method. The peak position of both Cloisite 30B nanocomposites and Cloisite 15A samples is lower than the peak positions in their corresponding clay, which indicates that the distance between the clay platelets has increased.

In-situ polymerization is useful in producing nanocomposites with a relatively high degree of exfoliation. Before the polymerization is initiated, monomer and initiator can enter the gallery space between the silicate platelets. After the polymerization is initiated, the polymer chains grow in this region between the silicate platelets and expands the gallery space.

3.2.4 Flammability measurement of *in-situ* Polymerized Samples

The gasification data from *in-situ* polymerized samples are shown in figure 3.7. The nanocomposites showed a lower mass loss rate than the pure polymer samples. The high molecular weight pure PMMA sample showed lower flammability than the low molecular weight pure PMMA sample. However, the high molecular weight nanocomposite samples showed similar flammability behavior to the low molecular weight nanocomposite samples, which can be explained by the presence of residual monomer in the nanocomposite. The Somasif MAE120 nanocomposite

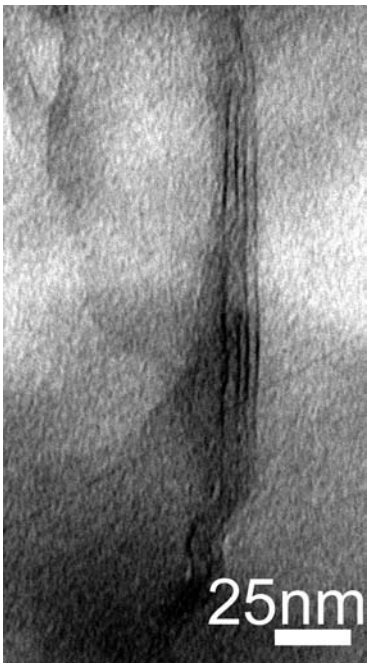

Figure 3.3: TEM of *in-situ* Polymerized Cloisite 15A Nanocomposites

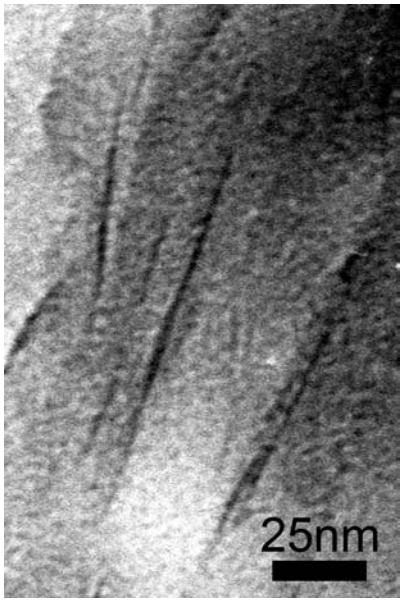

Figure 3.4: TEM of *in-situ* Polymerized Cloisite 30B Nanocomposites

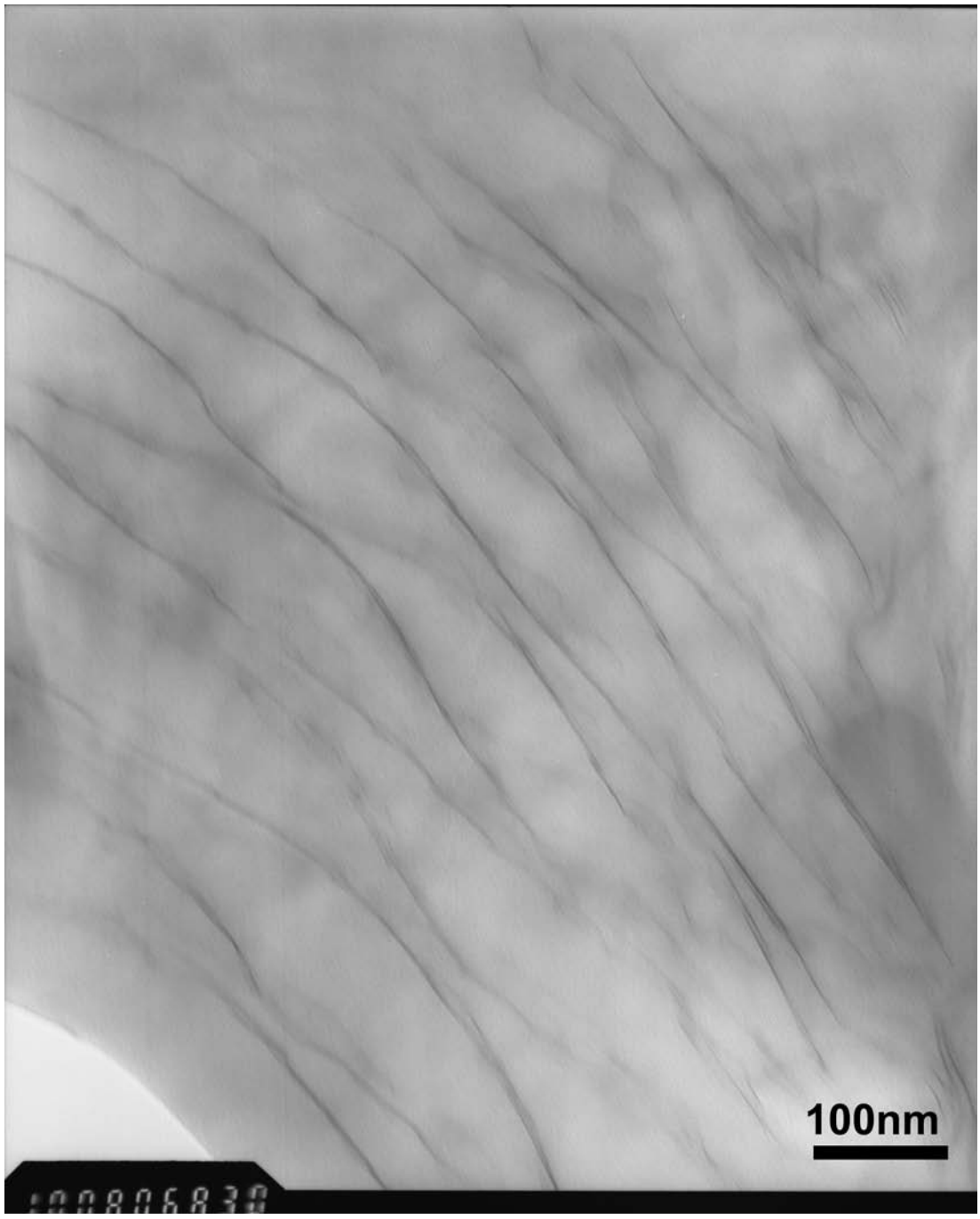

Figure 3.5: TEM of *in-situ* Polymerized MAE120 Nanocomposites

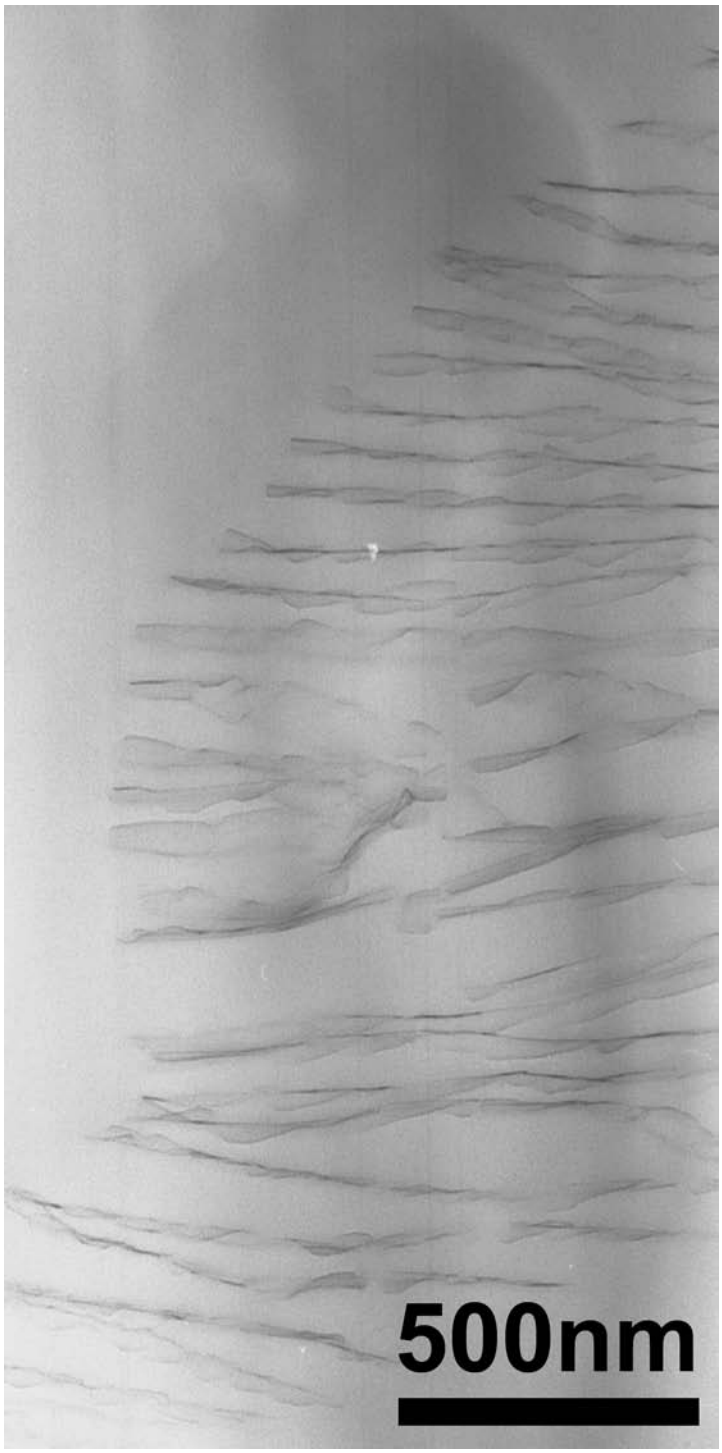

Figure 3.6: TEM of *in-situ* Polymerized MAE120 Nanocomposites Showing Clay Stacks Being Spread Apart

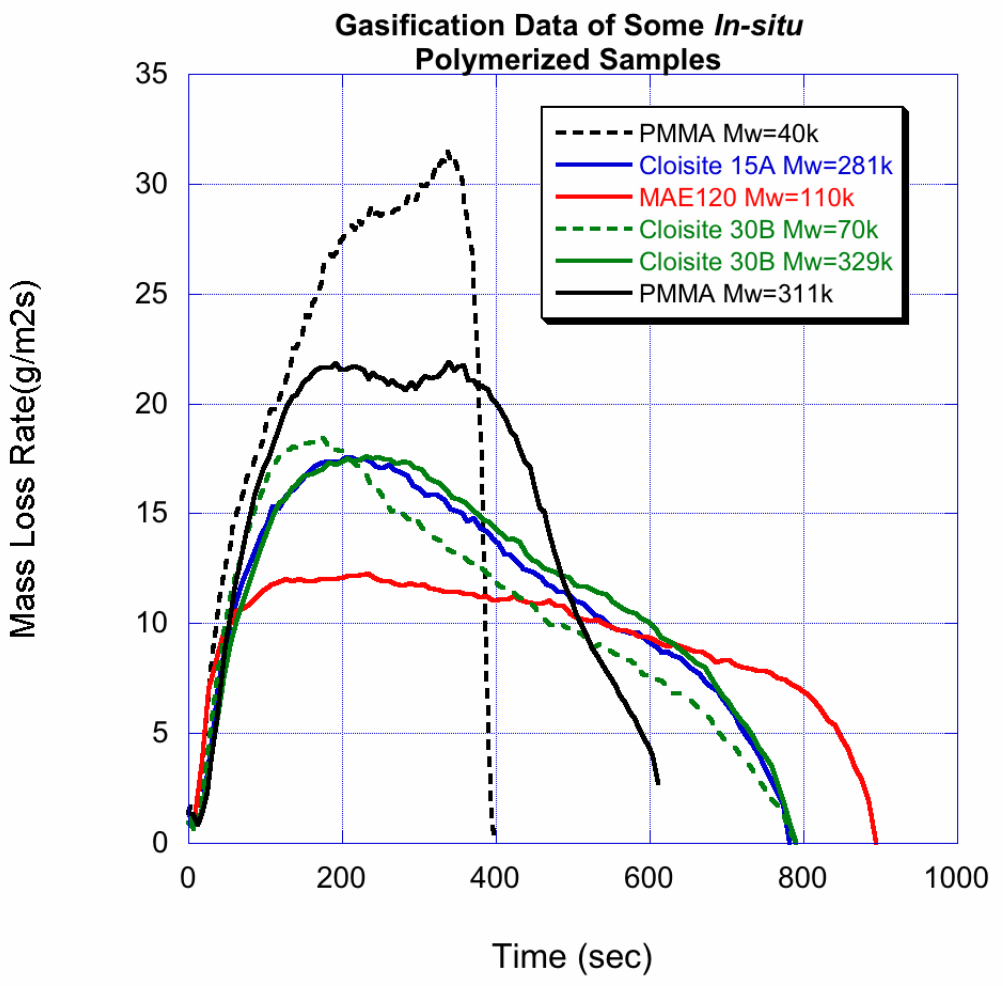

Figure 3.7: Gasification Data from *in-situ* Polymerized Nanocomposites

sample showed lowest mass loss rate in this group of data, despite its relatively low molecular weight. This may due to the effect of the large platelet size of the Somasif mica.

3.2.5 Summary of *in-situ* Polymerized Nanocomposites

Although the *in-situ* polymerization method makes nanocomposites with clay particles well dispersed in the polymer matrix, there were several problems which are difficult to solve. The difficulties are repeatability, monomer residue and molecular weight control. The *in-situ* polymerization method was dropped in favor of solution mixing to produce samples.

3.3 Solution Mixing Nanocomposite Structure

3.3.1 Transmission Electron Microscopy

Micrographs of nanocomposites with 5 wt% Cloisite 15A, Cloisite 30B and MAE 120 clay produced by solution mixing were taken using a JEOL JEM-2100 TEM. Two different molecular weights were used, a high molecular weight with a nominal Mw of 350kDa and a low molecular weight with a nominal Mw of 25kDa. Charging and electron beam degradation were a problem for the low molecular weight nanocomposites and the TEM samples were unstable and moved during observation, resulting micrographs of poor quality. Only micrographs from the high molecular weight samples (sample numbers 2, 4, and 6) are shown here. Nonetheless, the low molecular weight nanocomposites showed a similar clay dispersion as the

high molecular weight nanocomposites.

An example TEM micrograph of a 5 wt% Cloisite 15A/PMMA nanocomposite (350k g/mol molecular weight) is shown in figure 3.12. The Cloisite 15A primarily exists as 10-20 nm thick stacks. The distance between layers in the stacks was measured to be 2.3-2.5 nm. In contrast to the 30B samples (figure 3.13), only few double layer stacks were observed. Also in contrast to the 30B samples, the silicate stacks in the Cloisite 15A samples are generally thicker and less warped. A clay stack count is given in fig 3.8

An example TEM micrograph of nanocomposite of a 5 wt% Cloisite 30B/PMMA (350k g/mol molecular weight) is shown in micrograph 3.13. The Cloisite 30B clay shows a mixed morphology of thin stacks containing less than 5 silicate layers along with thick stacks with more than 5 layers. Double layers were widely present in the image(s). The silicate stacks are also highly warped. Compared with Cloisite 15A and MAE120, Cloisite 30B has a relatively high affinity to the PMMA matrix because of its more polar surfactant, which leads to a higher level of clay exfoliation. The higher level of intercalation (and some exfoliation) in the 30B samples results in more deformation of the clay platelets during molding of the samples. The distance between clay layers measured from TEM ranges from 2.3-2.5 nm for the Cloisite 30B while the stack thickness varied from a single layer to 15 nm (8 layers). A clay stack count is given in figure 3.9.

An example TEM micrograph of a nanocomposite of 5 wt% MAE120/PMMA (350k g/mol molecular weight) is shown in micrograph 3.14. The stack thickness is

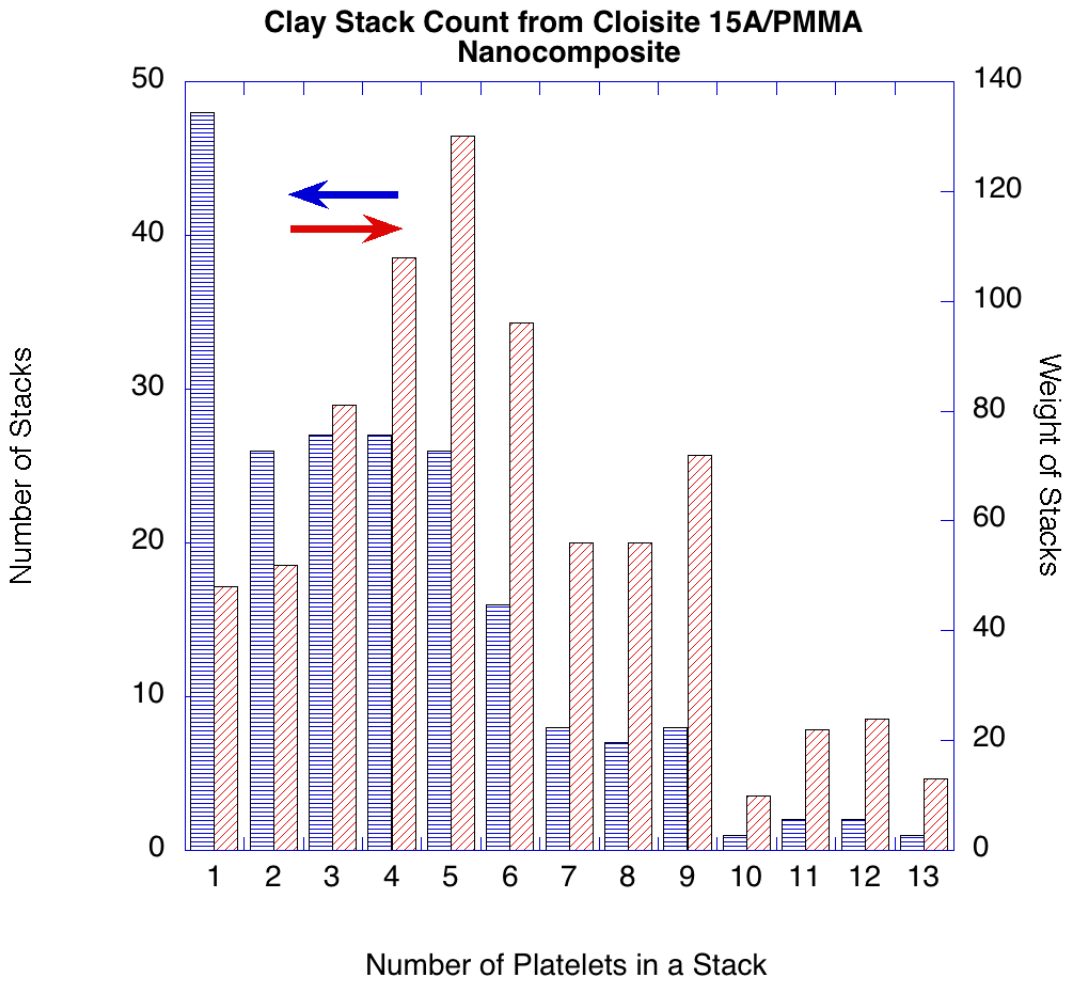

Figure 3.8: Clay Stack Count from the Cloisite 15A/PMMA Nanocomposites

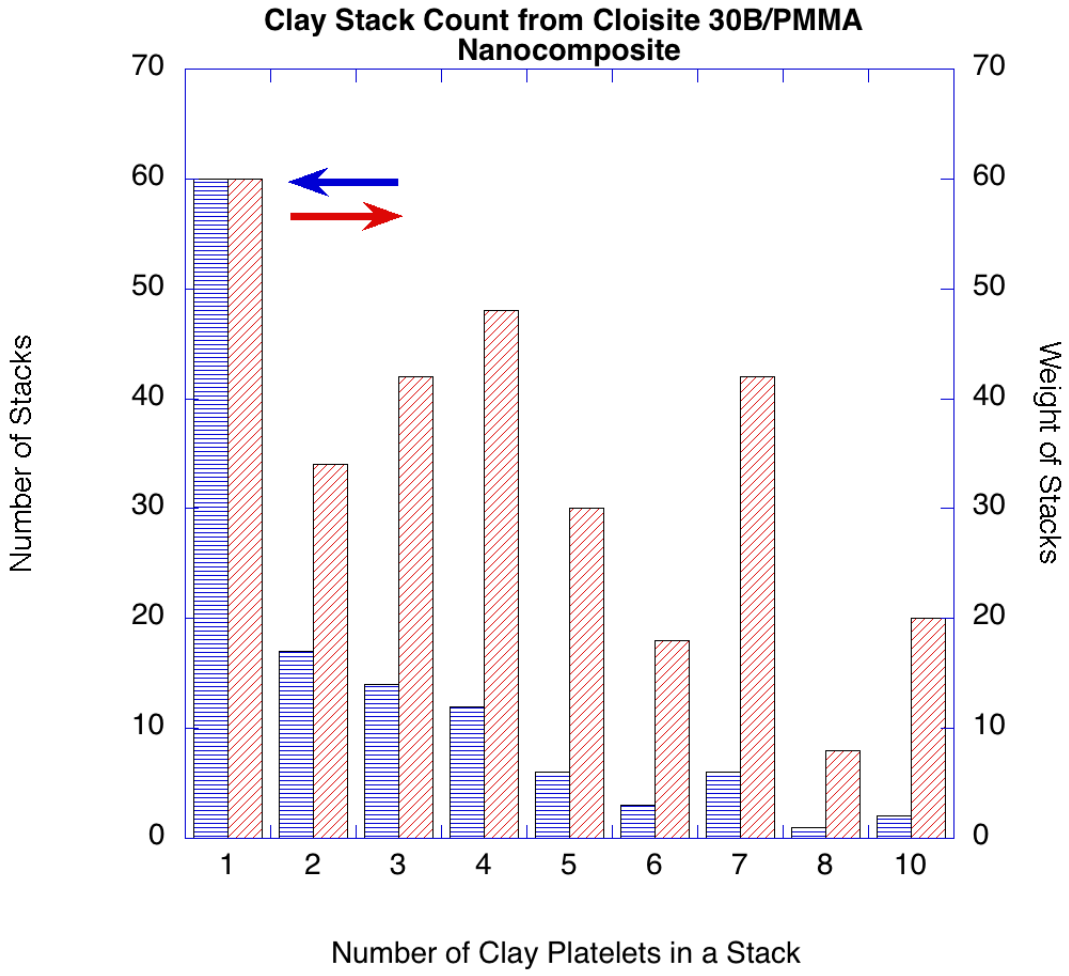

Figure 3.9: Clay Stack Count from the Cloisite 30B/PMMA Nanocomposites

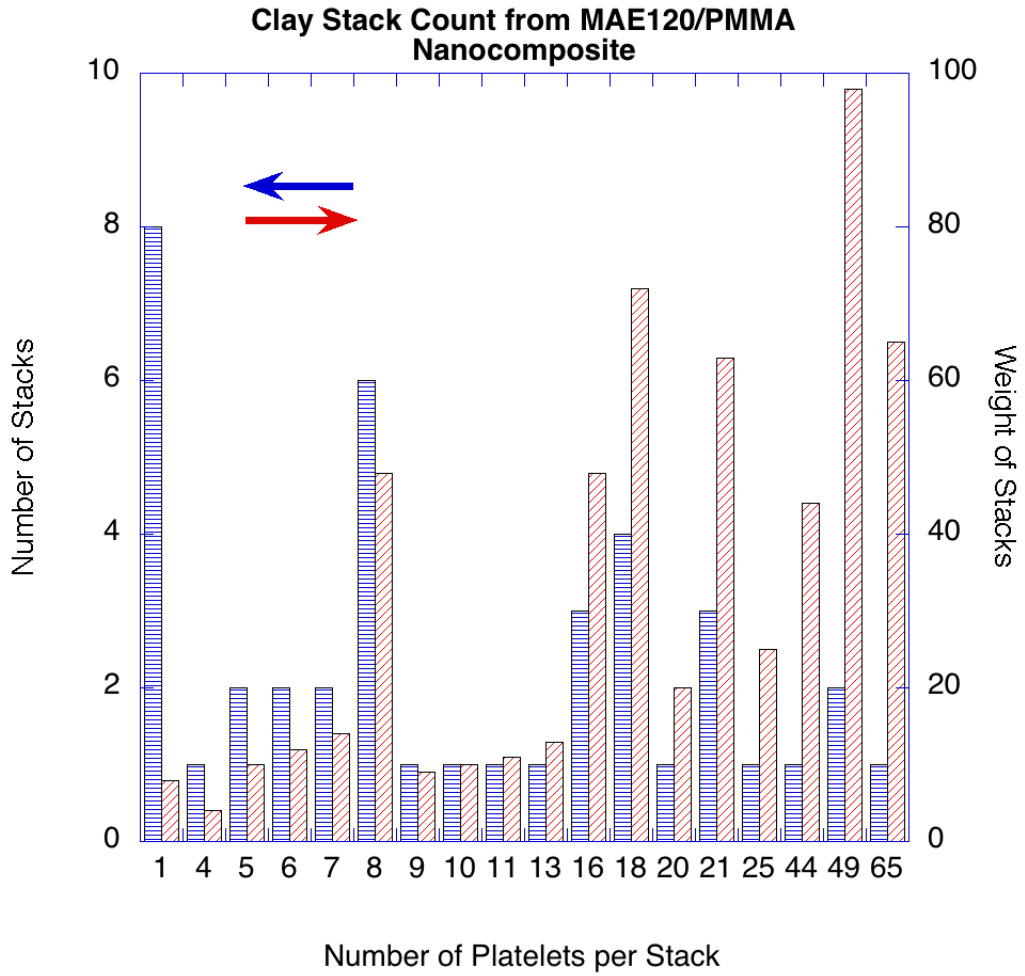

Figure 3.10: Clay Stack Count from the MAE120/PMMA Nanocomposites

several hundred nanometers and the PMMA/Somasif MAE120 samples should be classified as microcomposites rather than nanocomposites. The micrograph shows two different morphologies. One morphology is consistent of stacks with a platelet layer spacing of 2.6 nm and a second one with a spacing of 1.5 nm. The second morphology is consistent with MAE120 platelets without organic modification. A clay stack count is given in figure 3.10

An example TEM micrograph of nanocomposite of a 5 wt% PMMA grafted

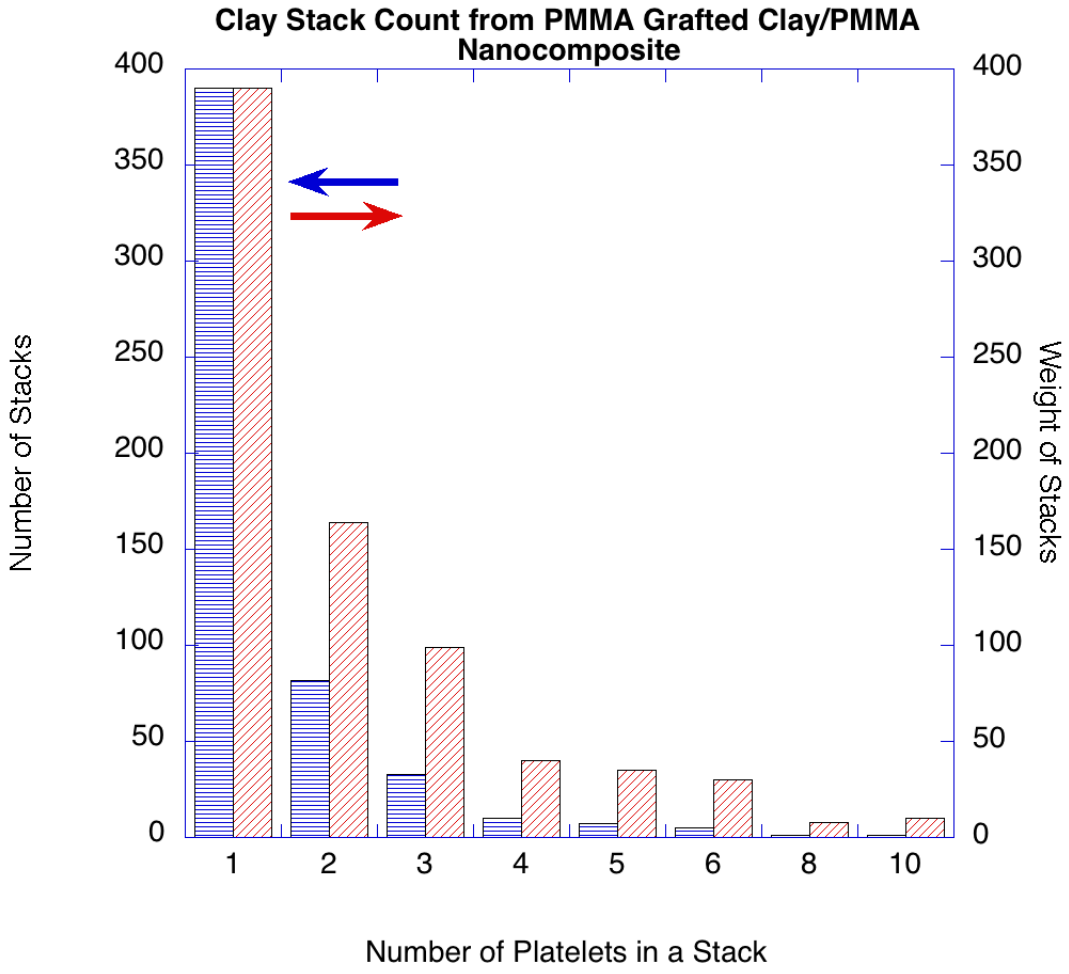

Figure 3.11: Clay Stack Count from the PMMA Grafted Clay/PMMA Nanocomposites

Cloisite 30B/PMMA (350k g/mol molecular weight) is shown in micrographs 3.15 and 3.16 at low and high magnification respectively. The PMMA grafted Cloisite 30B sample showed well distributed platelets in the PMMA matrix. A large number of single and double layers can be seen in the image. A clay stack count is given in table 3.11

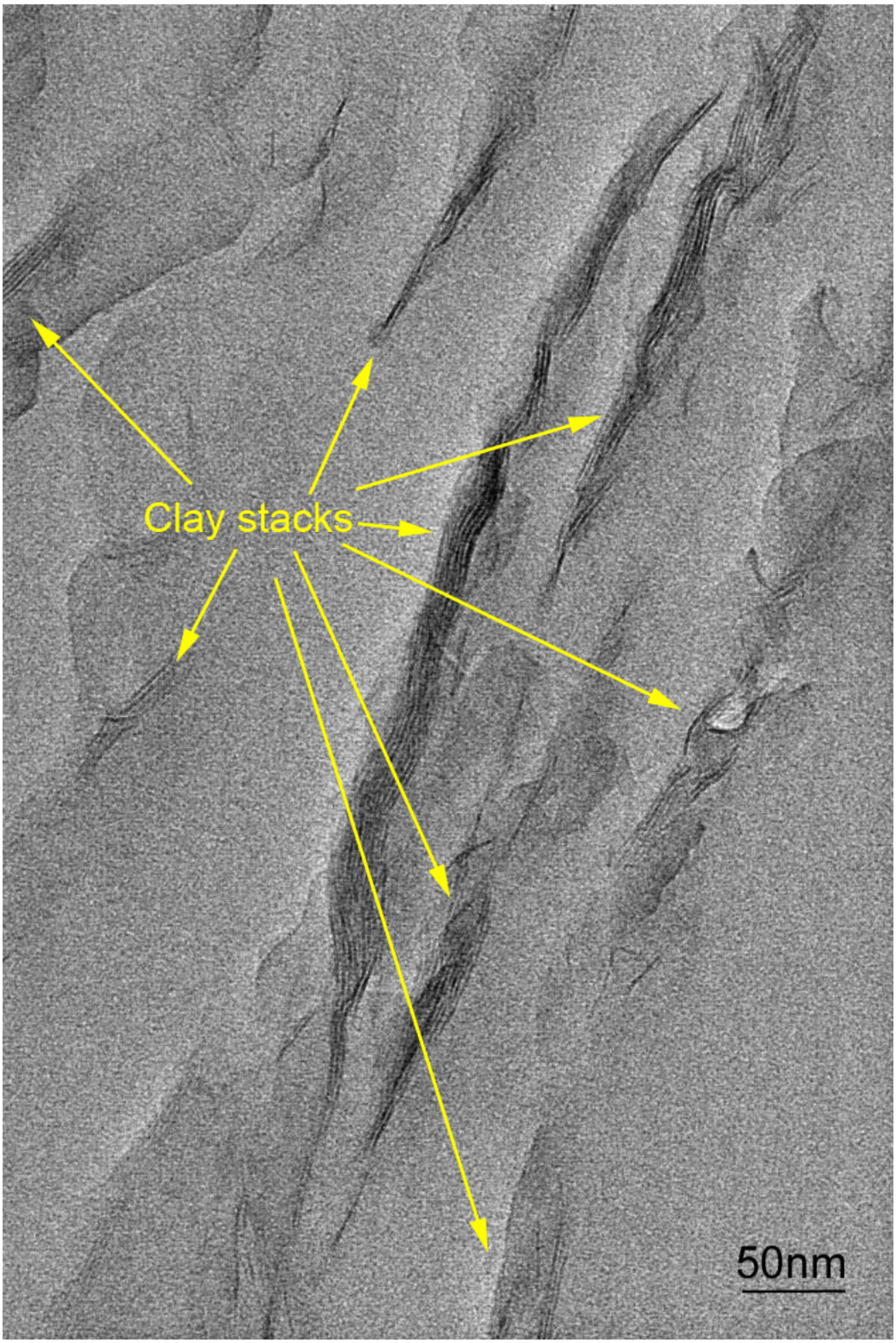

Figure 3.12: Intercalated Structure Produced with Cloisite 15A Clay

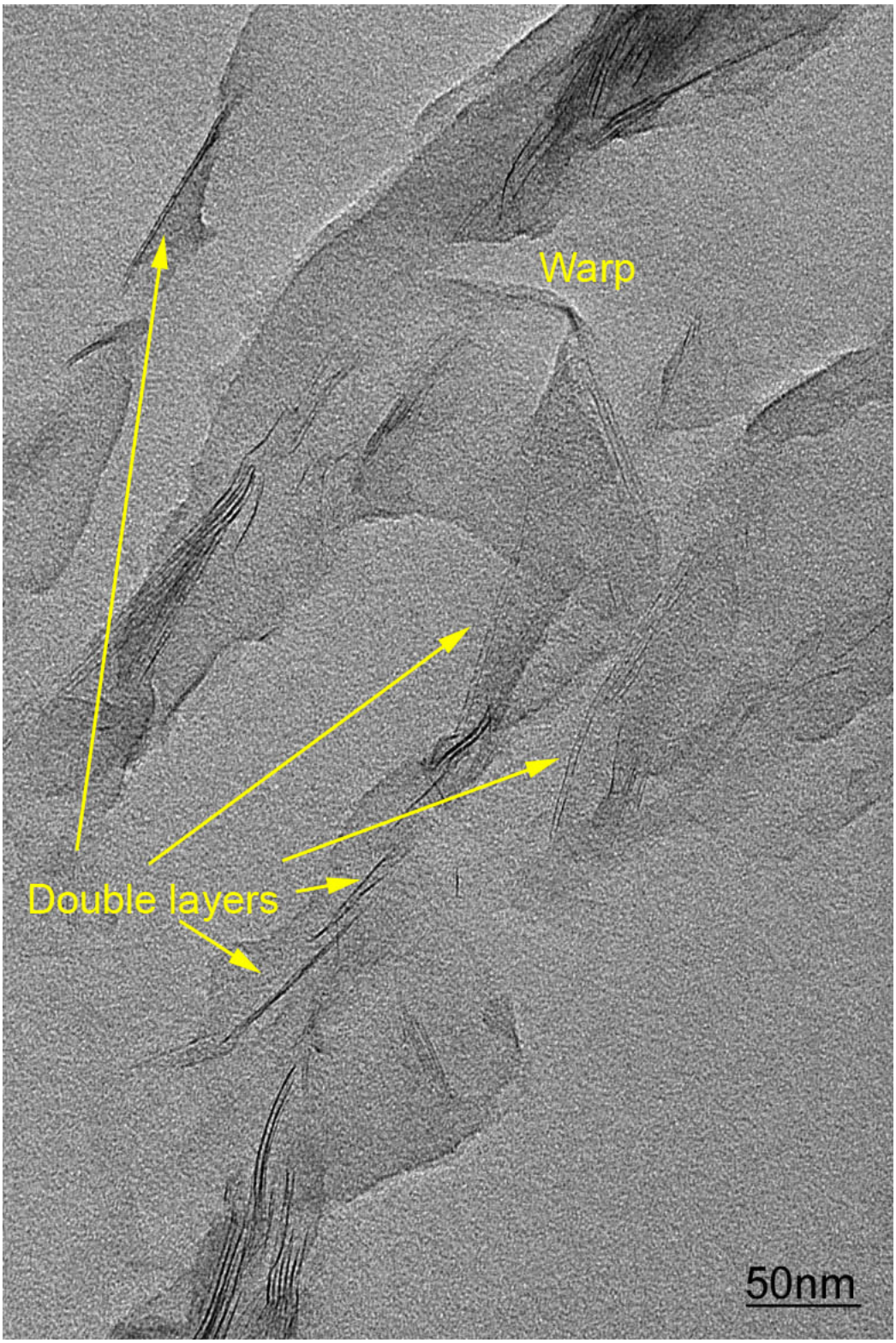

Figure 3.13: Exfoliated Structure Produced with Cloisite 30B Clay

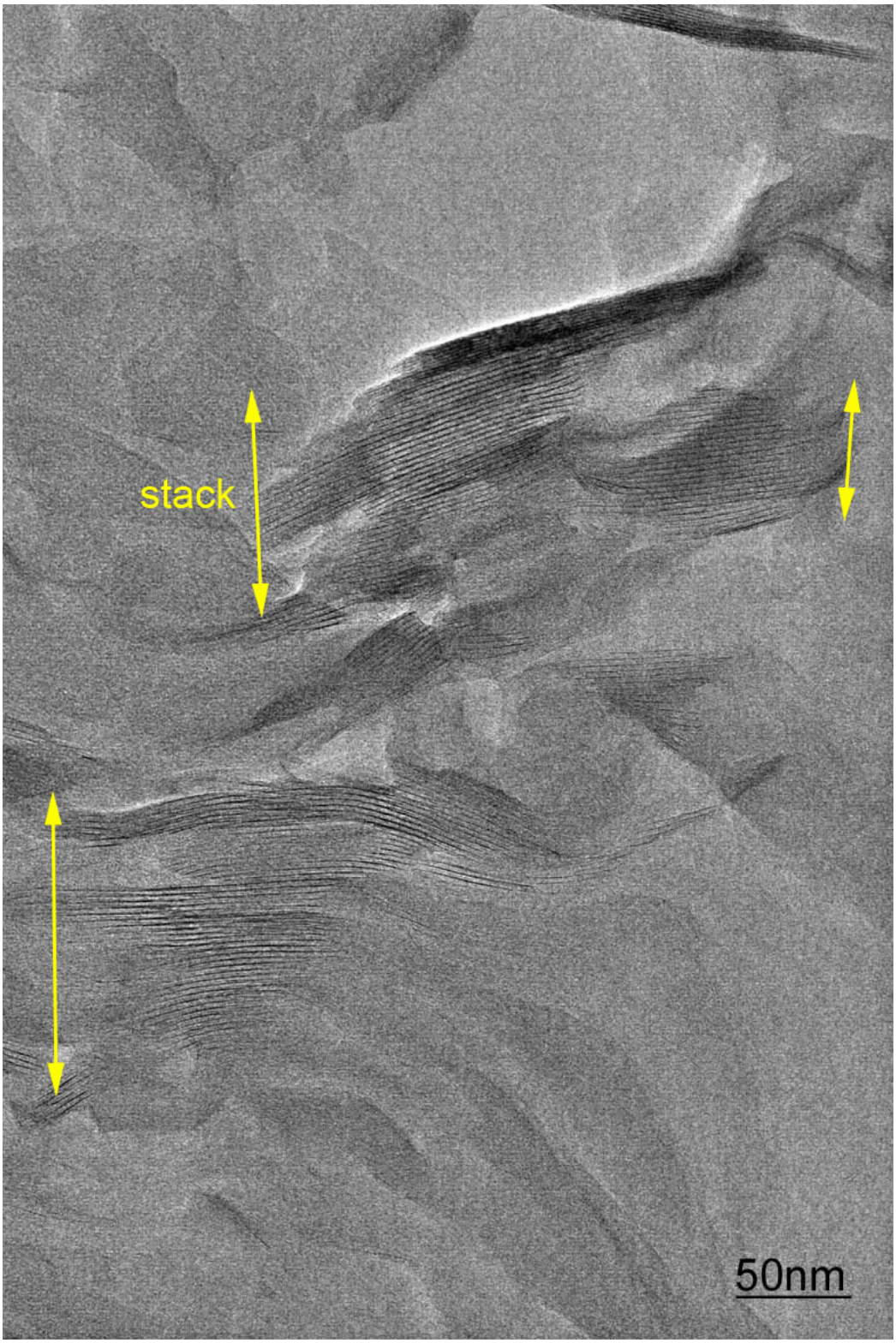

Figure 3.14: Intercalated Structure Produced with MAE120 Clay

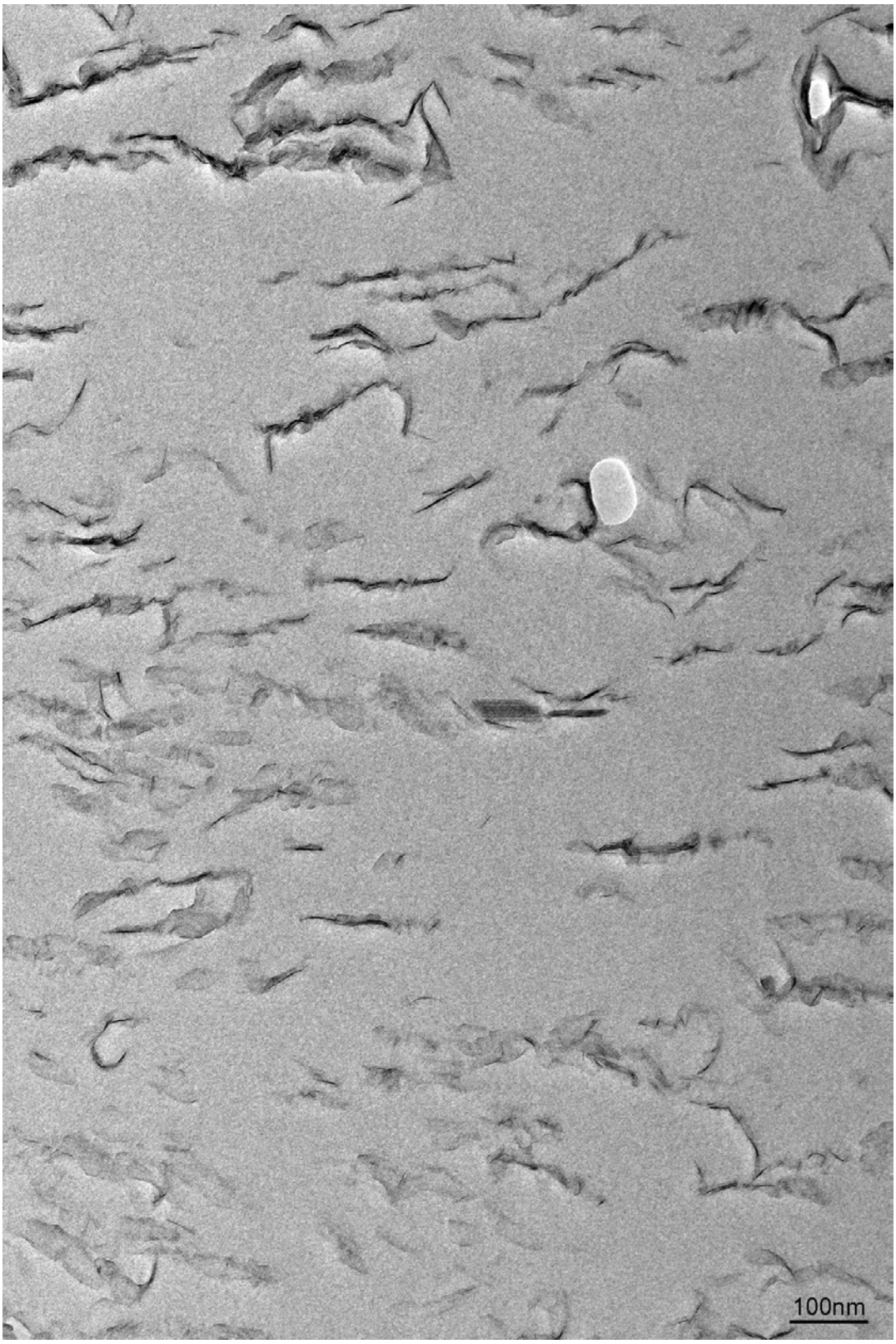

Figure 3.15: Exfoliated Structure from Nanocomposite with PMMA Grafted Clay

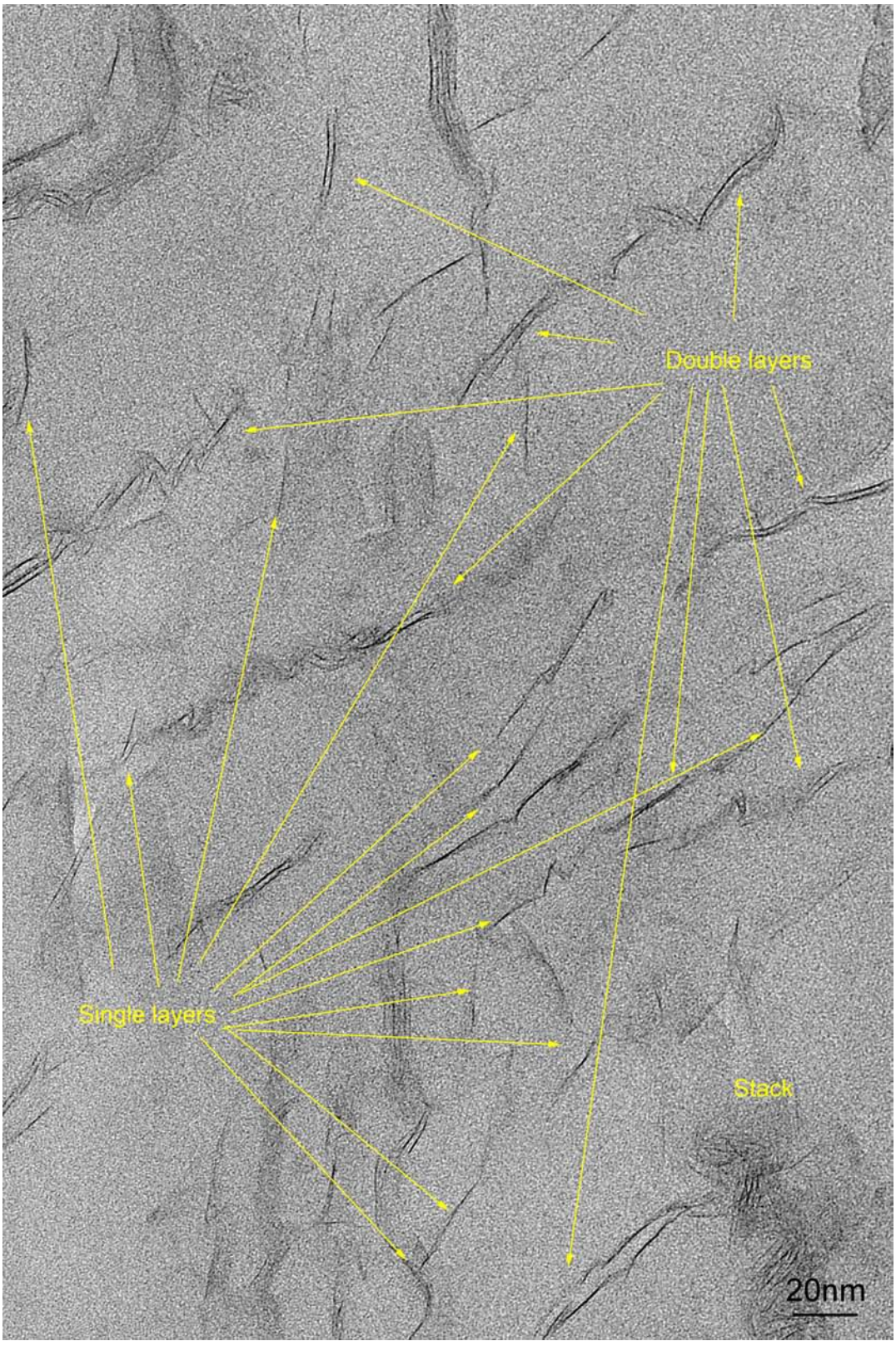

Figure 3.16: Exfoliated Structure from Nanocomposite with PMMA Grafted Clay

3.3.2 X-ray Diffraction

3.3.2.1 X-ray Diffraction from Nanocomposites

The XRD data from solution mixing 5 wt% Cloisite 15A, Cloisite 30B and MAE120 nanocomposites are shown in figure 3.17. The PMMA/MAE120 sample showed peaks at 3.60 nm, and 1.92 nm. These peaks can be indexed as (001), and (002) from the stacks of clay platelets. The primary gallery spacing of PMMA/MAE120 sample is approximately 3.6 nm. The Cloisite 15A and Cloisite 30B samples showed broad peaks at 3.43 nm, and 1.77 nm, which correspond to (001), and (002). PMMA grafted sample showed a shoulder at 3.43 nm. Cloisite 15A, Cloisite 30B and PMMA grafted samples had broader and weaker diffraction peaks than MAE120 (with the PMMA grafted sample being being broadest). The XRD patterns indicate that there are significant stacks of platelets present in the samples, and the increase in the gallery spacing indicates that the nanocomposite has an intercalated structure. The degree of order of the layered structure is MAE120, Cloisite 15A, Cloisite 30B and short PMMA chain grafted samples from high to low.

Comparing the XRD data from the pure clay to that from the nanocomposites, it can be concluded that some intercalation has occurred in all samples.

An analysis of crystal size in the direction of X-ray beam was conducted based on Scherrer equation

$$t = 0.89\lambda / B\cos\theta \tag{3.1}$$

Where t is the thickness of crystal, λ is the wave length of X-ray, B is the half-peak

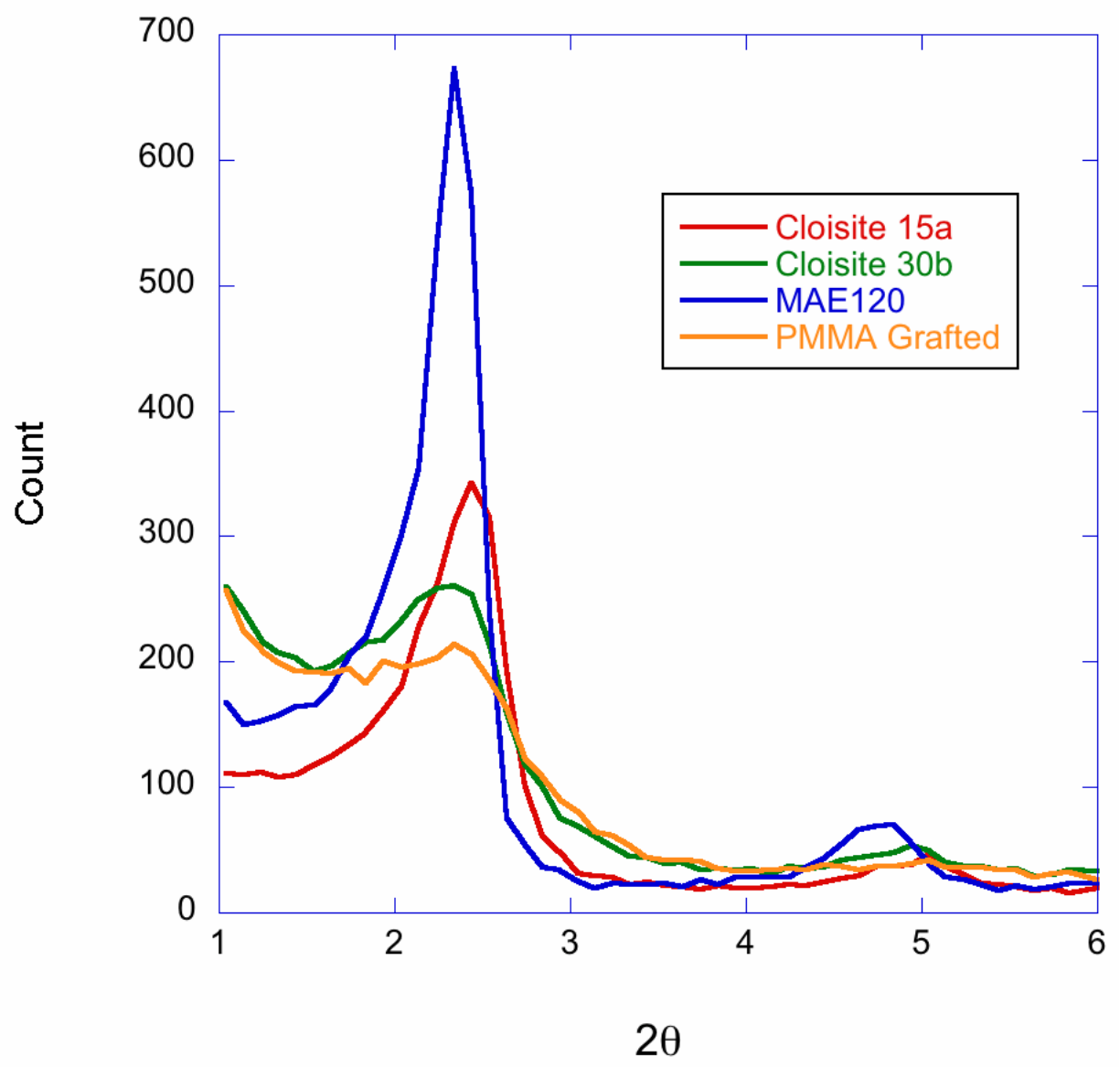

Figure 3.17: XRD Data from Precipitated Nanocomposites

Table 3.1: Silicate Stack Thickness Based on Scherrer Equation

Sample	2θ (°)	B	Thickness (nm)	# of layers
MAE120	2.4	0.1134	70.1	More than 20
Cloisite 15A	2.6	0.2456	32.4	10
Cloisite 30B	5	0.75	10.6	3

width and θ is the center of the peak.

The result of analysis is listed in table 3.1. It should be noted that the peak in the XRD data of PMMA grafted sample is too small and half peak width is hard to measure. So no analysis was done on PMMA grafted sample.

3.3.3 Small Angle X-ray Scattering

SAXS data for the nanocomposites are shown in figure 3.18 as a log-log plot. Over the q range from 0.02 to 0.05, the PMMA grafted nanocomposite sample showed a slope of -2.25, the Cloisite 30B nanocomposite sample showed a slope of -2.42, the Cloisite 15A sample showed a slope of -2.73 and the MAE120 nanocomposite showed a slope of -3.21.

The slope of scattering data of the PMMA grafted sample is similar to the slope of exfoliated clay in water [123, 124, 125], where 2 dimensional disk shaped single sheets are expected. The slope of the SAXS data from the MAE120 nanocomposite is consistent with a 3 dimensional object. The slope of the SAXS data from the Cloisite 30B nanocomposite was consistent with a 2 dimensional structure and the

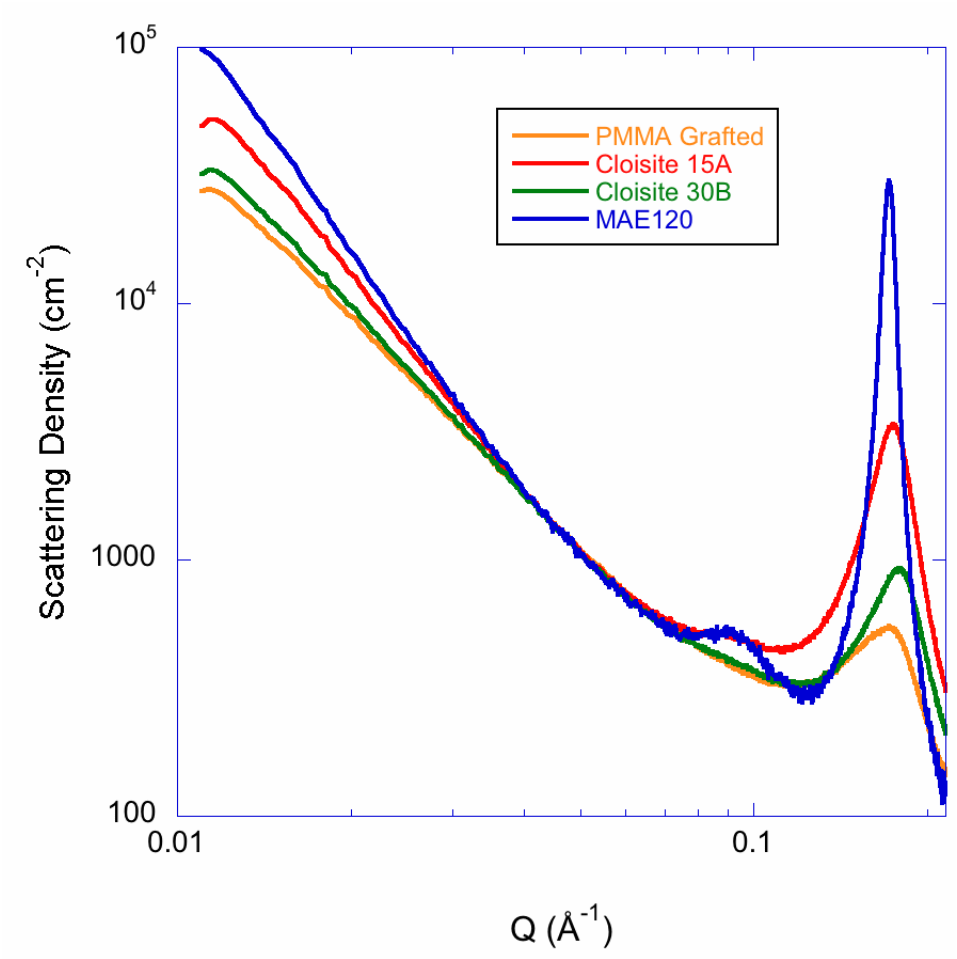

Figure 3.18: Small Angle X-ray Scattering from Nanocomposites

Cloisite 15A nanocomposite showed a structure closer to a 3 dimensional object.

Using the average stack method (equation 2.3), the average number of platelets in a stack is calculated as 1.1, 1.5, 3 and 6 for the PMMA grafted, Cloisite 30B, Cloisite 15A, Somasif MAE120 nanocomposite samples respectively. It should be noted that the model did not fit the 15A or Somasif MAE120 samples well as those nanocomposites have a structure that is not captured by the model. The fits using the average stack method is shown in figure 3.19 (the PMMA grafted sample) and figure 3.20 (the Cloisite 30B sample).

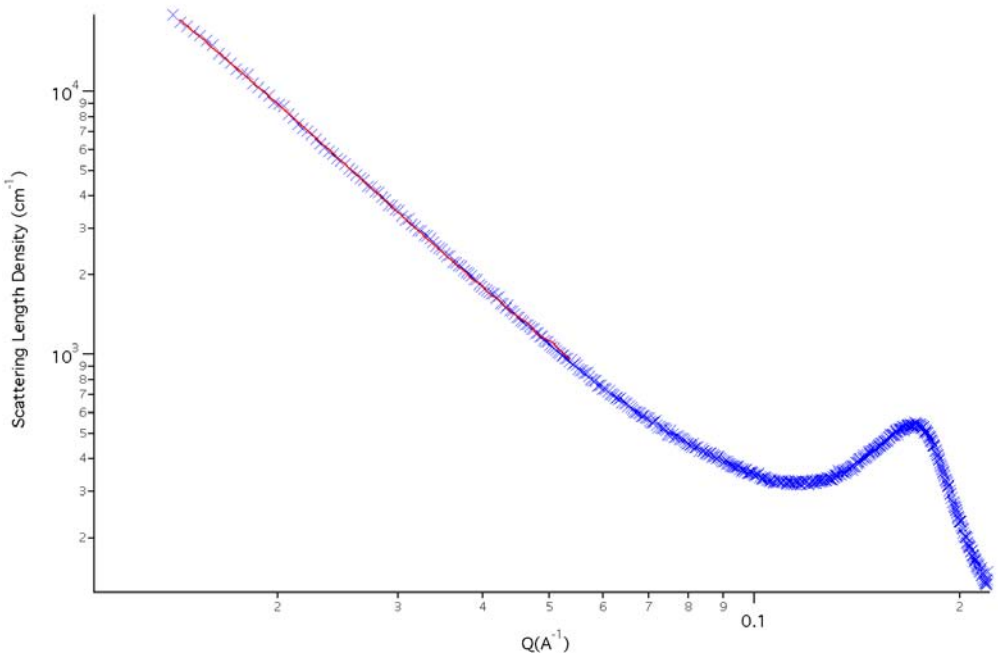

Figure 3.19: Fitting of PMMA Grafted Sample with Average Stack Model

Fits based on the multiple stack summation model (equation 2.4) are shown in figure 3.21 (PMMA grafted sample), 3.22 (Cloisite 30B sample) and 3.23 (Cloisite 15A). The multiple stack summation model can fit the nanocomposites which have a high degree of exfoliation, such as the PMMA grafted samples and the Cloisite 30B samples. For the nanocomposites with a mostly intercalated structure such as the Cloisite 15A, the model can show the trends but the fits are not very good. The multiple stack summation model fails to fit the MAE120 sample as the model can not capture the microcomposite structure.

Based on the multiple stack summation model, the PMMA grafted sample had about half of the clay platelets as single layers and the average stack thickness was 2.2 layers. The Cloisite 30B sample showed 40% of clay platelets in single layers and the average stack thickness is close to 2.6 layers. The Cloisite 15A had essentially

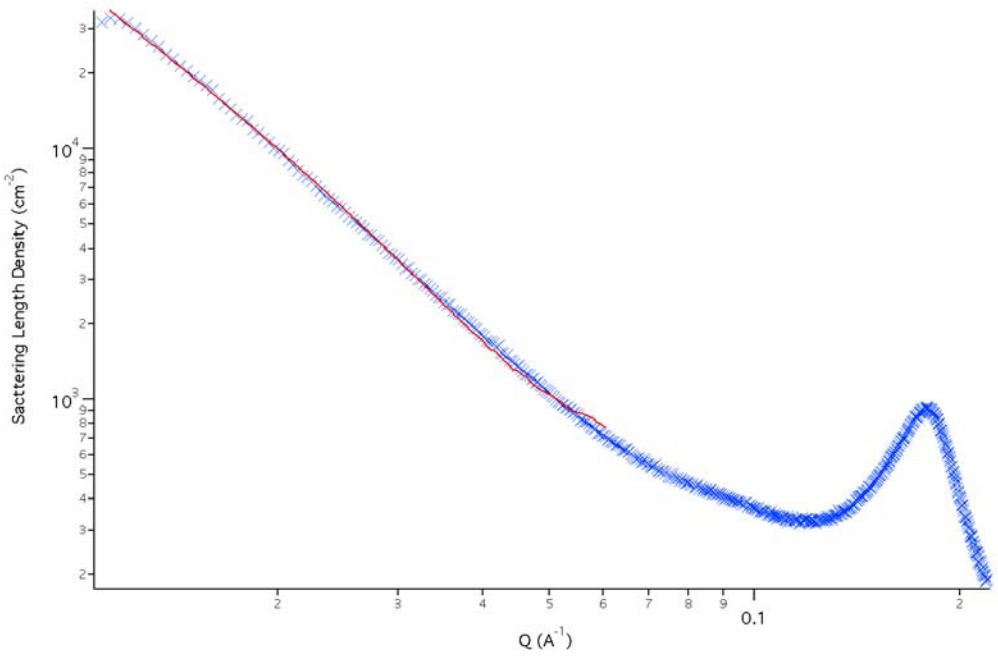

Figure 3.20: Fitting of Cloisite 30B Sample with Average Stack Model

no single layers and the MAE120 sample had multiple thick stacks.

3.4 Discussion on the Dispersion of Layered Silicate in Polymer

By comparing the XRD, TEM and SAXS measurements, it can be found that different techniques have their advantages and disadvantages. TEM observation provides a direct image where it is easy to observe the exfoliated structure, but due to possible compression during the sample preparation process (ultramicrotoming), the measurement of the layer distance in the intercalated structure may be less accurate than XRD. The XRD gives an accurate distance between the clay layers and clay stack thickness, but the amount of isolated clay platelets can not be easily deduced from XRD. SAXS measurements can be used to study both the shape and

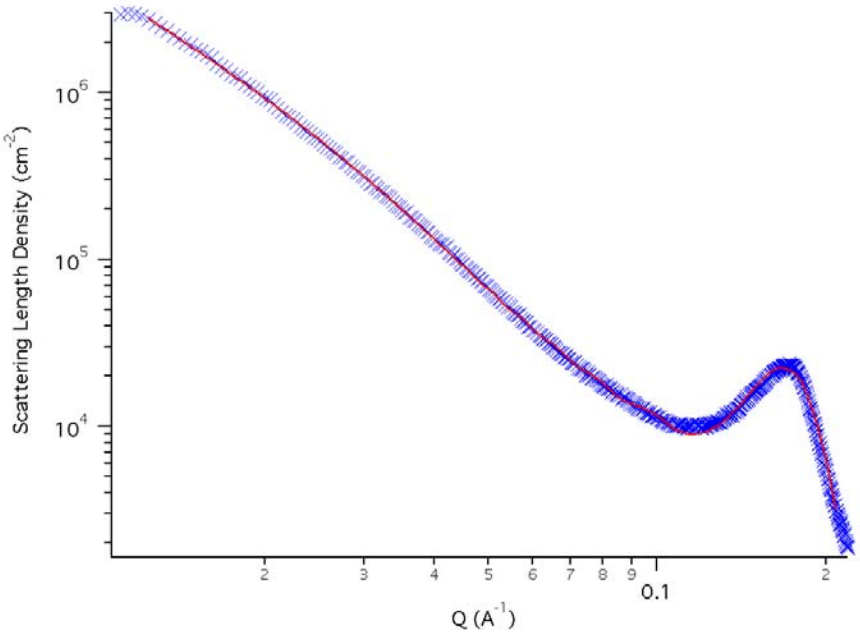

Figure 3.21: Fitting of PMMA Grafted Sample with Multiple Stack Summation Model

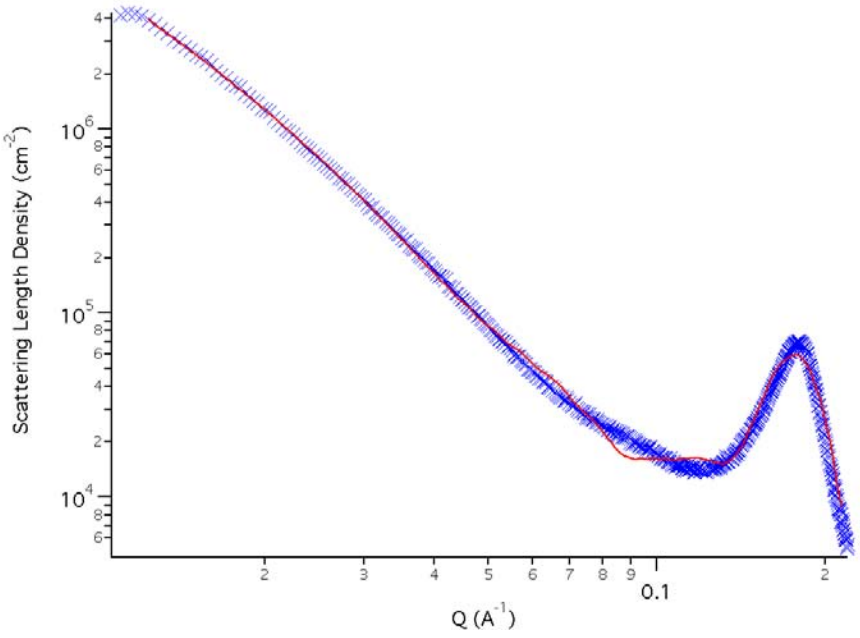

Figure 3.22: Fitting of Cloisite 30B Sample with Multiple Stack Summation Model

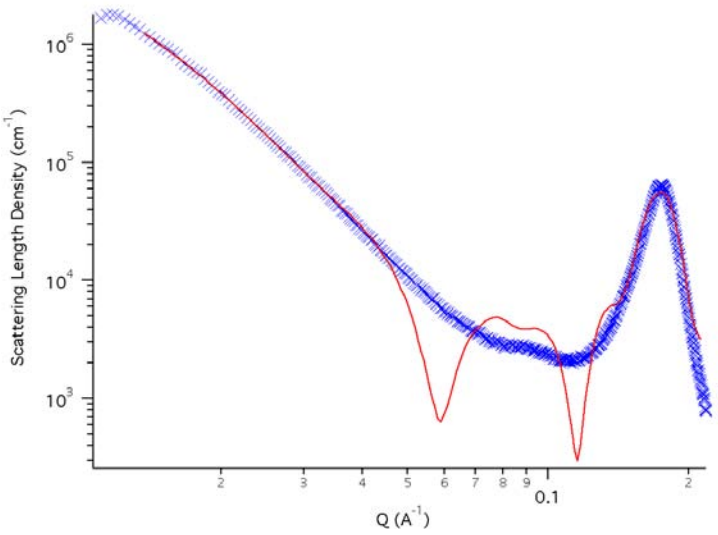

Figure 3.23: Fitting of Cloisite 15A Sample with Multiple Stack Summation Model

thickness of clay stacks. This can be used to deduce the degree of exfoliation of clay particles in the nanocomposite. In summary, SAXS probably has the largest advantage, however, SAXS is not widely used in industry.

In reference to flammability applications, the degree of clay particle dispersion in the polymer matrix should be measured at different length scales: the microscale and the nanoscale. The dispersion of clay particles at the microscale can be measured by optical microscopy and can be described by the average dimension ($D_{average}$) of the particle. This factor can be quantitated by the following equation

$$F_{micro} = 1 - \frac{D_{average}}{D_{allowed}} \tag{3.2}$$

In the experiments reported in this thesis, all samples with visible particles by optical microscopy have been rejected, which means

$$F_{micro} = 1 \tag{3.3}$$

The nanoscale dispersion can be expressed in similar manner, by using the clay stack thickness ($T_{average}$)

$$A_{nano} = 1 - \frac{T_{average} - 1}{T_{allowed}} \tag{3.4}$$

Nanocomposites with a stack thicker than 51 nm will give a A_{nano} less than 0. The fully exfoliated nanocomposite will give a A_{nano} of 1.

The over all dispersion can be expressed as

$$A_{total} = A_{nano} + A_{micro} - 1 \tag{3.5}$$

If the sample has A_{total} less than 0 then it will be rejected as not suitable for low flammability applications. In our experiments, the PMMA grafted, Cloisite 30B and Cloisite 15A samples gives numbers A_{total} 1 to 0.5 and Somasif MAE120 samples gives A_{total} less than 0.

3.5 Flammability Tests

3.5.1 Thermogravimetric Analysis of Nanocomposites Made by the Solution Mixing Method

3.5.1.1 Clay Samples

The TGA data acquired from the clays are shown in figure 3.24.

The Cloisite 30B, Cloisite 15A and MAE120 samples showed significantly different degradation behavior.

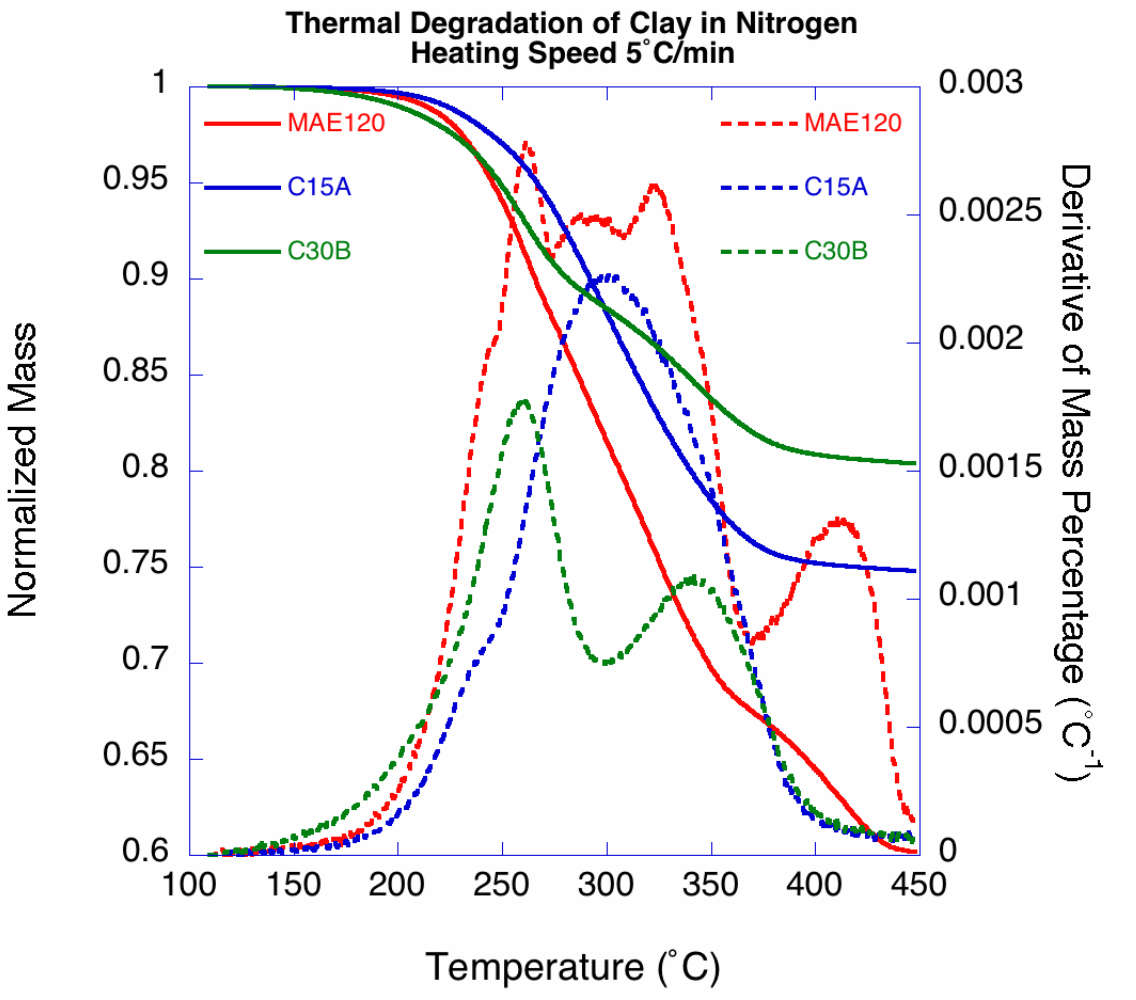

Figure 3.24: TGA Data from Various Clay Samples

Cloisite 30B lost about 20% of its mass at $450°C$. Cloisite 15A lost about 25% of its mass at $450°C$. The degradation of the clay contributes about 1 wt% mass loss for a nanocomposite with 5 wt% clay. MAE120 lost 40% of its mass at $450°C$. The clay degradation will contribute about 2 wt% of the mass loss for a nanocomposite with 5 wt% of MAE120 clay.

The thermal degradation process of Cloisite 30B organically modified clay shows two steps, the first step is at $257°C$, the second step is at $342°C$. The degradation of Cloisite 15A can be separated into 3 peaks, the first one is at $228°C$, the second one is at $290°C$ and the third one is at $341°C$. MAE120 shows 4 steps in the degradation process. The first MAE120 degradation step is at $253°C$, the second step is at $298°C$, the third step is at $334°C$ and the fourth step is at $410°C$.

3.5.1.2 Nanocomposite Samples

Thermal degradation of PMMA has been well studied [126, 127, 128, 129, 130, 131, 132, 133]. The degradation of PMMA has three steps. The first step is at 150 °C to 200°C. The degradation at this step is due to head-to-head defects in the polymer backbone. A second step is at 250°C to 320°C. This step is attributed to unsaturated bonds. The third step is at 300°C to 400°C. This step is the main PMMA chain undergoing random scission.

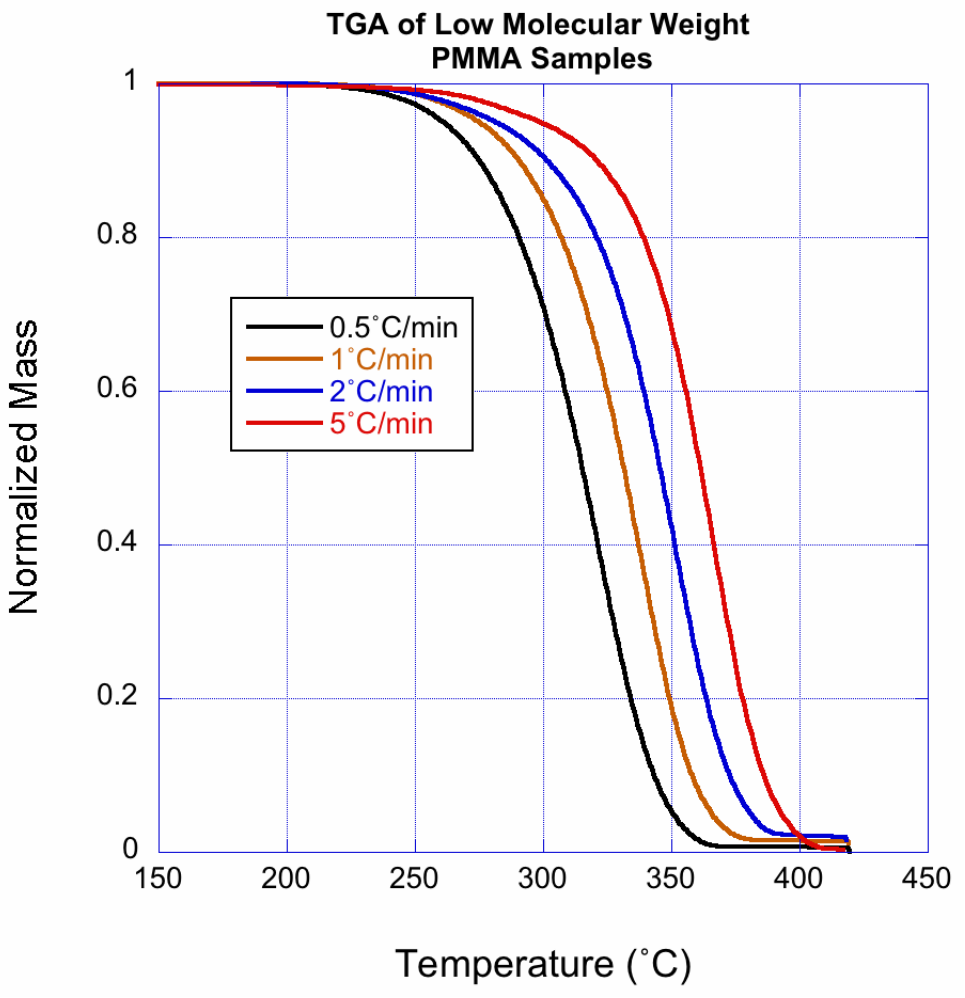

Figure 3.25: TGA Data from Pure PMMA Samples

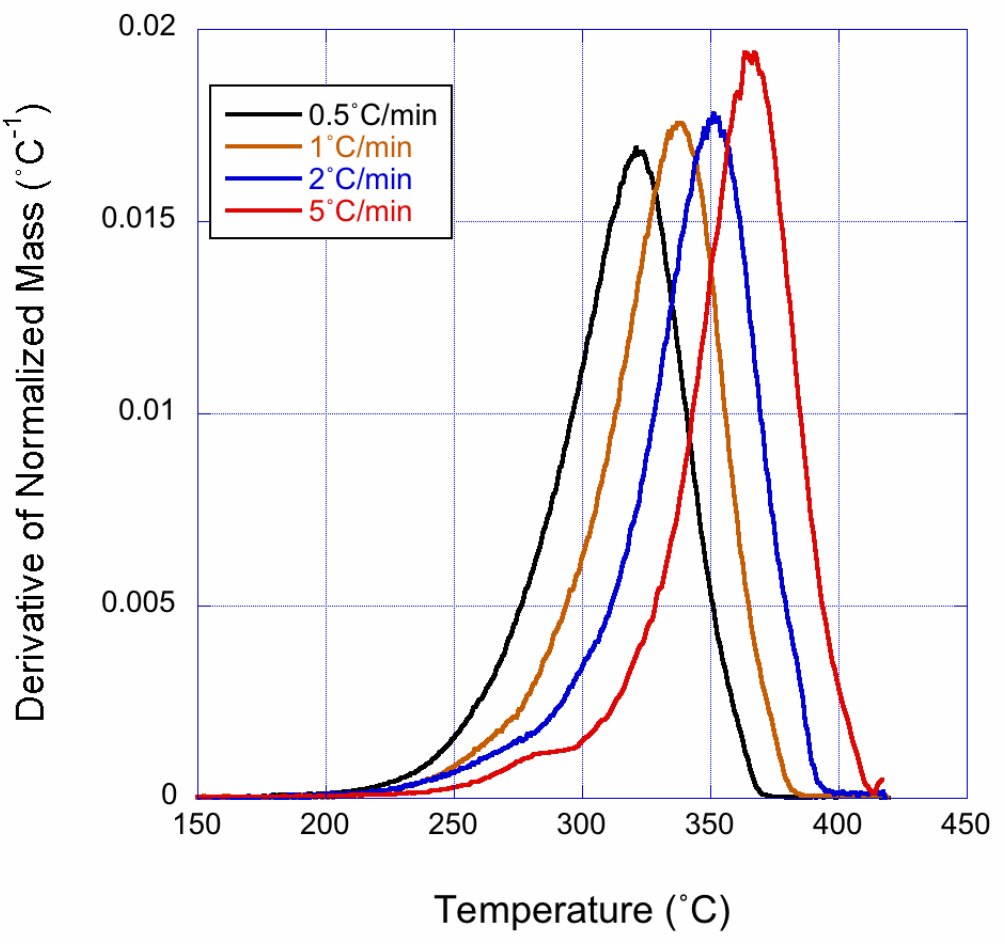

Figure 3.26: Derivative of TGA Data from Pure PMMA Samples

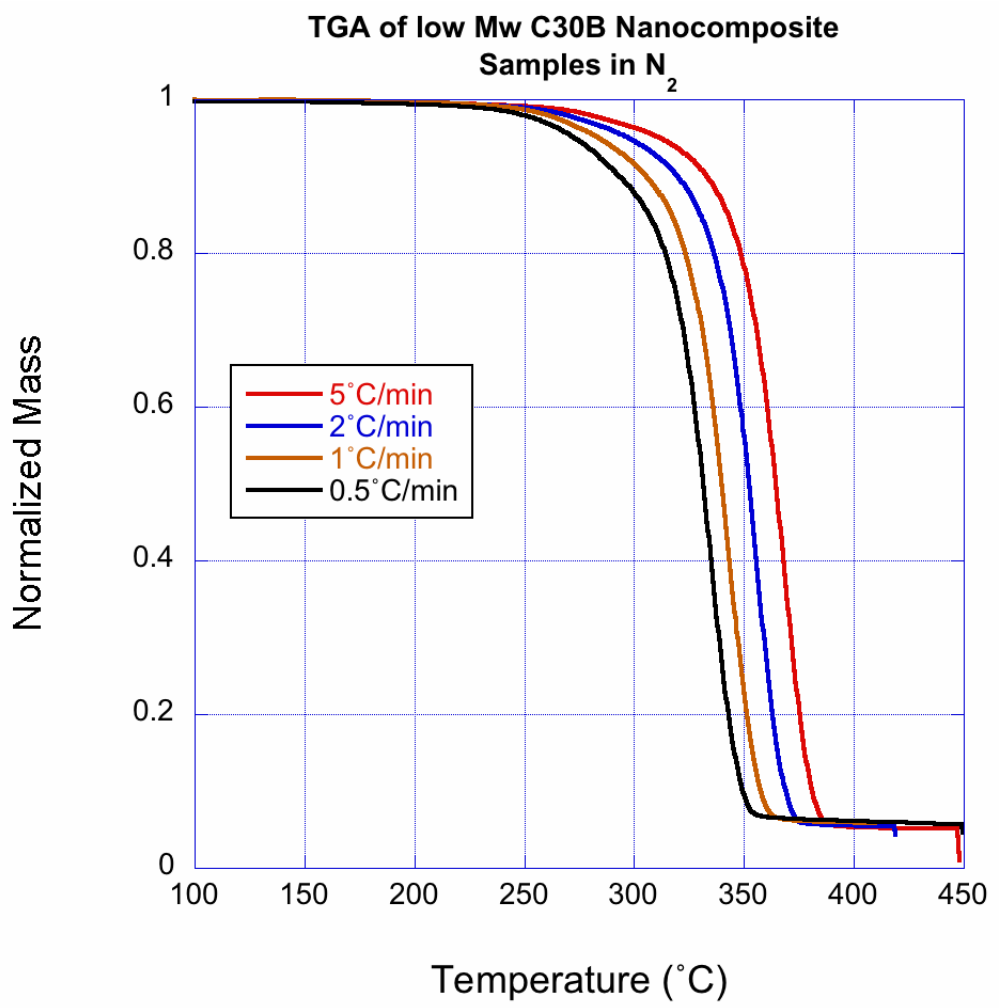

Figure 3.27: TGA Data from Cloisite 30B/PMMA Low Molecular Weight Nanocomposite Samples

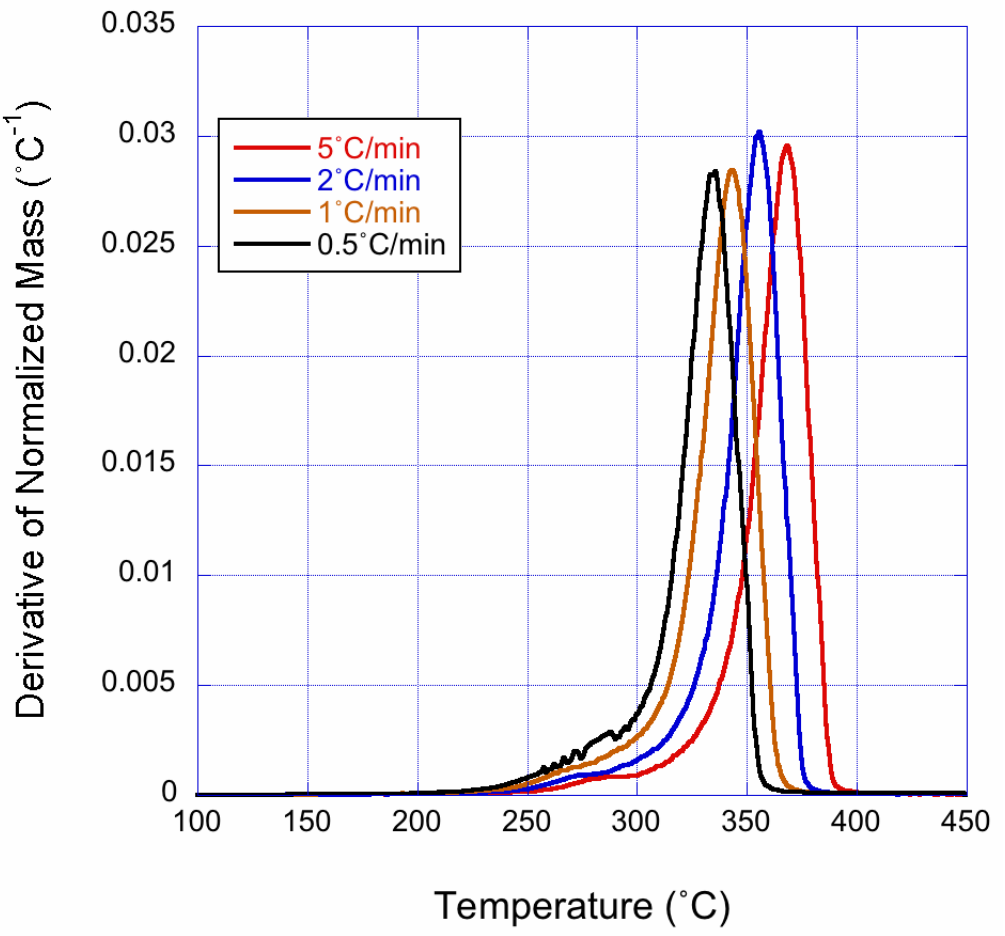

Figure 3.28: TGA Data from Cloisite 30B/PMMA Low Molecular Weight Nanocomposite Samples

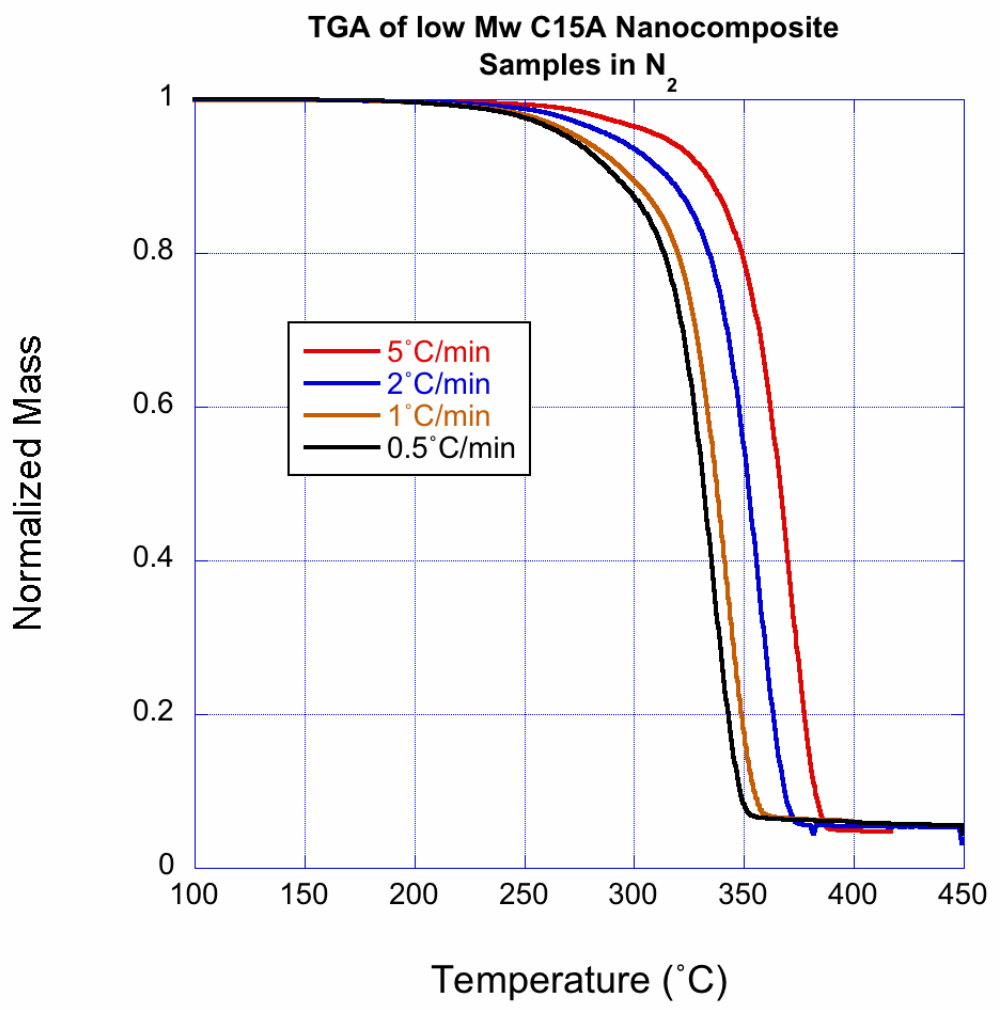

Figure 3.29: TGA Data from Cloisite 15A/PMMA Low Molecular Weight Nanocomposite Samples

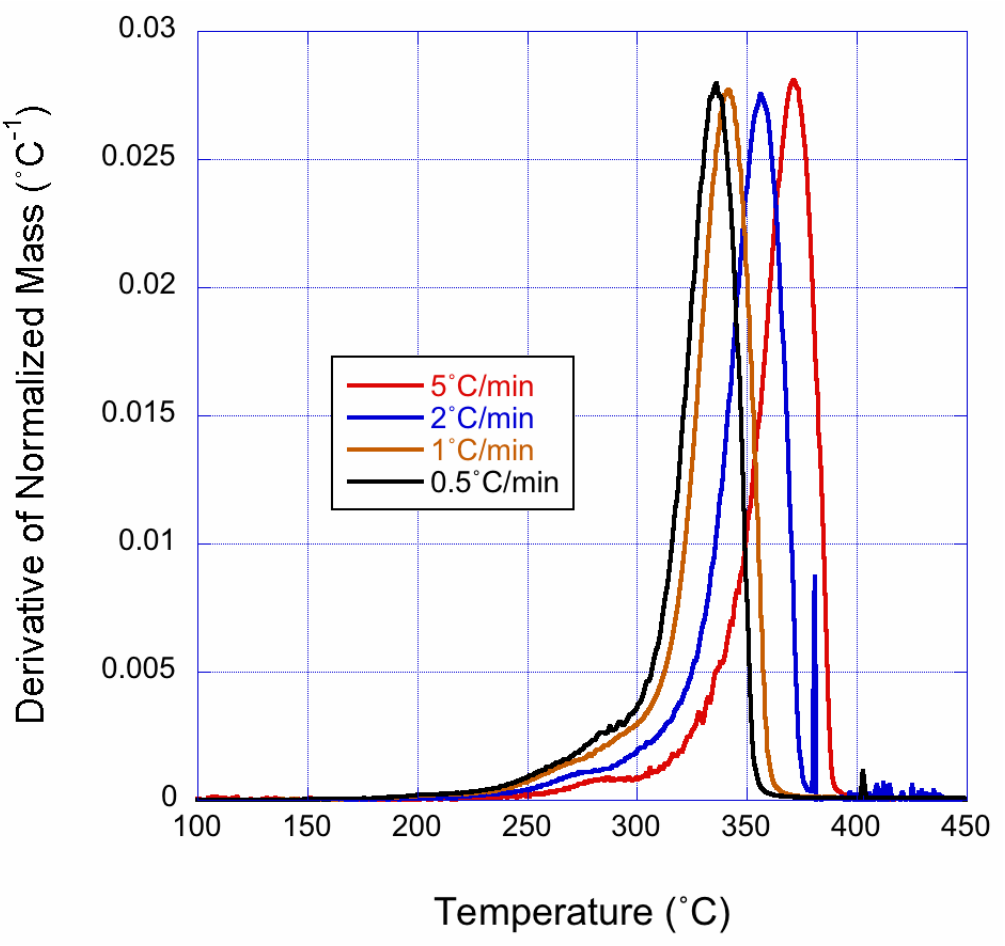

Figure 3.30: TGA Data from Cloisite 15A/PMMA Low Molecular Weight Nanocomposite Samples

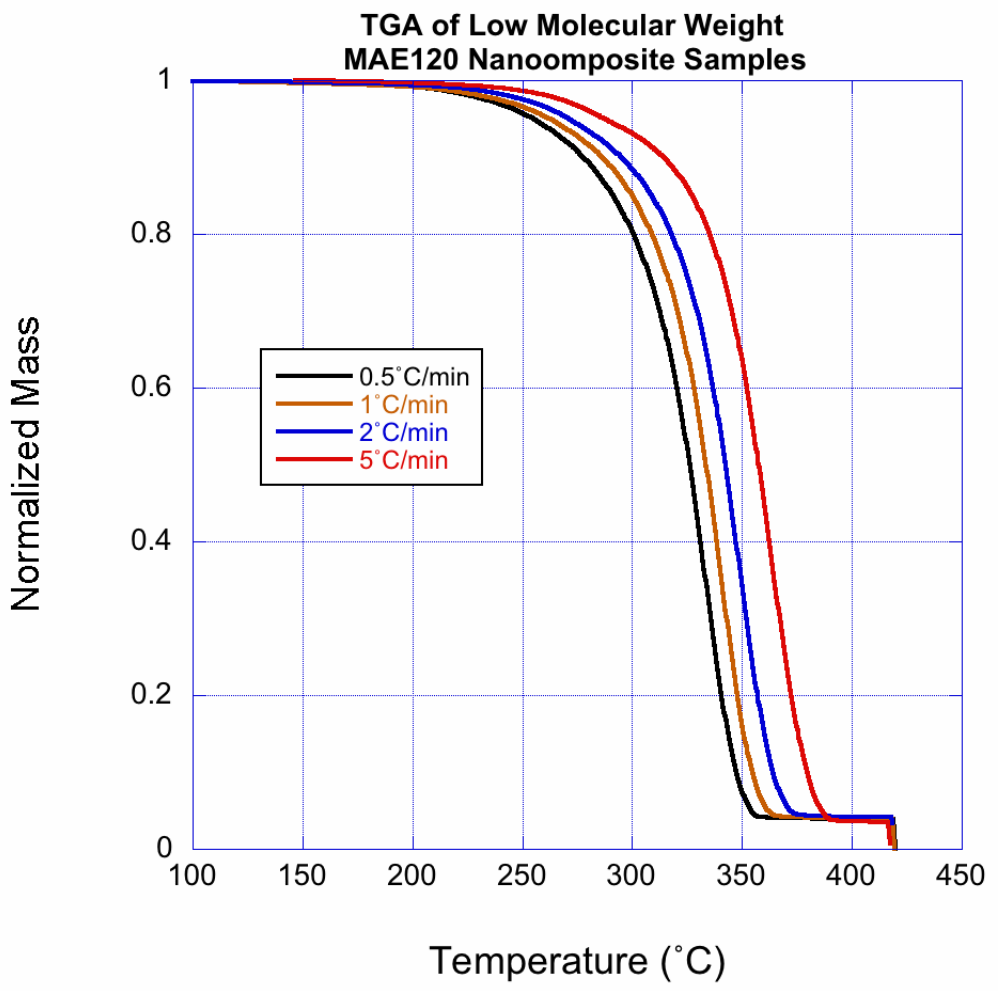

Figure 3.31: TGA Data from MAE120/PMMA Low Molecular Weight Nanocomposite Samples

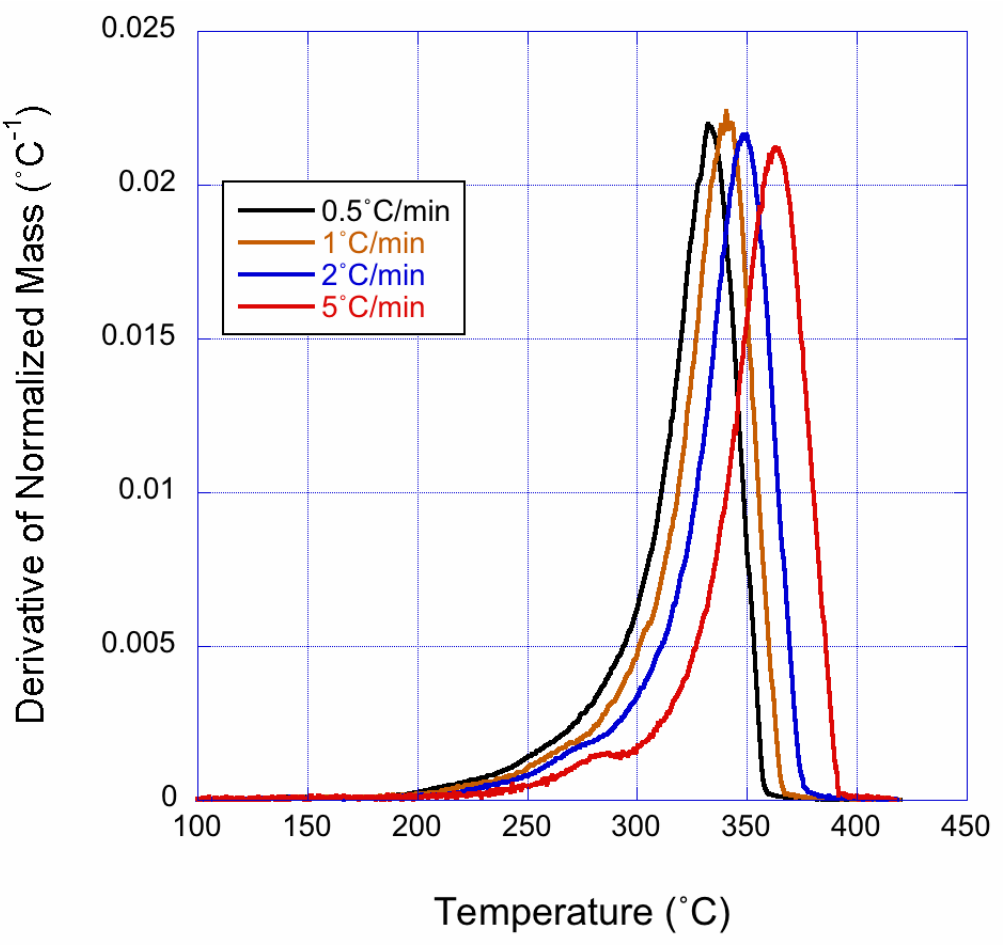

Figure 3.32: TGA Data from MAE120/PMMA Low Molecular Weight Nanocomposite Samples

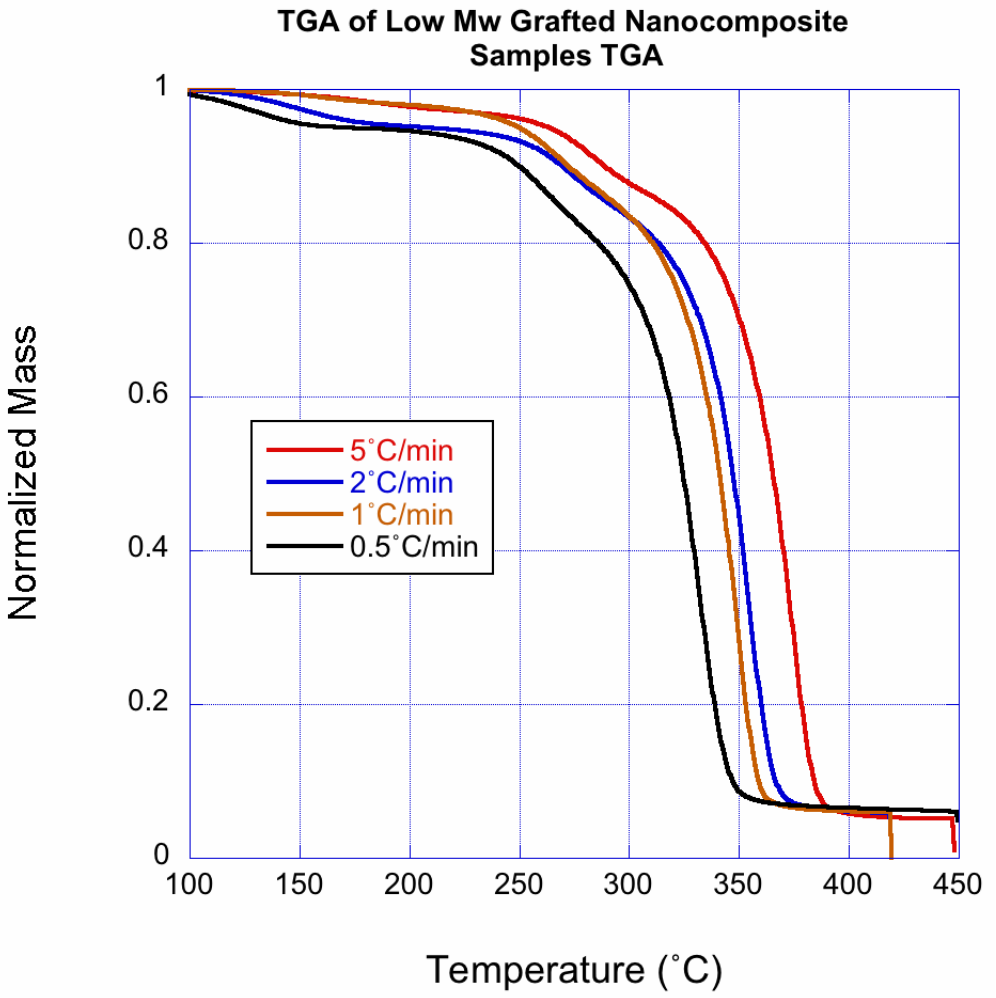

Figure 3.33: TGA Data from Grafted Clay/PMMA Low Molecular Weight Nanocomposite Samples

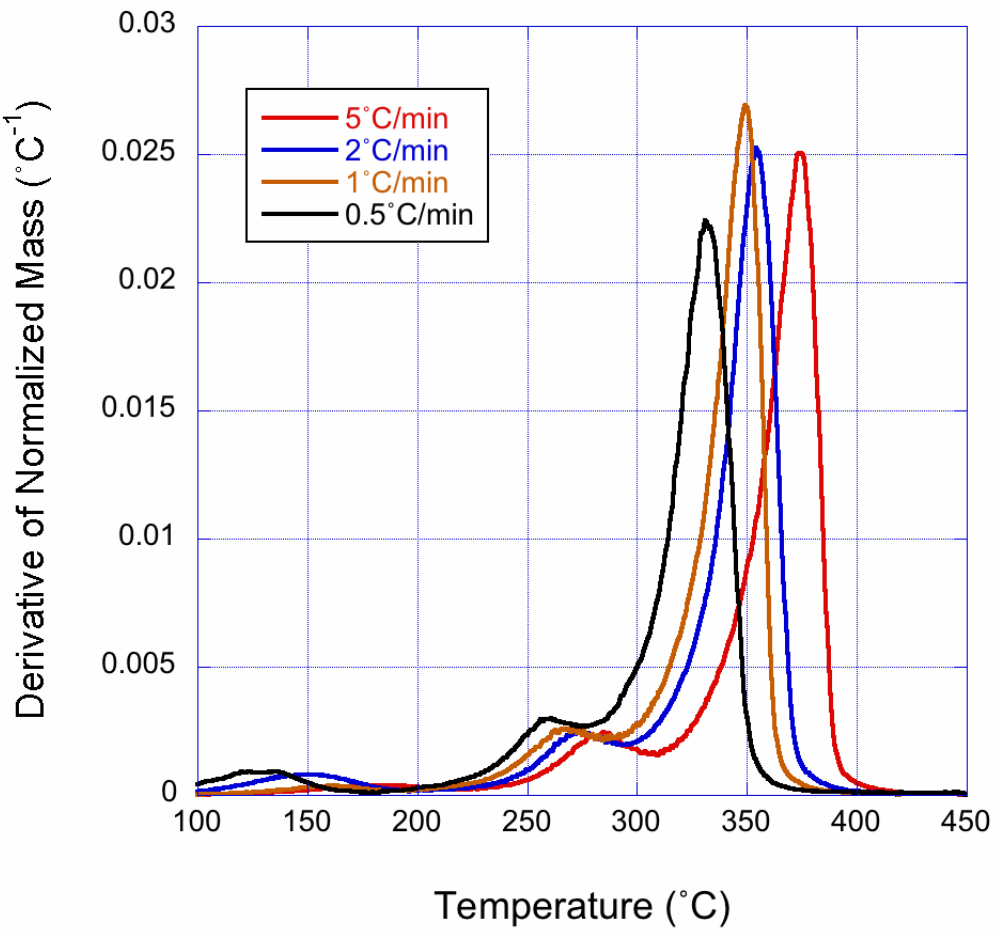

Figure 3.34: TGA Data from Grafted Clay/PMMA Low Molecular Weight Nanocomposite Samples

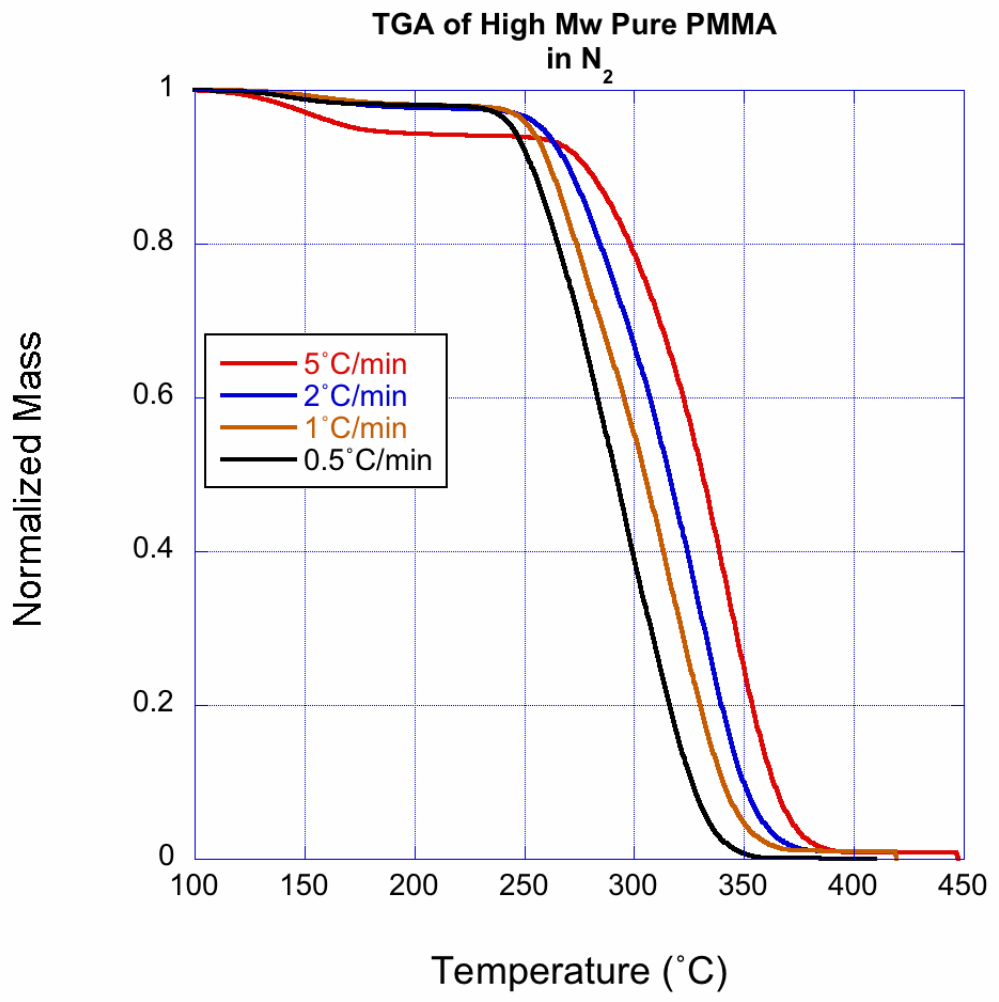

Figure 3.35: TGA Data from Pure PMMA High Molecular Weight Samples

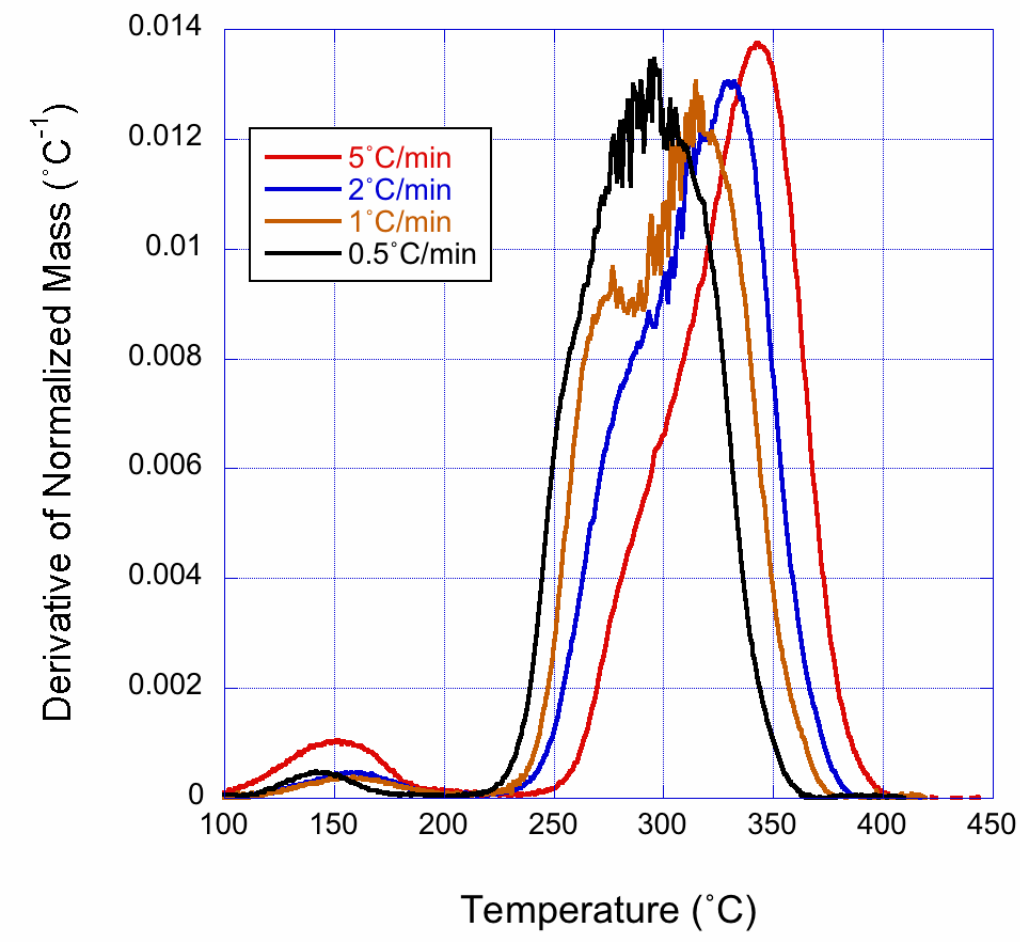

Figure 3.36: TGA Data from Pure PMMA High Molecular Weight Samples

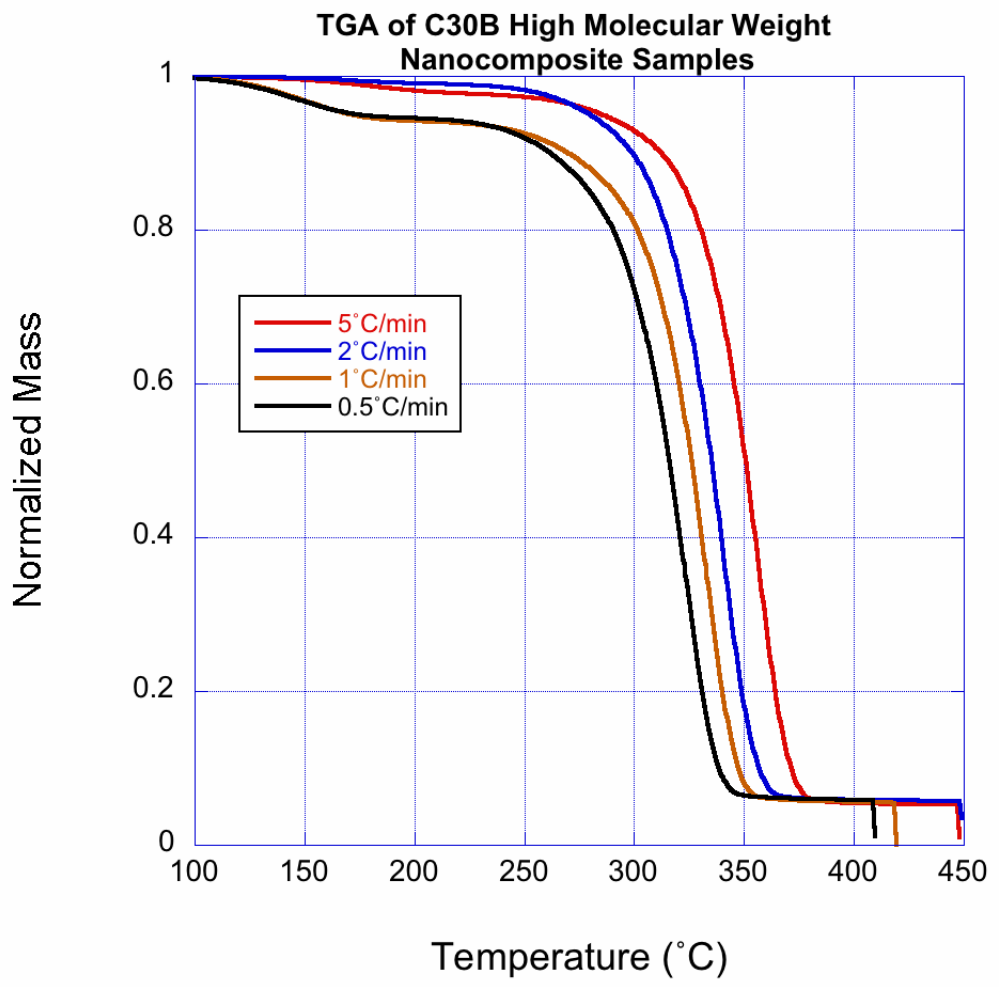

Figure 3.37: TGA Data from Cloisite 30B/PMMA High Molecular Weight Nanocomposite Samples

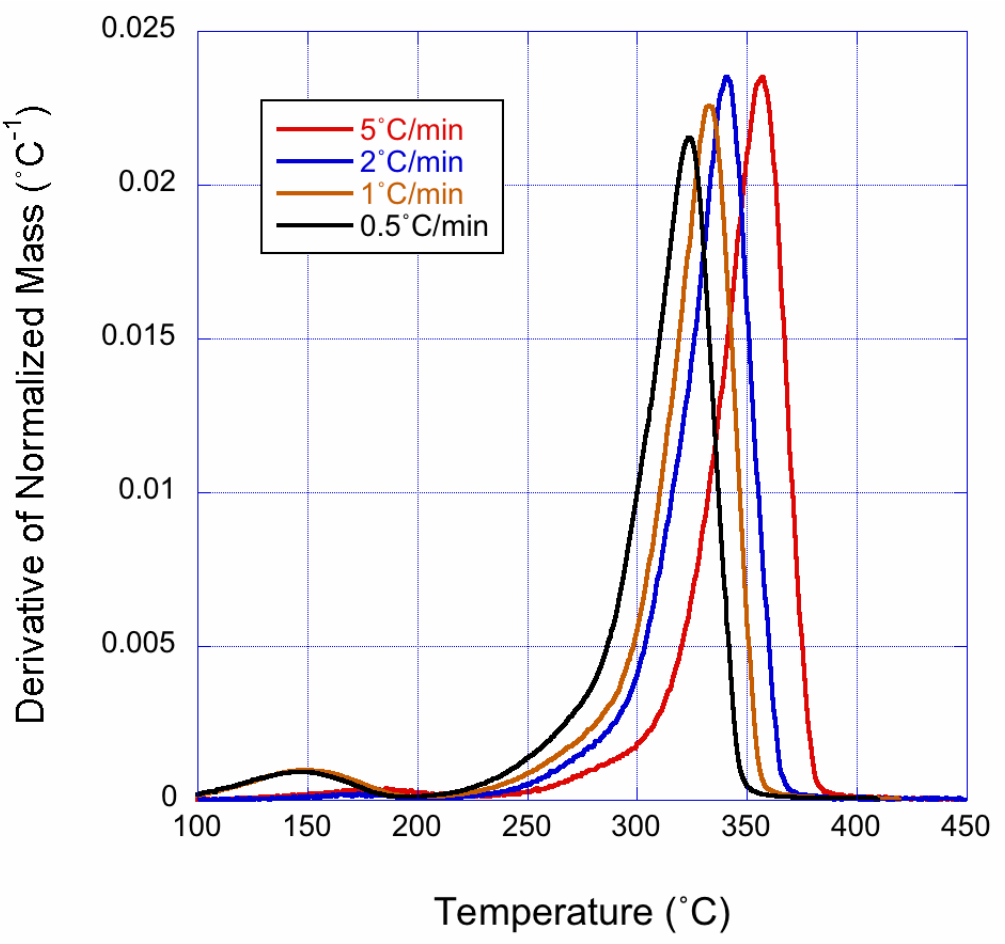

Figure 3.38: TGA Data from Cloisite 30B/PMMA High Molecular Weight Nanocomposite Samples

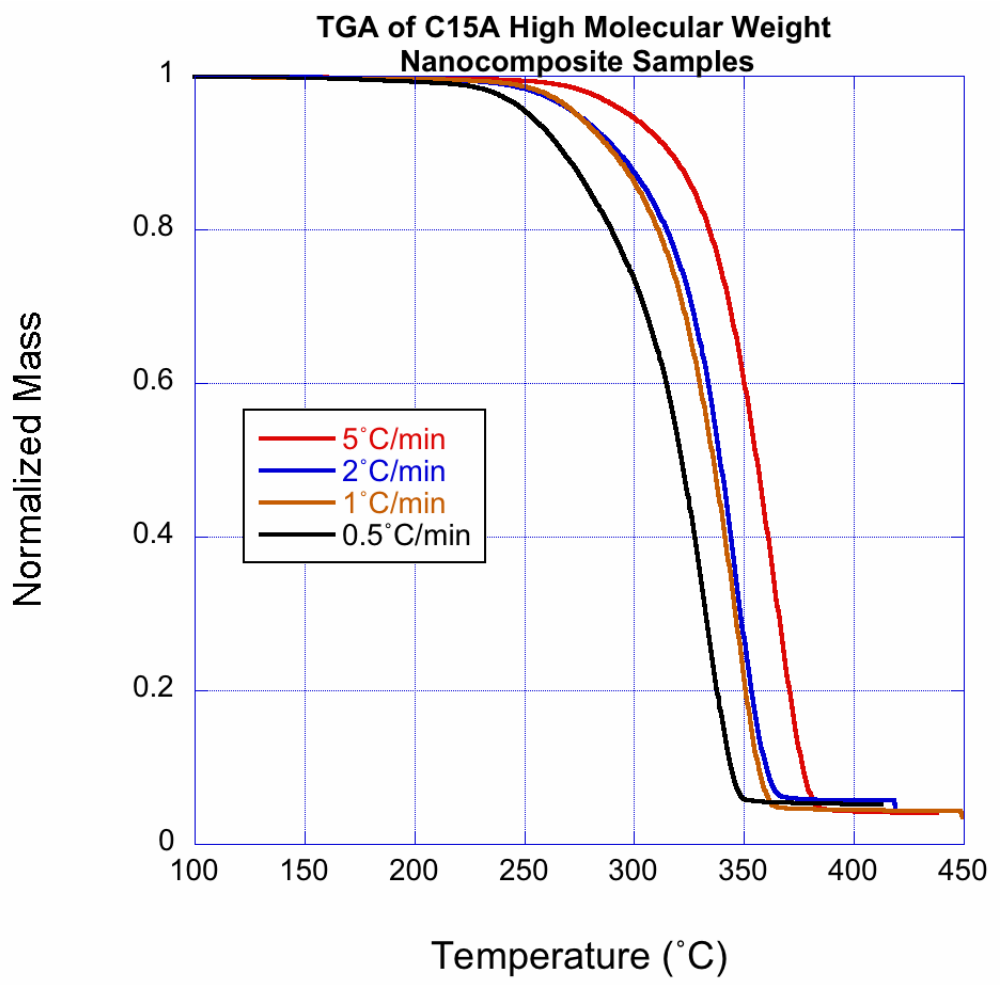

Figure 3.39: TGA Data from Cloisite 15A/PMMA High Molecular Weight Nanocomposite Samples

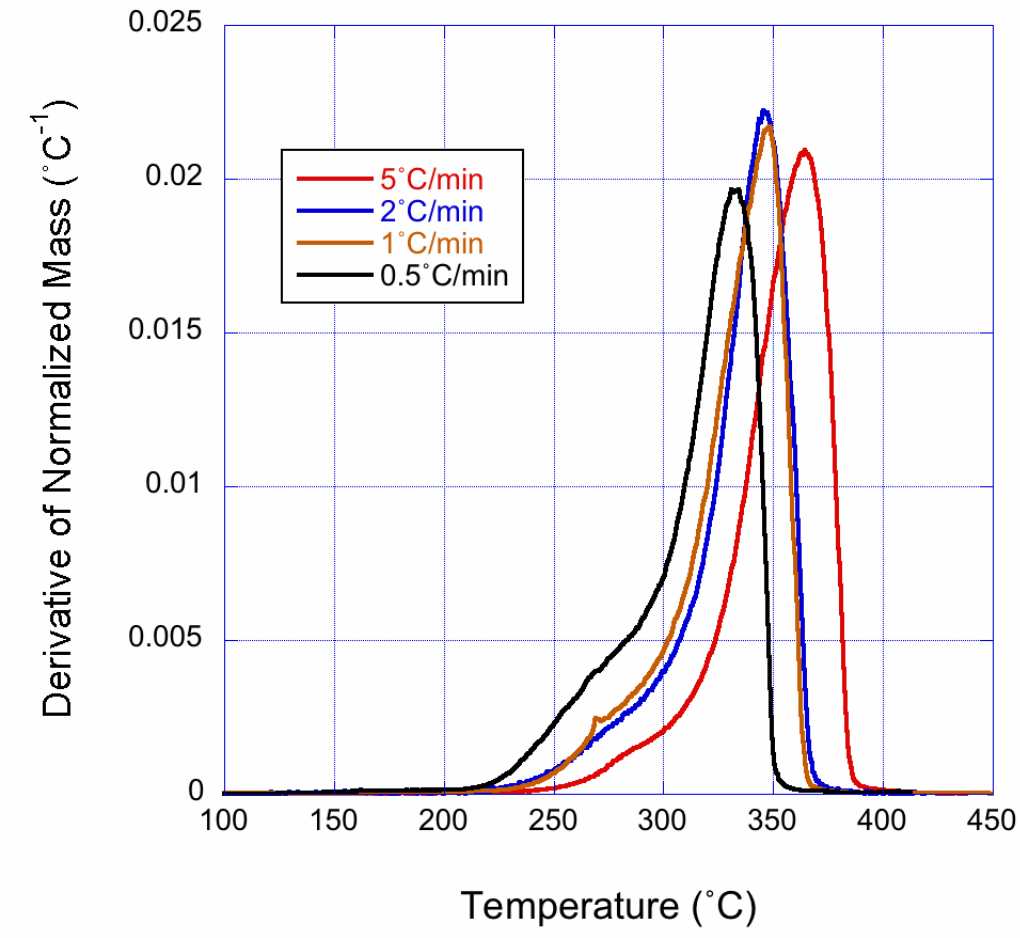

Figure 3.40: TGA Data from Cloisite 15A/PMMA High Molecular Weight Nanocomposite Samples

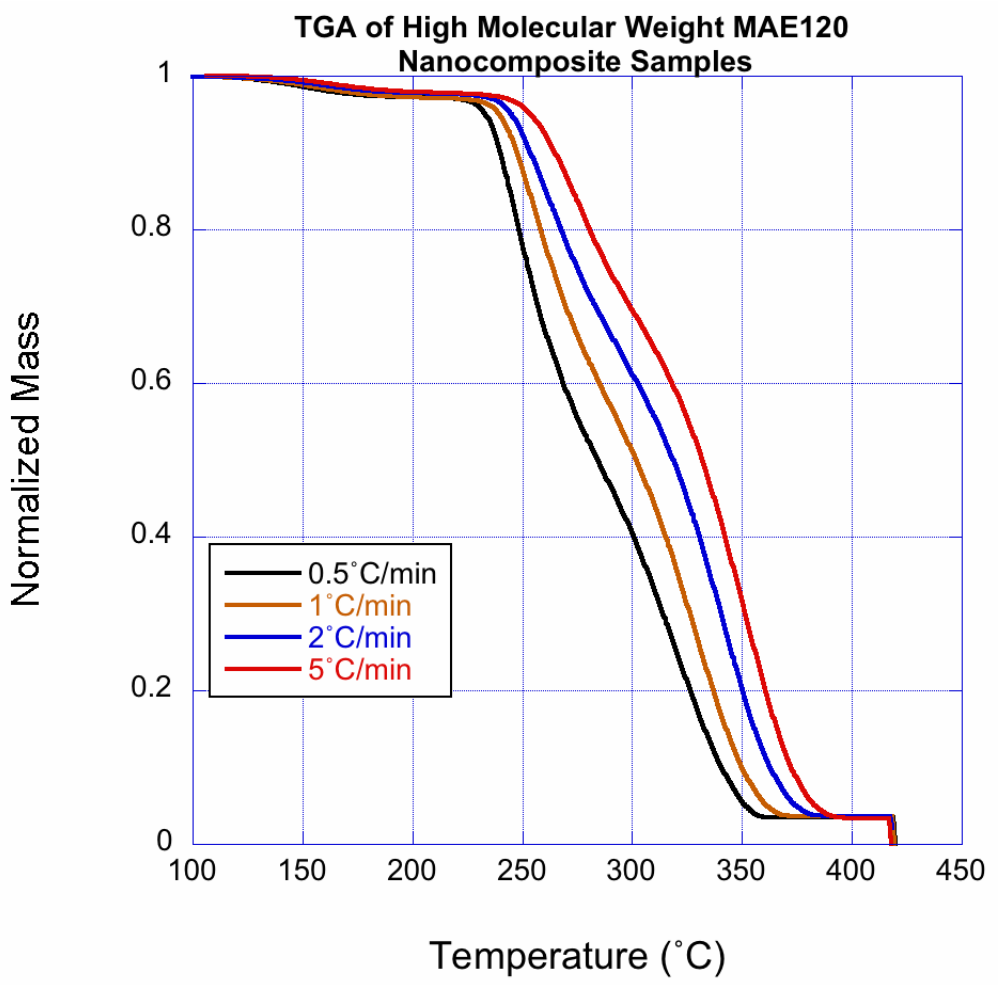

Figure 3.41: TGA Data from MAE120/PMMA High Molecular Weight Nanocomposite Samples

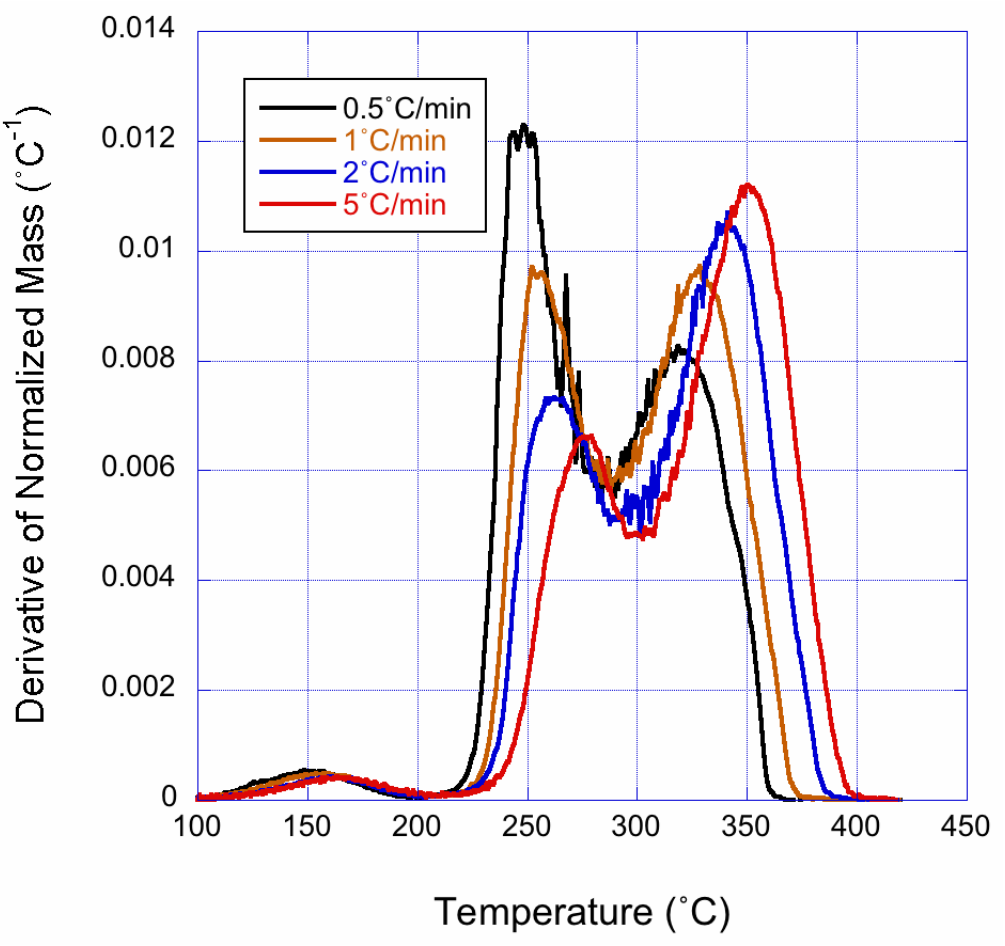

Figure 3.42: TGA Data from MAE120/PMMA High Molecular Weight Nanocomposite Samples

By comparing the TGA data (figure 3.41 and 3.42) from the MAE 120 nanocomposite and TGA data from other nanocomposites with that of the pure polymer, it can be noticed that the MAE 120 samples have distinct thermal degradation characteristics. A large mass loss event can be observed in the 250°C to 300°C range . The ratio between the degradation event at 250°C to 300°C range and degradation event at 300°C to 400°C is related to the heating rate. At low heating rates, the degradation from 250°C to 300°C is more prominent. The different degradation behavior can be explained by the interaction between the clay degradation and the polymer degradation. The TGA data from the MAE 120 synthetic mica (figure 3.24) showed strong degradation at 250°C, the free radicals produced during the degradation of organically modified silicate can attack the polymer chains and lead to a mass loss in the nanocomposites in this temperature range. Polymer degradation due to the surfactant of organically modified clay degradation has also been reported in polycarbonate nanocomposites [134], LLDPE [135] and PA6 nanocomposites [136], and change of thermal degradation behavior of matrix polymer has been reported in PS nanocomposites [137, 138].

The TGA data from nanocomposites with the different clays and the low molecular weight matrix polymer are shown in figure 3.25 (Pure PMMA), 3.27 (Cloisite 30B), 3.29 (Cloisite 15A), 3.31 (MAE120) and 3.33 (Grafted Clay). The derivative TGA curves are shown in 3.26 (Pure PMMA), 3.28 (Cloisite 30B), 3.30 (Cloisite 15A), 3.32 (MAE120) and 3.34 (Grafted Clay).

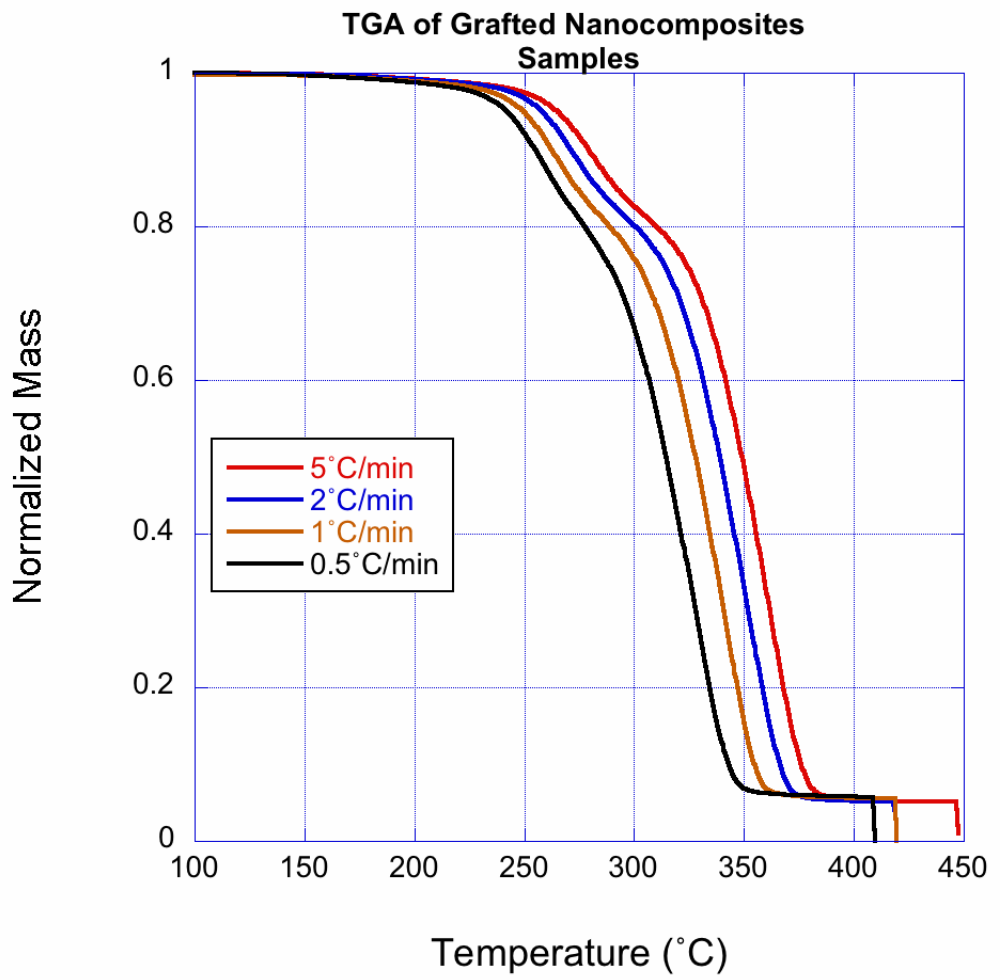

Figure 3.43: TGA Data from Grafted Clay/PMMA High Molecular Weight Nanocomposite Samples

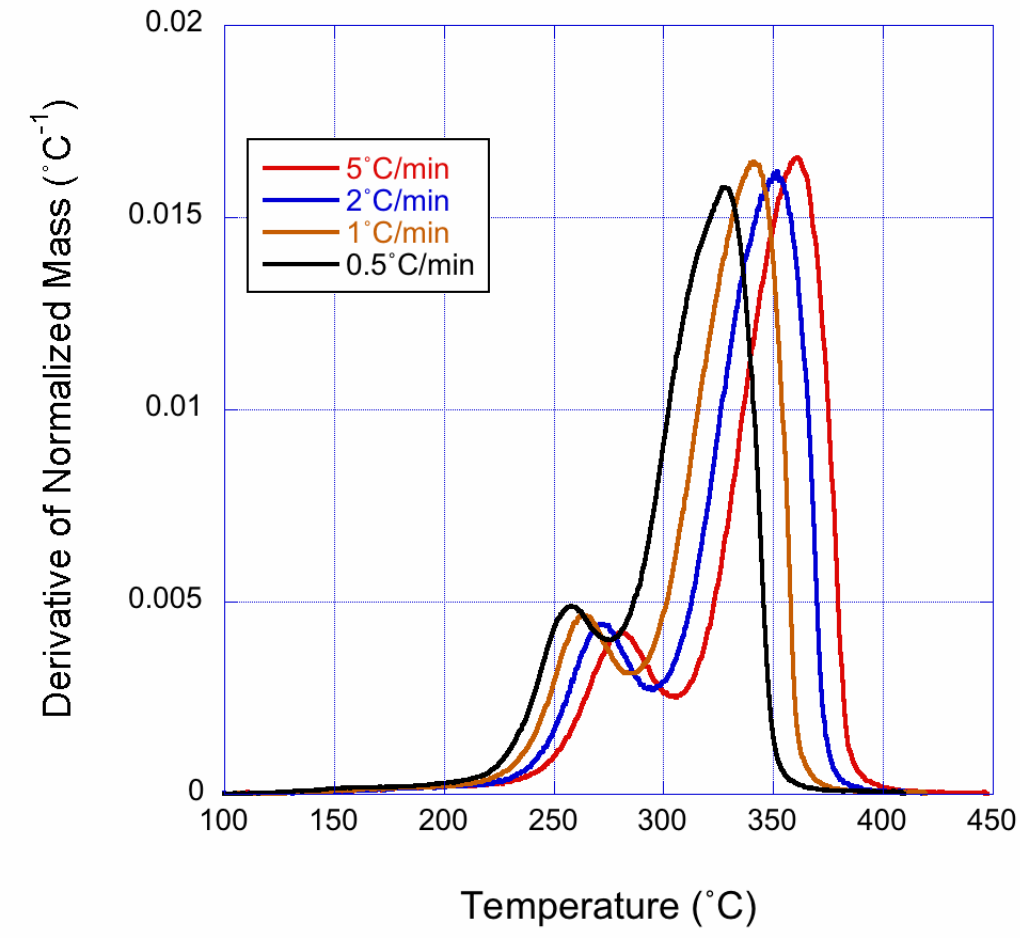

Figure 3.44: TGA Data from Grafted Clay/PMMA High Molecular Weight Nanocomposite Samples

The TGA data from nanocomposites with different clays and high molecular weight matrix polymer are shown in figure 3.35 (Pure PMMA), 3.37 (Cloisite 30B), 3.39 (Cloisite 15A), 3.41 (MAE120) and 3.43 (Grafted Clay). The derivative of the TGA curves are shown in 3.36 (Pure PMMA), 3.38 (Cloisite 30B), 3.40 (Cloisite 15A), 3.42 (MAE120) and 3.44 (Grafted Clay).

From figures 3.25 and 3.35, it can be observed that the 25k molecular weight PMMA begins to degrade at higher temperatures than the 350k molecular weight PMMA. It is possible that the low molecular weight PMMA is synthesized using a chain transfer agent, thus the chain ends of low molecular weight samples were saturated bonds (due to the chain transfer agents). The high molecular weight PMMA was probably synthesized using simple free radical polymerization which would result in the chain ends being mostly unsaturated bonds. Unsaturated bonds begin to degrade at a lower temperature than saturated bonds.

The reaction order and other degradation kinetic parameters calculated by Kissinger method and shape factor methods from low molecular weight samples are listed in table 3.2 (pure low molecular weight PMMA), 3.3 (low molecular weight Cloisite 15A 5 wt% nanocomposite), 3.4 (low molecular weight Cloisite 30B 5 wt% nanocomposite), 3.5 (low molecular weight MAE 120 5 wt% nanocomposite), and 3.6 (low molecular weight PMMA grafted 5 wt% nanocomposite). The activation energies of degradation reaction for different samples were also calculated by Ozawa method.

Because for of high molecular weight sample, the degradation process in the 250°C - 300°C range and degradation process in the 300°C - 400°C range overlap

with each other, the degradation activation energy of high molecular weigh samples were only calculated by the Ozawa method. The calculation results are listed in table 3.7.

The data showed that the in the low molecular weight samples, all low nanocomposites showed higher activation energies than the pure polymer. The high molecular weight samples also showed higher activation energies than the pure polymer, with the exception of the MAE120 sample, which has an activation energy lower than the pure polymer. The reason high molecular weight MAE 120 sample showed a lower activation energy than the pure polymer is that the nanocomposite degradation is controlled by the degradation of the surfactant rather than the matrix polymer.

It can also be observed that the reaction order for the nanocomposites decrease as the heating speed and the mass of the samples increase. The pure polymer samples do not show this behavior over the tested range of heating rates and sample mass. The MAE120 sample, which has a structure between a microcomposite and a nanocomposite also were not affected by the change in the heating rate and sample mass. This phenomenon can be explained as the nanocomposites forms a residue layer that acted as a small molecule barrier and a heat insulating layer. However TGA is not suitable when such mass and heat transportation barrier exist. Interestingly, the formation of such residue/char barrier can be used to identify the quality of the dispersion for the nanocomposites as materials with well dispersed layered silicate show different reaction orders compared to poorly dispersed nanocomposites.

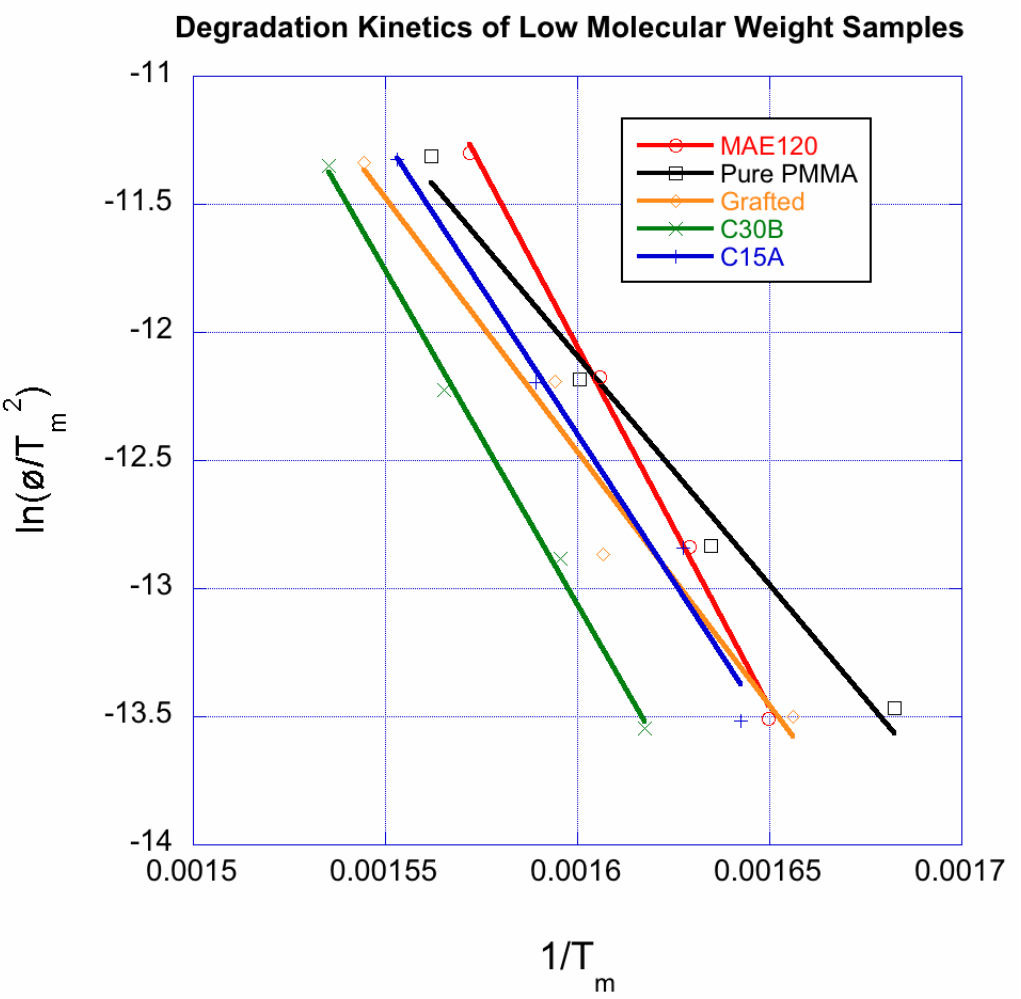

Figure 3.45: Kissinger Analysis of Low Molecular Weight PMMA and Nanocomposite Degradation Kinetics

Table 3.2: Kinetic Parameters Derived from Pure Polymer TGA Data

Sample Weight (mg)	Heating Speed (K/s)	Reaction Order	Kissinger Activation Energy (J/mol)	A Pre-exponential Factor (1/s)	Ozawa Activation Energy (J/mol)
2.7953	0.5	0.978	148205	2.43e+11	141555
2.5706	1	0.965			
1.7672	2	1.051			
2.3850	5	1.098			
31.034	2.5	0.972			
16.646	5	0.967			
16.657	10	1.151			

Table 3.3: Kinetic Parameters Derived from Cloisite 15A Low Molecular Weight Nanocomposite TGA Data

Sample Weight (mg)	Heating Speed (K/s)	Reaction Order	Kissinger Activation Energy (J/mol)	A Pre-exponential Factor (1/s)	Ozawa Activation Energy (J/mol)
5.4852	0.5	0.957	190823	8.42E+14	191249
2.8123	1	1.000			
5.9433	2	0.979			
7.4183	5	0.903			
17.874	2.5	0.767			
18.63	5	0.755			
28.807	10	0.652			

Table 3.4: Kinetic Parameters Derived from Cloisite 30B Low Molecular Weight Nanocomposite TGA Data

Sample Weight (mg)	Heating Speed (K/s)	Reaction Order	Kissinger Activation Energy (J/mol)	A Pre-exponential Factor (1/s)	Ozawa Activation Energy (J/mol)
8.4561	0.5	1.098	210477	4.17E+16	206056
6.9799	1	1.028			
8.4127	2	1.051			
8.4719	5	0.981			
58.94	2.5	0.829			
41.018	5	0.786			
57.238	10	0.642			

Table 3.5: Kinetic Parameters Derived from MAE120 Low Molecular Weight Nanocomposite TGA Data

Sample Weight (mg)	Heating Speed (K/s)	Reaction Order	Kissinger Activation Energy (J/mol)	A Pre-exponential Factor (1/s)	Ozawa Activation Energy (J/mol)
4.7121	0.5	0.947	234613	6.674e+18	214270
2.4946	1	0.946			
2.1487	2	0.984			
1.9742	5	1.025			
9.1827	2.5	0.983			
24.564	5	1.060			
9.9289	10	0.999			

Table 3.6: Kinetic Parameters Derived from PMMA Grafted Clay Low Molecular Weight Nanocomposite TGA Data

Sample Weight (mg)	Heating Speed (K/s)	Reaction Order	Kissinger Activation Energy (J/mol)	A Pre-exponential Factor (1/s)	Ozawa Activation Energy (J/mol)
4.3296	0.5	0.992	164875	4.61E+12	171669
6.6164	1	0.840			
5.6903	2	0.980			
8.3840	5	0.862			
27.203	2.5	0.726			
29.097	5	0.798			
26.083	10	0.813			

Table 3.7: Kinetic Parameters Derived from TGA Data of High Molecular Weight Samples

Sample	Ozawa Activation Energy (J/mol)
Pure PMMA	157159
PMMA C15A 5%	207094
PMMA C30B 5%	196913
PMMA MAE120 5%	129447
Grafted Clay 5%	192725

3.5.2 Gasification Experiments

Gasification results are shown in figure 3.46, and table 3.8 lists the values of ignition time, peak mass loss rate, time to peak mass loss rate and average mass loss rate. Photographs of the sample residue after gasification are shown in figure 3.47. The photographs on the left are residues from the low molecular weight samples, and the photographs on the right are from the high molecular weight samples. The pure PMMA samples left no residue after gasification or cone calorimetry and are not shown here.

The gasification data is separated into three groups, pure polymer, low molecular weight samples, and high molecular weight samples. The pure polymer showed a continuously increasing mass loss rate until reaching a maxima and then dropped

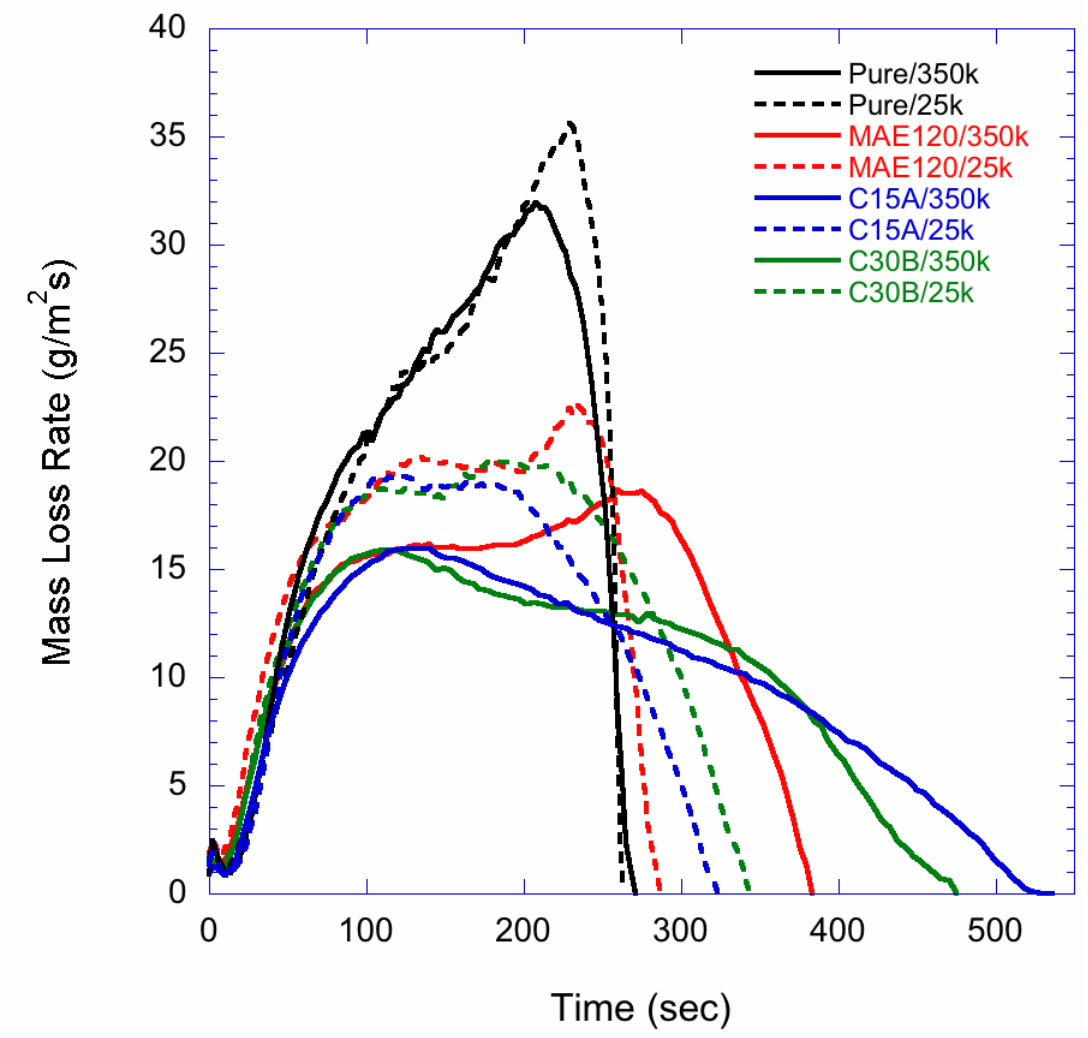

Figure 3.46: Mass Loss Rate Curve from Gasification Experiments

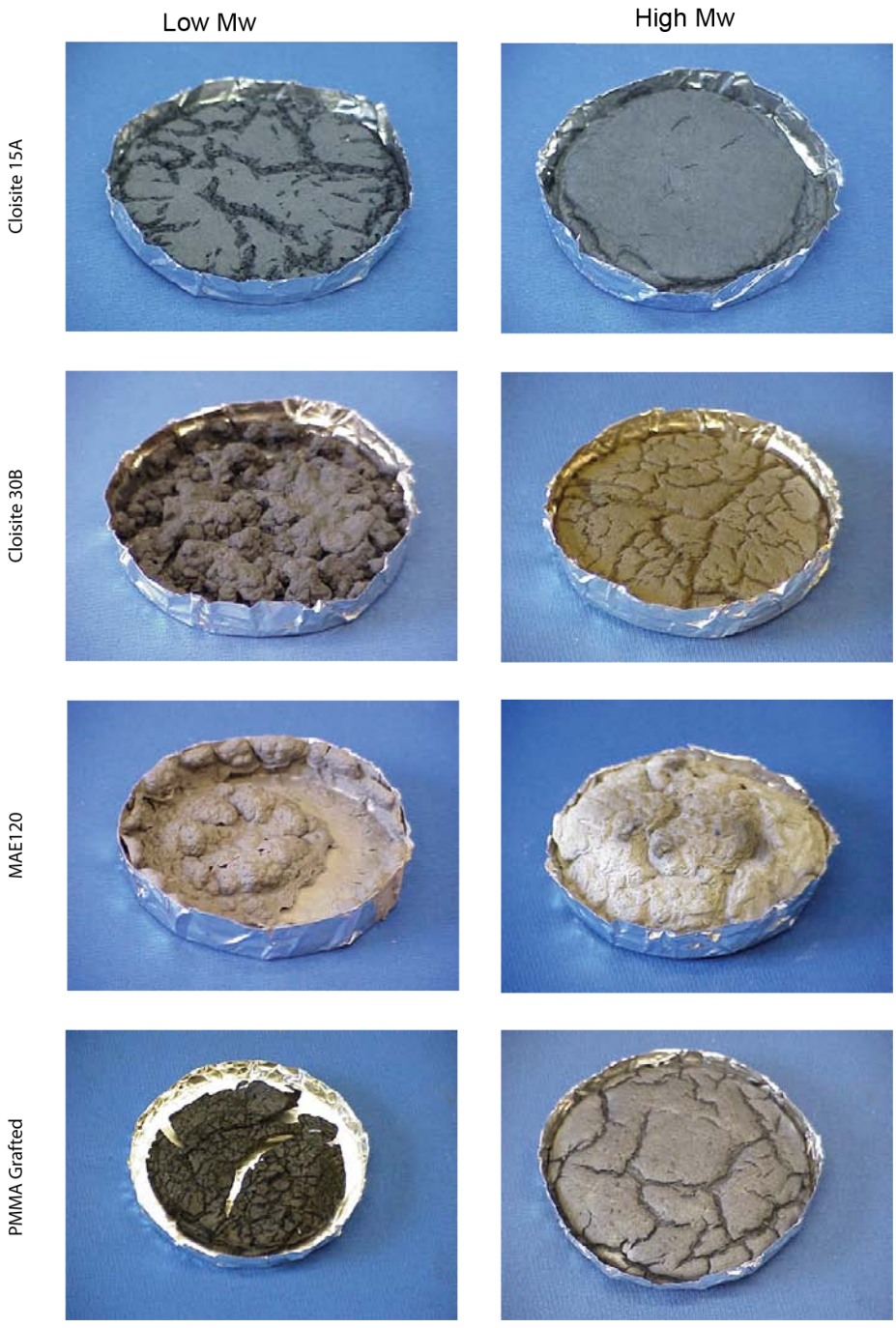

Figure 3.47: Residue After Gasification Experiments

quickly to zero. The nanocomposites all showed significantly lower mass loss rates compared with the pure polymers. All low molecular weight samples showed higher mass loss rates compared to their corresponding high molecular weight samples, while the mass loss rate of the MAE 120 samples increased after a plateau but the Cloisite 30B and 15A samples dropped slowly after a plateau as shown in figure 3.46. During the gasification experiments, decomposition products formed bubbles in the polymer melt and these bubbles rose to the surface of the polymer melt and erupted. The motion of bubbles directly affects the formation of any protective residue layer at the surface of the degrading sample. At beginning of the experiment, the residue layer is very thin, the eruption of bubbles can break the residue layer as shown in figure 3.48. In the low molecular weight samples, bubbles can keep the residue from forming a continuous film on the residue even after the residue layer has become thick. Such a case is illustrated in figure 3.49. In the case of high molecular weight samples, because of the relatively high melt viscosity, the disturbance of bubbles was suppressed and generally resulted in the formation of a protective residue layer with better integrity. It is also interesting to note that decomposition gases built up under all sample disks causing the samples to swell up due to the increasing gas pressure. During swelling, the surface area of the sample increased, the protective residue layers often cracked and broke, exposing new polymer melt to the incident radiation, which in turn increased the decomposition rate. The swelling-cracking situation is illustrated in figure 3.50. In general, the high molecular weight samples have a higher storage modulus and as a result are more resistant to swelling. The low molecular weight samples were more prone to swelling, reaching the dramatic

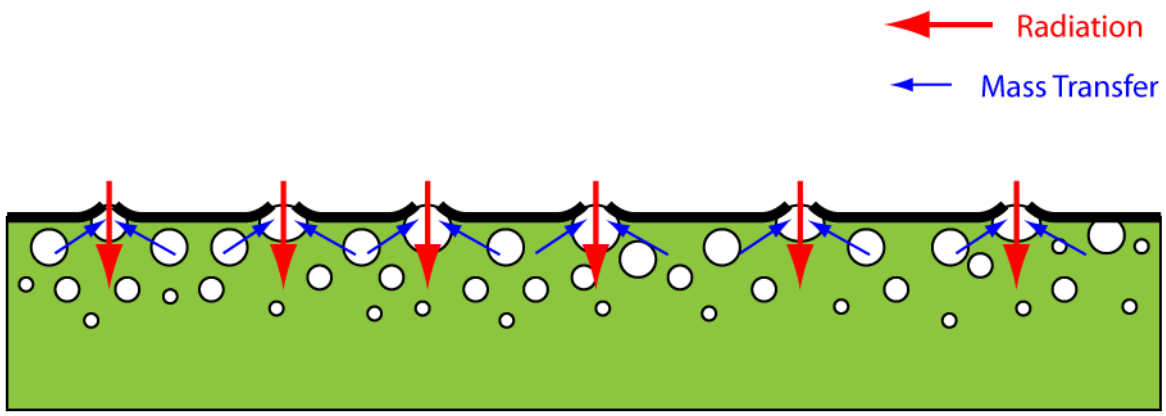

Figure 3.48: Effect of Bubbles on Thin Residue Layer

situation for the low molecular weight MAE120 sample when the melt erupted catastrophically due to melt being stretched beyond the elastic limit by the build up of decomposition products.

3.5.3 Cone Calorimetry

Cone calorimetry data are shown in figure 3.53. Table 3.9 lists ignition time, peak heat release rate (PHRR), time to peak heat release rate, peak mass loss rate, time to peak mass loss rate. The cone calorimetry behavior showed similar trends as the gasification data, but due to the heat from the burning polymer, the degradation

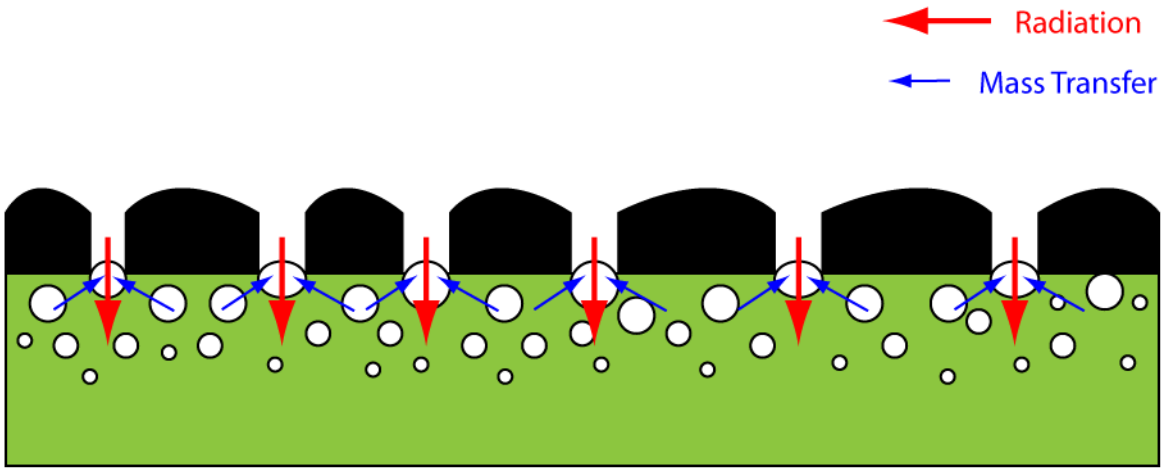

Figure 3.49: Effect of Bubbles on Thick Residue Layer

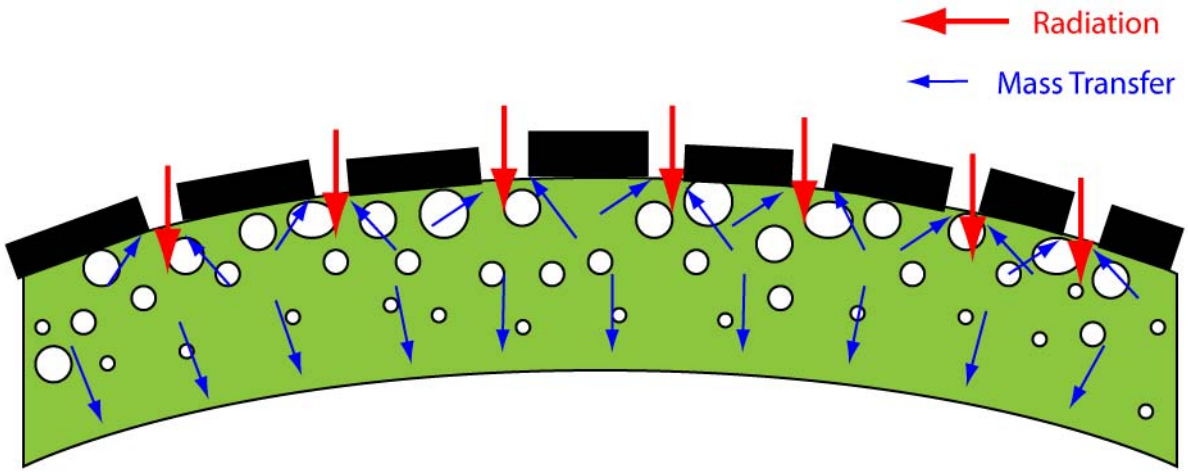

Figure 3.50: Effect of Disk Warping on the Flammability

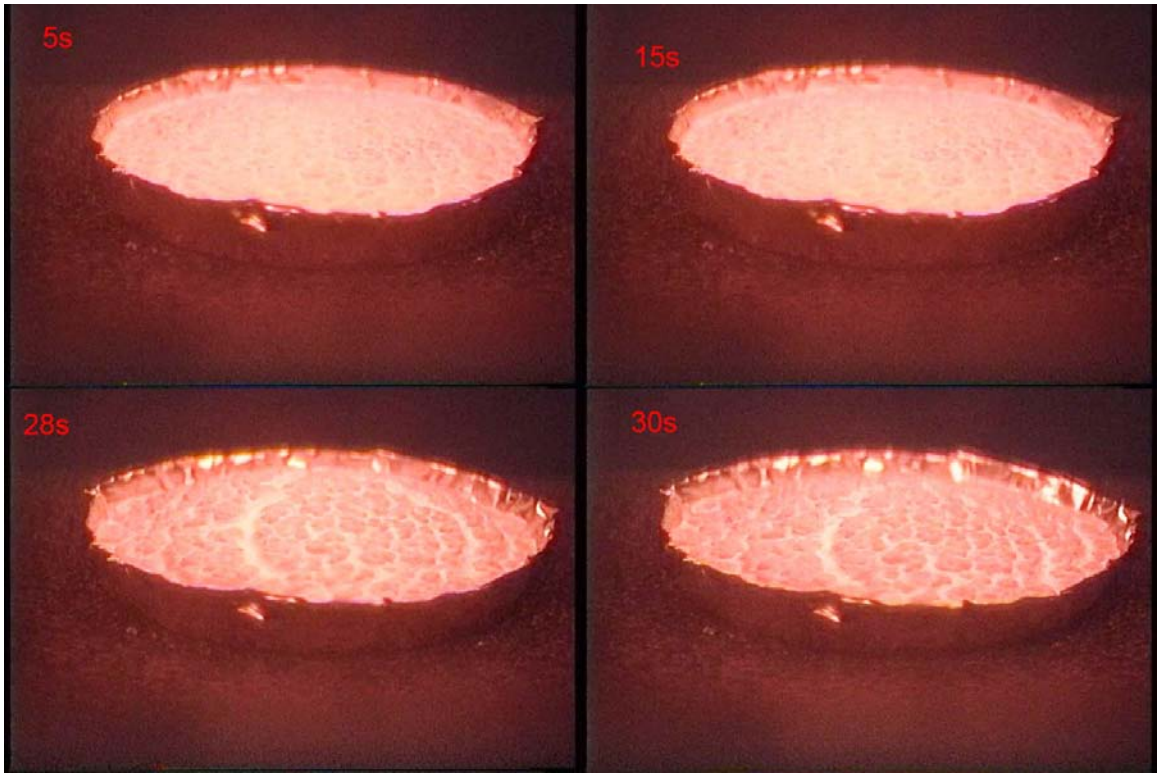

Figure 3.51: Video images captured during the gasification of a high molecular weight sample, showing stacks in thin residue (5s, 10s), swelling (28s), and large cracks formed during swelling (28s, 30s).

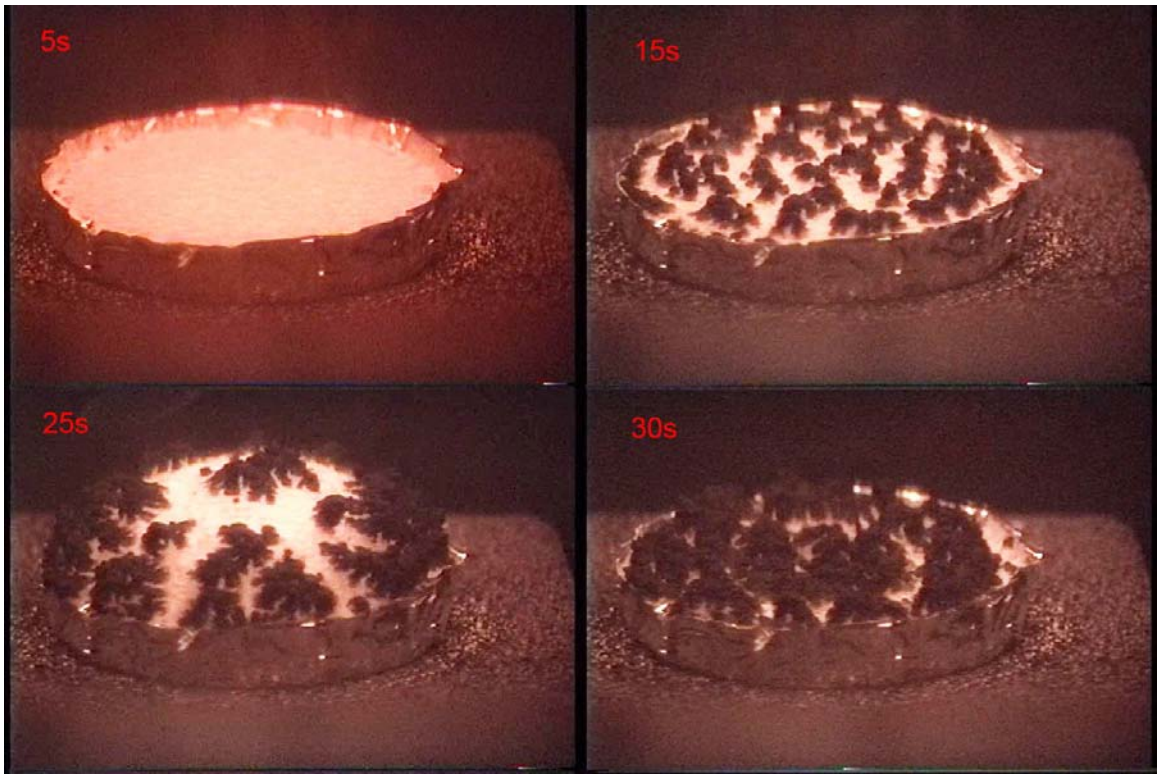

Figure 3.52: Video images captured during the gasification of a low molecular weight sample, showing cracks in thin residue (5s), island like structure formed because of bubbles pushing residue (15s), swelling (25s), and large cracks formed during swelling (25s, 30s).

Table 3.8: Results from Gasification Experiments for Samples with 5wt.% Filler

Sample	PMMA	PMMA	Cloisite 30B	Cloisite 30B	Cloisite 15A	Cloisite 15A	MAE 120	MAE 120
Molecular Weight (g/mol)	25K	350k	25k	350k	25k	350k	25k	350k
Ignition time (s)	22.5	27.5	21	21.5	30	28	17	22.5
Peak MLR (g/m^2s)	40.045	35.747	23.982	17.195	21.267	17.647	26.244	20.326
Time to PMLR (s)	230.5	201.5	206.5	107.5	104	128.5	236	257.5
Average MLR (g/m^2s)	21.13	19.86	14.26	10.57	11.05	10.95	16.15	13.37

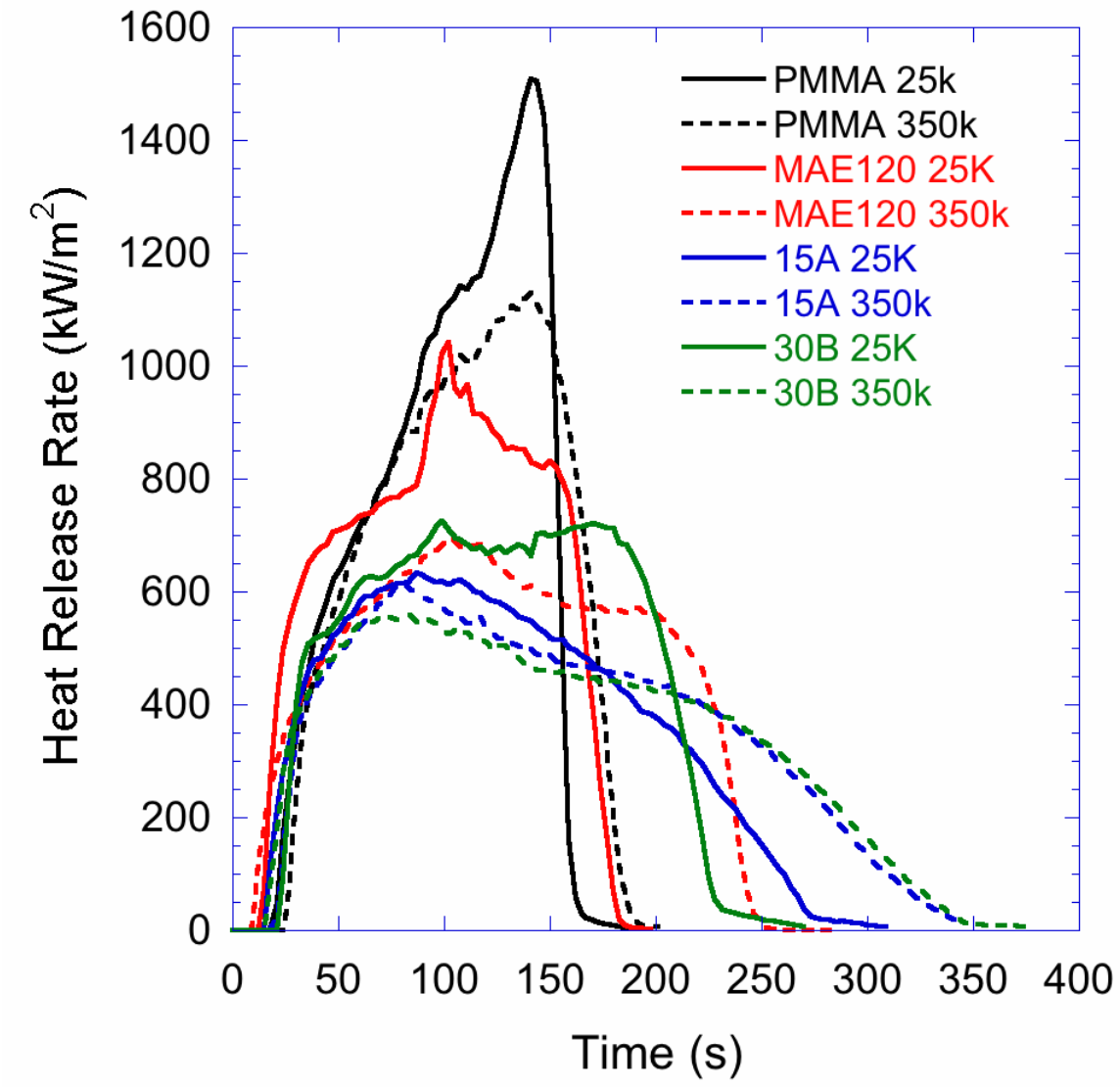

Figure 3.53: Heat Release Rate Curve from Cone Calorimetry Experiments

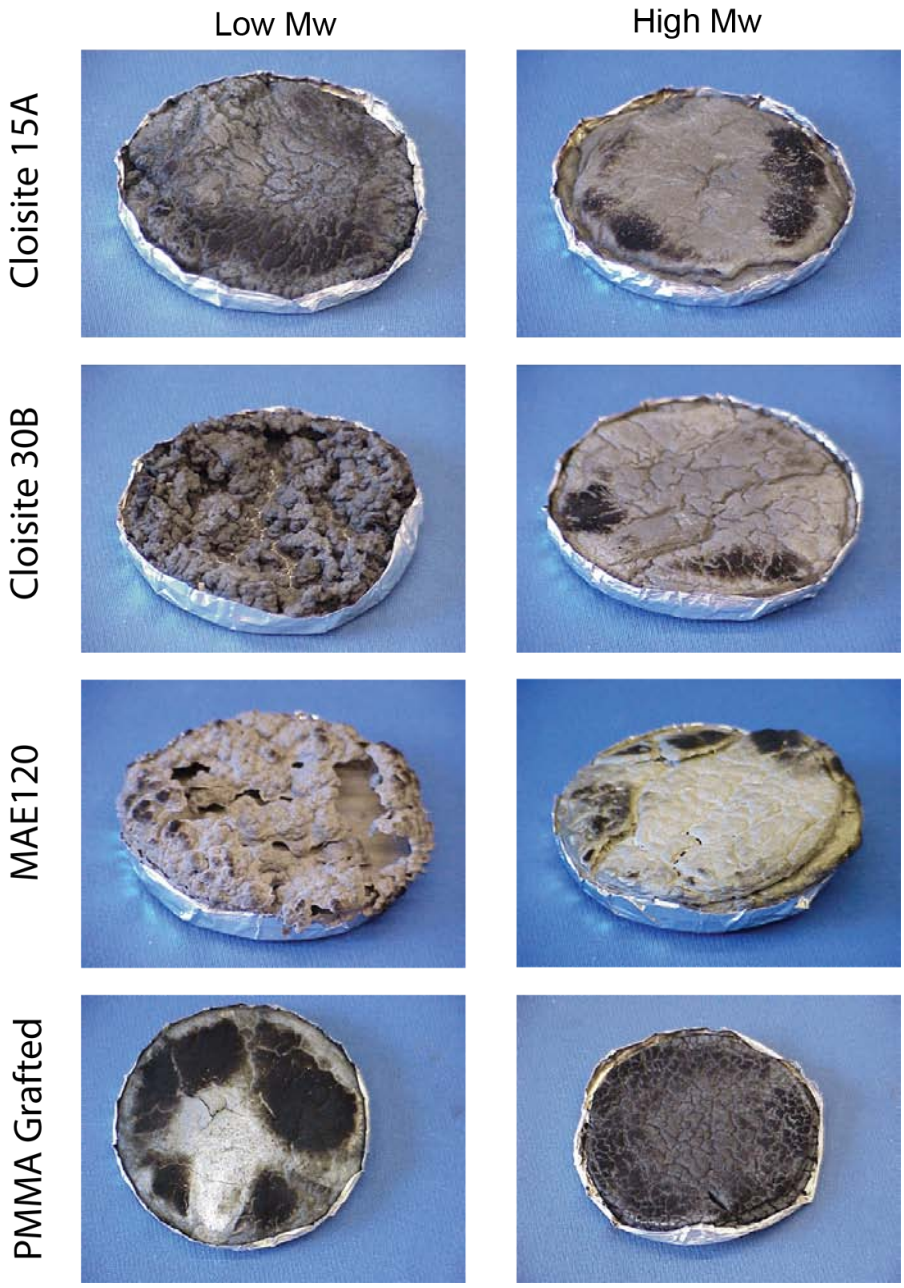

Figure 3.54: Residue After Cone Calorimetry Experiment

Table 3.9: Results from Cone Calorimetry Experiments

Sample	PMMA	PMMA	Cloisite 30B	Cloisite 30B	Cloisite 15A	Cloisite 15A	MAE 120	MAE 120
Molecular Weight (g/mol)	25K	350k	25k	350k	25k	350k	25k	350k
Ignition time (s)*	21	27	24	18	22	18	15	12
PHRR (kW/m2)	1508.8	1111.3	726	559.7	621.2	632.7	1041.7	696
Time to PHRR (s)*	141	144	99	81	78	87	102	102
Peak MLR (g/m2s)	59.06	44.815	29.522	22.916	25.535	26.227	38.993	27.089
Time to PMLR (s)*	141	141	96	96	84	78	99	96

* data were acquired every 3s.

process is faster. Image of the residue are shown in figure 3.54.

3.5.4 Effect of Clay Dispersion

3.5.4.1 Solvent Introduced Dispersion Change

One possible method to improve the stability of the residue layer is to alter the clay dispersion, although it has been reported that the clay dispersion is a secondary issue affecting the flammability of nanocomposites [109, 139], this has been explored in further detail.

An experiment was designed to examine the effect of clay dispersion on flammability. MAE120 synthetic mica disperses better in chloroform than in tetrahydrofuran (THF), so a sample was cast from chloroform and the gasification measured to compare with the previous gasification data on materials precipitated from THF. The results are shown in 3.55.

The TEM of the samples cast from chloroform revealed that the Cloisite 15A sample has a microcomposite structure with relatively poor clay dispersion (figure 3.56), while the MAE120 sample has a higher degree of intercalation (figure 3.57). TEM observation of the samples formed by precipitation from THF revealed that the MAE120 sample was more like a microcomposite and Cloisite 15A sample is more like a nanocomposite.

The maximum mass loss rate of the MAE120 sample cast from chloroform is lower than the sample from THF, which is consistent with an improvement of the dispersion in the chloroform cast sample. The mass loss rate data for the the

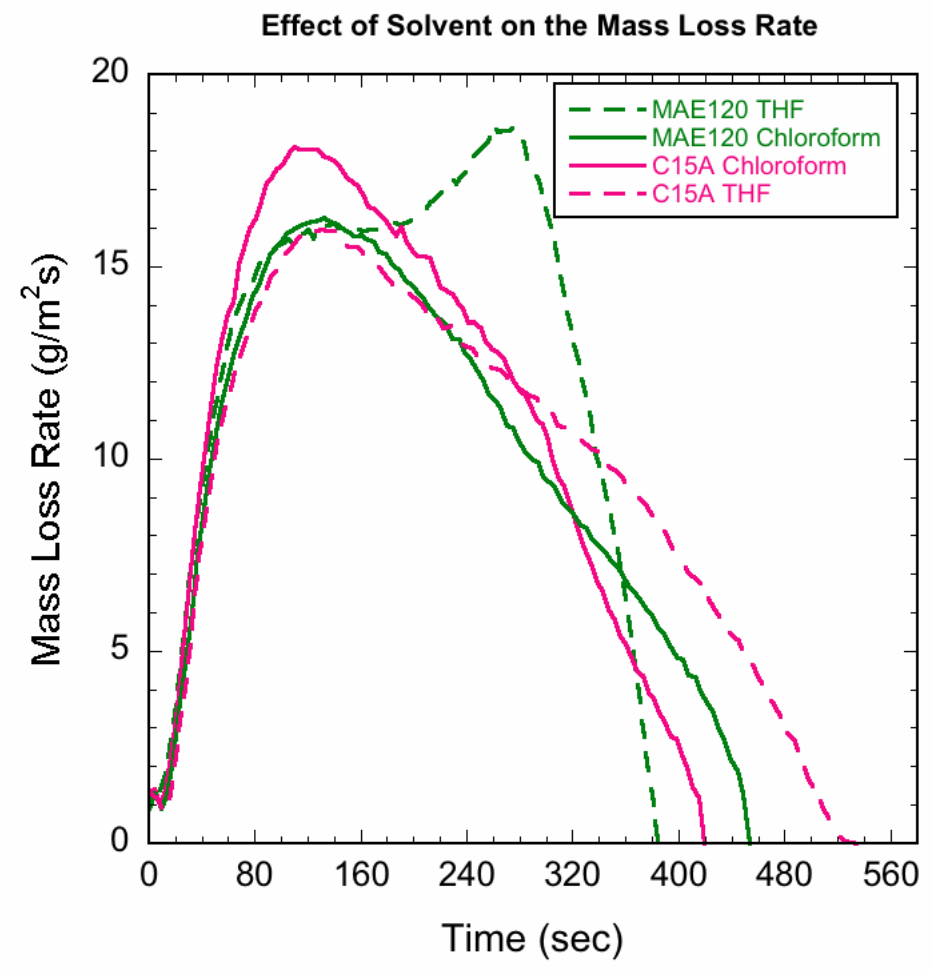

Figure 3.55: Mass Loss Rate Curve from Gasification Experiment of Samples Cast from Chloroform Compared to Samples from THF

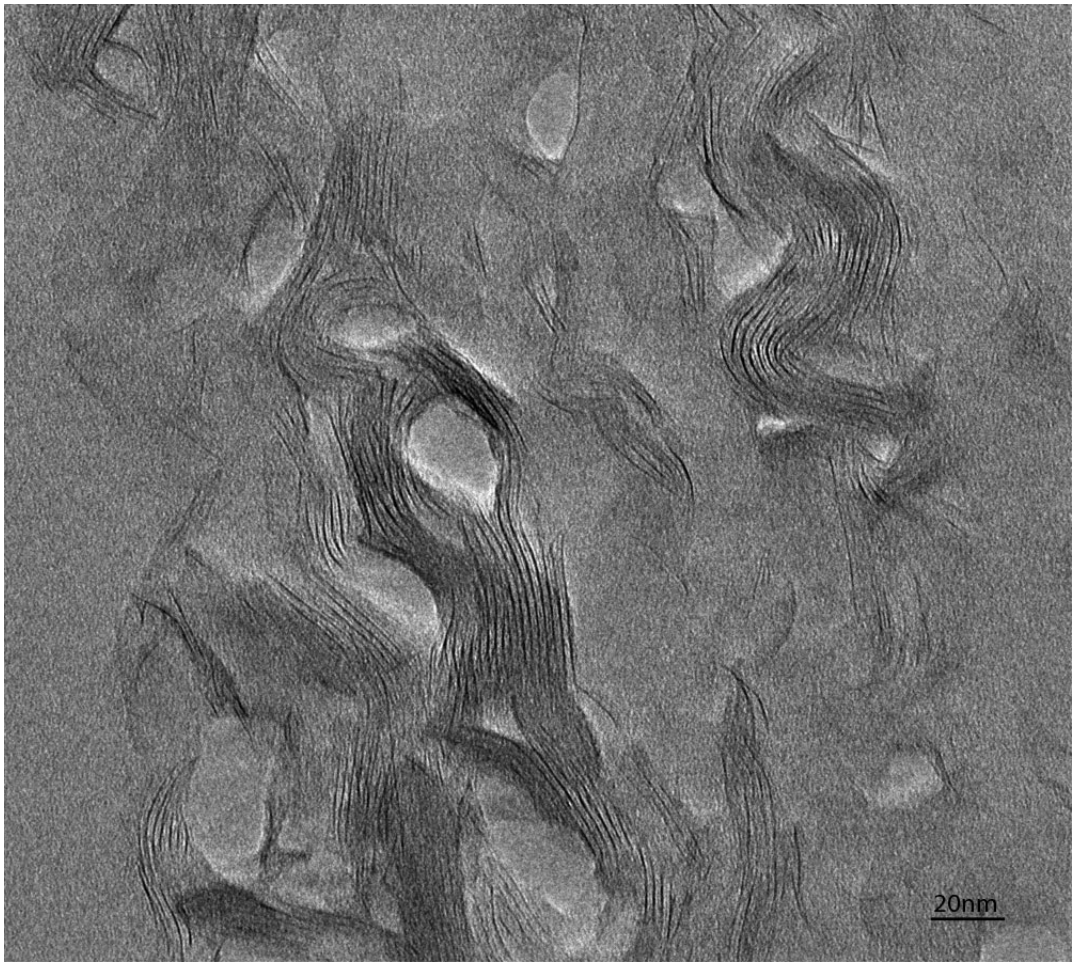

Figure 3.56: Intercalated/Microcomposite Structure Formed when Cloisite 15A/PMMA Sample Cast from Chloroform

Cloisite 15A sample cast from chloroform is higher than the sample cast from THF, which is also consistent with a decrease in the dispersion.

These experiments indicate changing the dispersion of the clay from a microcomposite to an intercalated nanocomposite does affect the flammability, with the intercalated systems showing improved flammability.

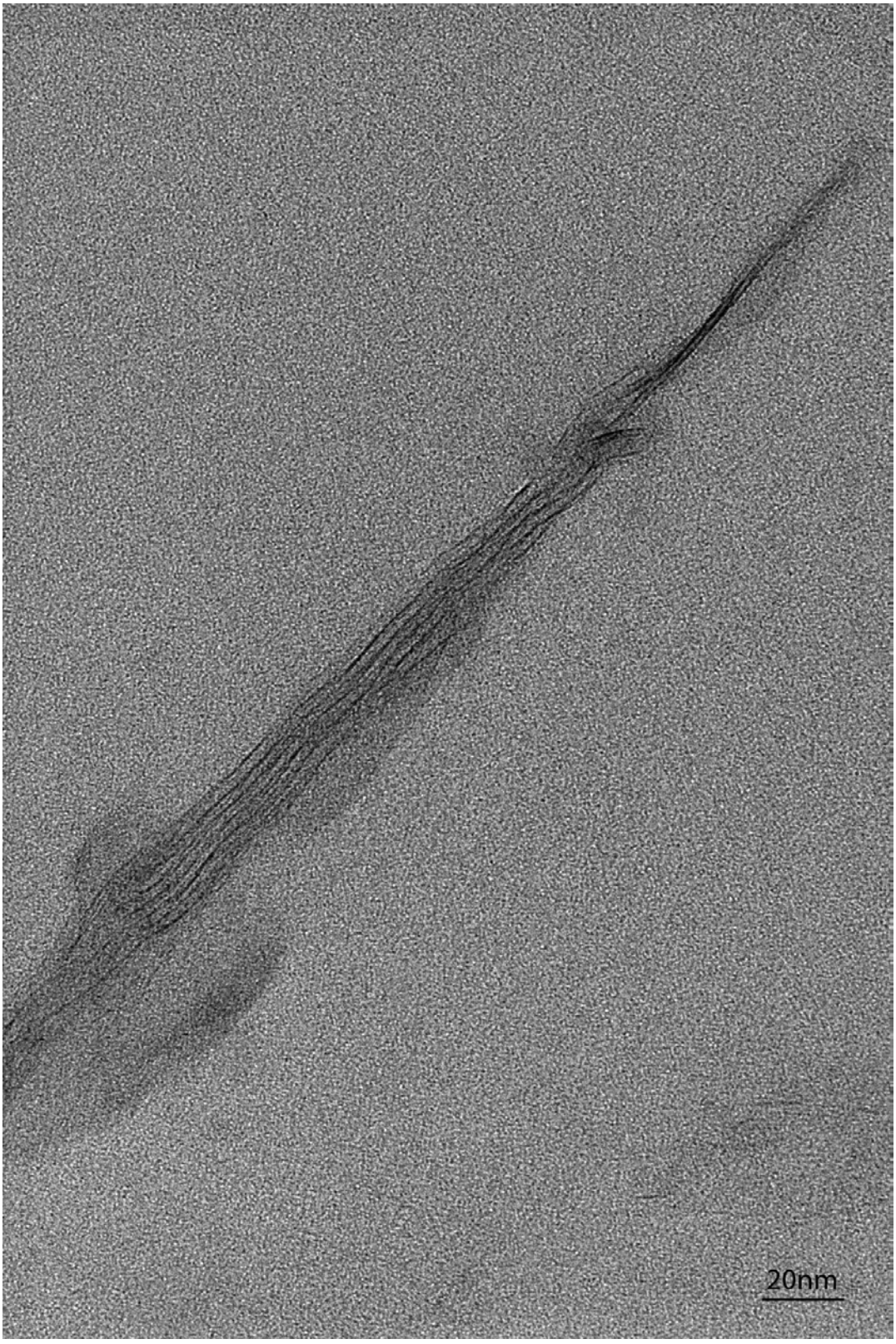

Figure 3.57: Intercalated Structure Produced from MAE120/PMMA Cast from Chloroform.

3.5.4.2 PMMA Grafted Clay Introduced Dispersion Change

The PMMA grafted clay disperses in the PMMA matrix in a more exfoliated manner than the Cloisite 30B. However, the PMMA grafted clay did not produce significant improvement in the flammability.

The TGA data are shown in figure 3.33 (low molecular weight sample), 3.43 (high molecular weight sample), 3.34 (derivative TGA data for the low molecular weigh sample), 3.44 (derivative TGA data for the high molecular weigh sample). The data shows three peaks during the thermal degradation. The first peak is in the range from 150°C to 200°C, which is attributed to head to head defects, the second peak is in the range of 250°C to 330°C, which is attributed to unsaturated bonds. The third peak is in the range of 300°C to 400°C, which is attributed to random chain scission.

Gasification data from the nanocomposite with the PMMA grafted clay is shown in figure 3.58. The mean mass loss rate of the grafted clay nanocomposite is lower than the Cloisite 30B nanocomposite (10.00 g/m^{2}s vs. 10.57 g/m^{2}s in the high molecular weight samples and 12.15 g/sm^2 vs. 14.26 g/sm^2 in low molecular weight samples, g/m^{2}s is gram per square meter per second), but the peak heat release rate is not reduced.

The cone calorimeter data are shown in figure 3.59.

The short PMMA chains grafted on the surface of clay are synthesized by free radical polymerization and are expected to have chain ends with double bonds. Although the dispersion showed improved exfoliation, the thermal degradation and

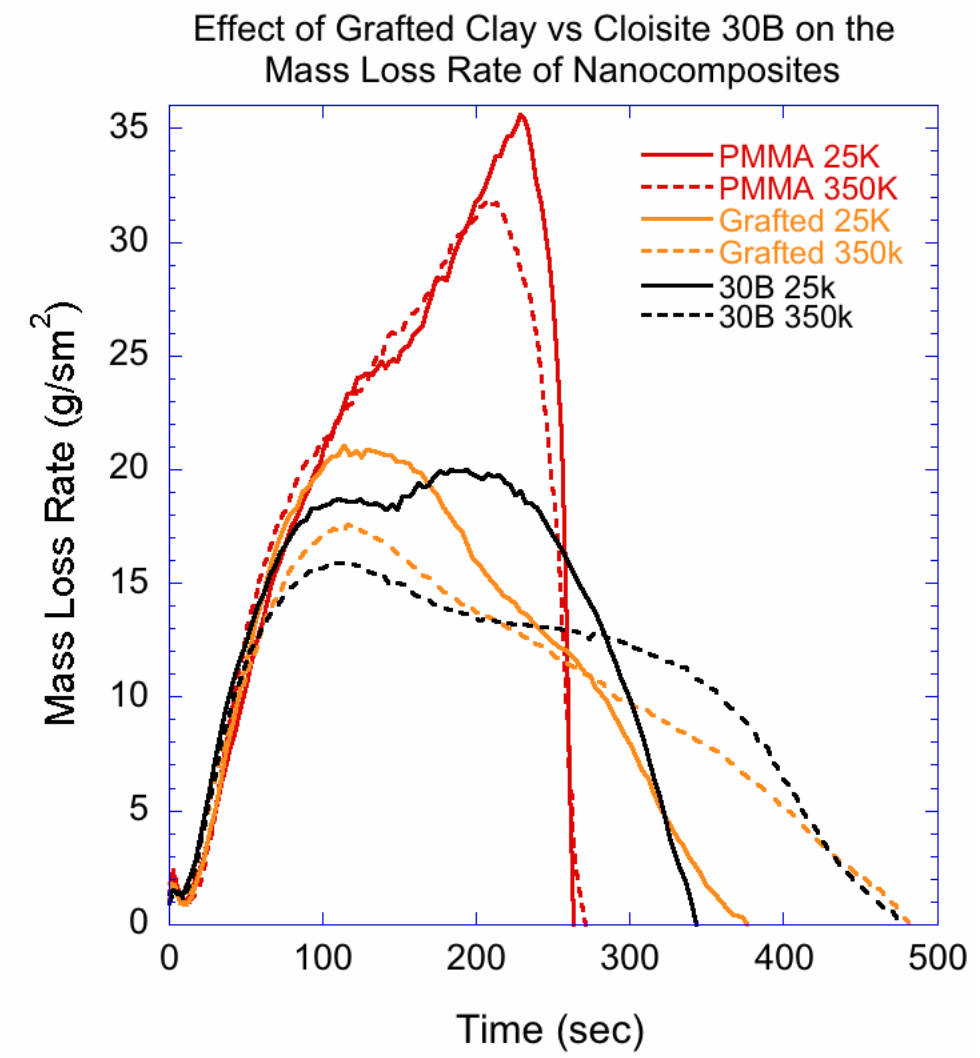

Figure 3.58: Mass Loss Rate Data from Nanocomposites with PMMA Grafted Clay

flammability was not significantly improved, probably due to the presence of the unsaturated chain ends.

3.5.5 Residue Layer

XRD data from residue are shown in figure 3.60. The diffraction peak from the Cloisite 30B nanocomposite residue and the Cloisite 15A nanocomposite residue

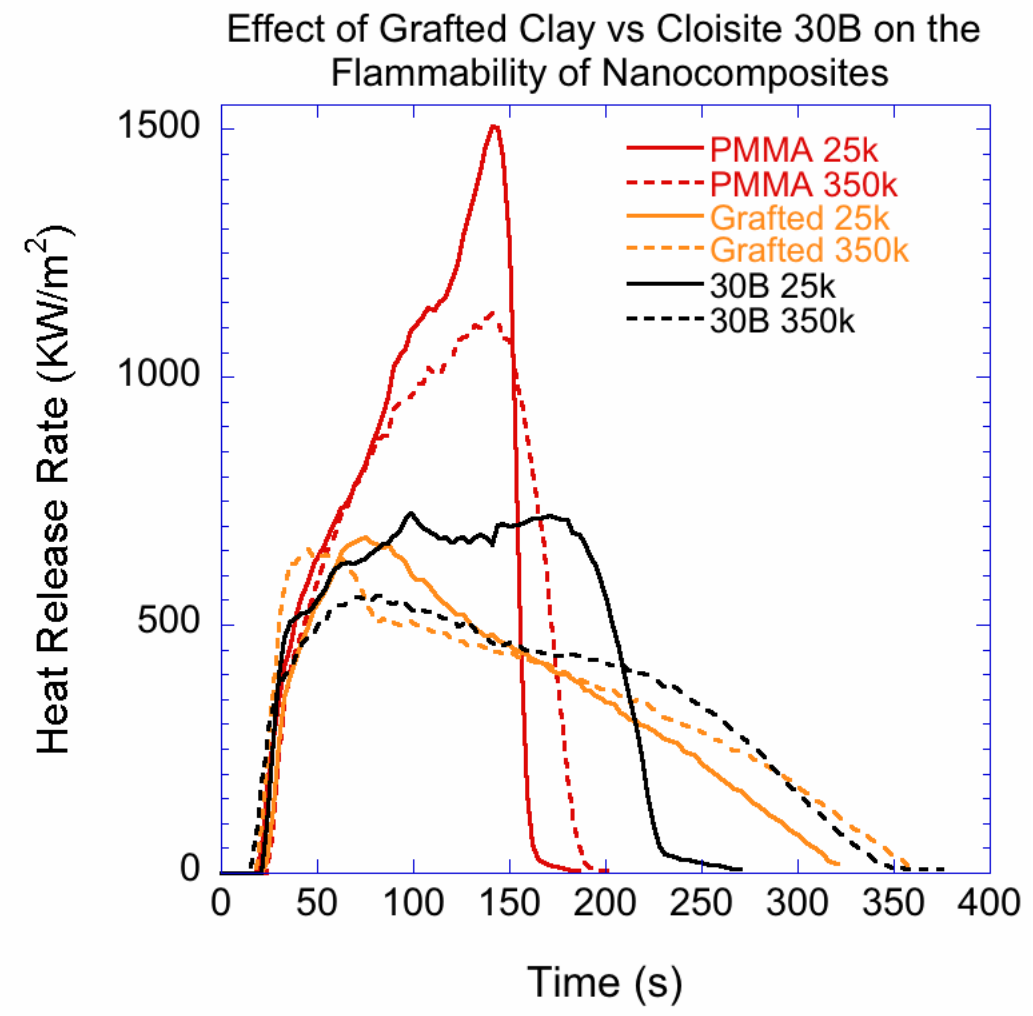

Figure 3.59: Heat Release Rate from Cone Calorimetry Experiment of Nanocomposite Samples with PMMA Chain Grafted Clay in Comparison with Nanocomposite Samples with Cloisite 30B Clay and Samples of Pure PMMA Polymer

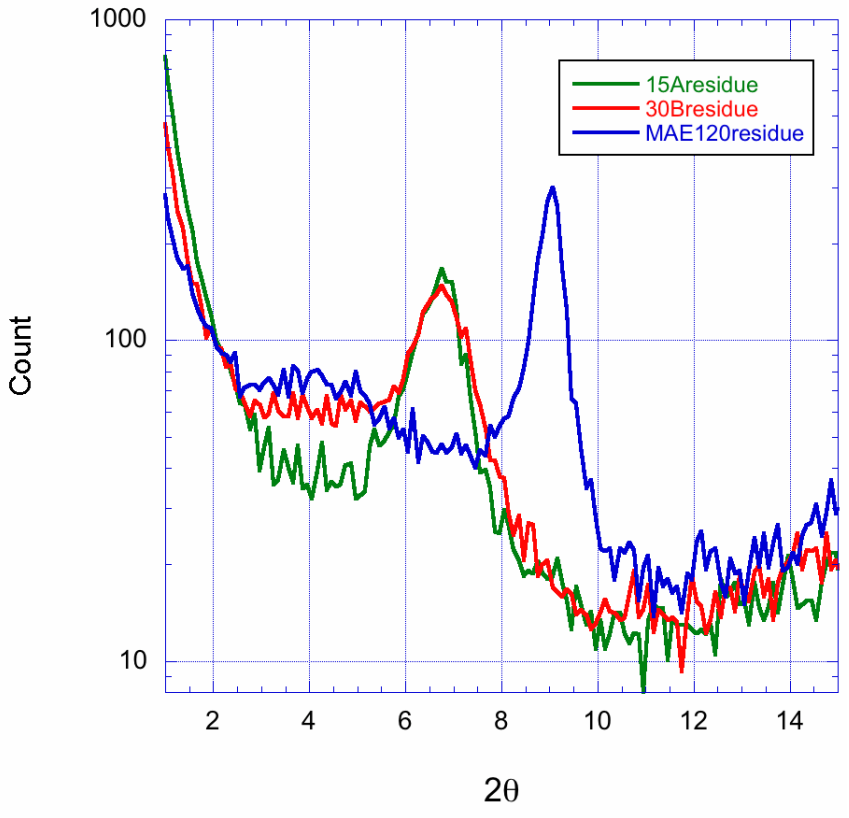

Figure 3.60: XRD Data from the Residues

is at 1.26 nm and the peak from the MAE120 nanocomposite residue is at 0.98 nm. The unmodified Cloisite Na+ clay has a spacing of 0.98 nm and the unmodified ME100 mica has a spacing of 0.93 nm. The XRD data shows that there is some char residue trapped inside the gallery space in the layered silicates.

A cross section SEM micrograph of the residue after the gasification experiment is shown in figure 3.61. The residue shows a porous structure, which is a good structure for heat insulation.

The characteristics of the char layer including the structure and uniformity are key factors related to the measured flammability. The effectiveness of the residue layer as a shield (radiation and/or mass loss) is maximized when the polymer melt surface is completely covered by the residue layer. For this to occur, the residue layer needs sufficient silicate to form and remain stable on top of the polymer melt to keep from cracking and disintegrating. If the protective residue layer forms cracks, radiation can penetrate into the polymer matrix and the decomposition products can escape.

There are several factors that affect the stability of the residue layer. First is the viscosity of the polymer resin. The lower the polymer resin viscosity, the more turbulent is the surface of the polymer melt during combustion, which makes it difficult for a uniform residue layer to form. A second factor is the toughness of the residue layer. In most cases, the residue layer is actually composed of porous silicates. By adding a coupling agent, bridges could form between the silicate layers and it may be possible to increase the toughness of the residue layer. The coupling

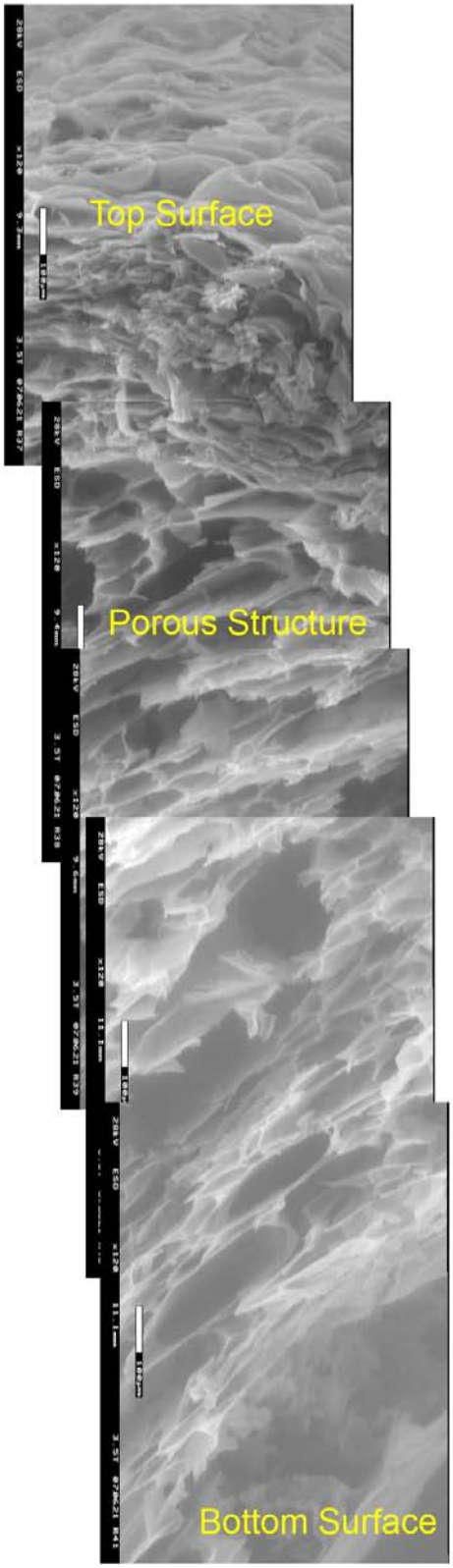

Figure 3.61: SEM Observation of Cross Section of a Residue from Gasification Experiment

agent could also be a low melting temperature glass or char.

3.6 Rheology Measurements

Measurement of the rheology showed that the viscosity of the nanocomposite is higher than the pure polymer resin (figure 3.62). The increased viscosity can help prevent bubble formation and slow the rising of the bubbles to the surface, which has two effects, first, the mass transfer from the polymer melt to the gaseous phase by the bubbles is slowed and second, the polymer melt surface is less turbulent.

3.7 Glass Transition Measurement

Increasing the surface or interface area can cause a change in the glass transition temperature. The glass transition temperature can increase or decrease depending on specific interactions at the polymer/clay interface. Layered silicates introduced into the polymer matrix result in a large interface between the silicate and the polymer and can shift the measured glass transition temperature. The shift can provide insight into the nature of the interface and the degree of dispersion. The glass transition temperature is often measured by Differential Scanning Calorimetry (DSC).

3.7.1 Differential Scanning Calorimetry

The glass transition temperatures of different samples measured by DSC are listed in table 3.10.

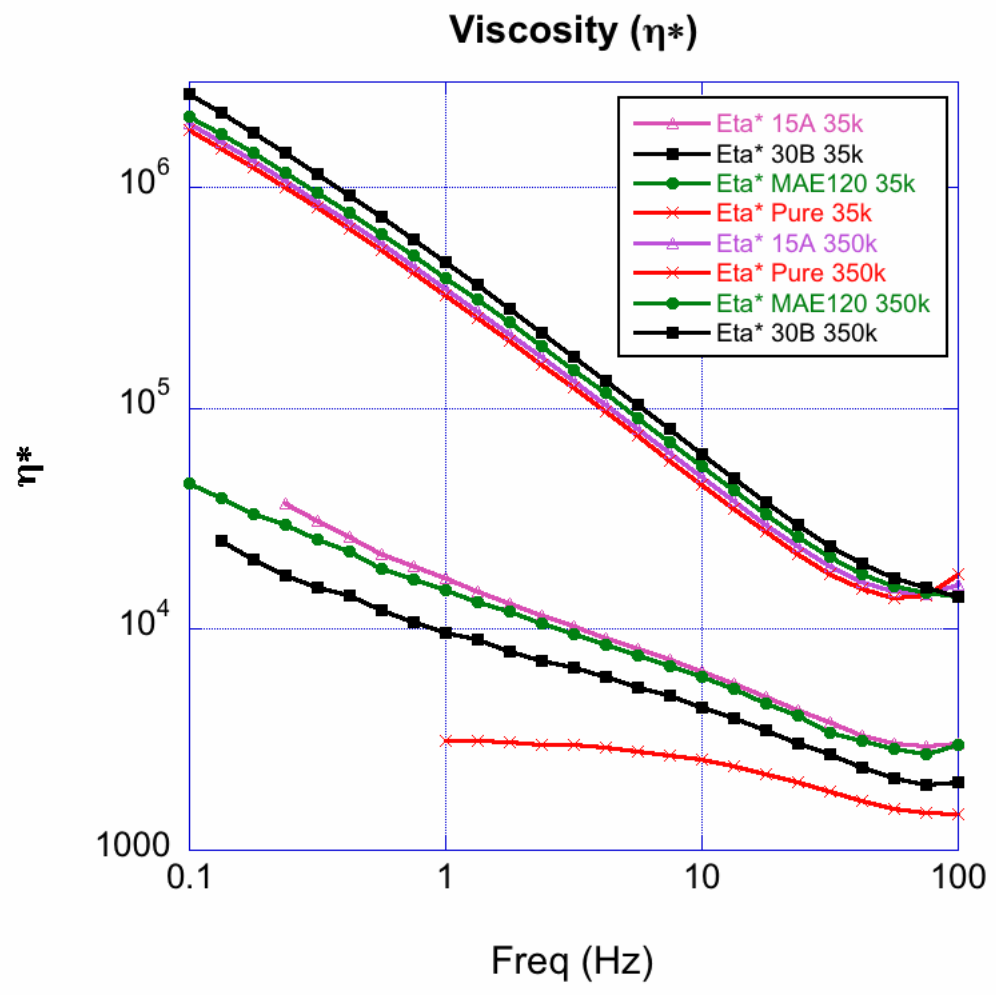

Figure 3.62: Viscosity of Different Nanocomposites

Table 3.10: Glass Transition Temperatures from DSC

Resin Molecular Weight	Filler Type	Filler Weight Percent	Glass Transition Temperature (°C)
25k	None	0	113
25k	C15A	5	115
25k	C30B	5	115
25k	MAE120	5	111
350k	None	0	118
350k	C15A	5	122
350k	C30B	5	101
350k	MAE120	5	106
350k	Grafted	5	113

The organically modified silicate has little impact on the glass transition of the low molecular weight nanocomposite. The high molecular weight Cloisite 30B nanocomposite sample showed a 17°C lower glass transition temperature than that of the pure polymer.

Polymer/layered silicate nanocomposites can be idealized as a polymer film between two impenetrable walls, and the glass transition temperature can be affected by several factors. Those factors include the thickness of the polymer film and wetability between the polymer film and wall [140, 141]. An additional factor is hydrogen bonding between the exposed hydroxyl groups on clay and the oxygen atoms on the PMMA [142]. The effect of film thickness is related to the wetability between the polymer film and the walls. If the the polymer film does not wet the walls, the thinner the film thickness the lower the glass transition temperature [140]. If the polymer film has a strong interaction with the wall, the glass transition temperature should increase with decreasing film thickness. If the film wets the wall but with no strong interactions, the glass transition temperature should not change with film thickness. Assuming the surface of the layered silicate is covered by the hydrocarbon tails of surfactant molecules, no hydrogen bonding should form between the silicate surface and the PMMA polymer and the silicate can be assumed to be non-wetting or poor wetting for the PMMA. There are two different film thicknesses in the nanocomposites, one is the polymer film in the gallery space and a second one is the polymer between the silicate stacks. The thickness of these two films contributes to the change of the glass transition temperature. The hydroxyl groups on the edge of silicates are exposed and can form hydrogen bonds, which should

increase the glass transition temperature. Cloisite 15A and Cloisite 30B clays were both made from Cloisite Na+ clay, so they have the same shape and size distribution and thus should have same amount of hydroxyl groups exposed. The Somasif MAE120 is a modified mica with all the hydroxyl groups replaced by fluorine, so no hydrogen bonding should form. The glass transition of polymer/layered silicate nanocomposites can be described by:

$$T_g = V_1 T_{g1} + V_2 T_{g2} + V_h T_{gh} \tag{3.6}$$

Where V_1 is the volume fraction of polymer in the gallery space, T_{g1} is the glass transition temperature of polymer in the gallery space, V_2 is the volume fraction of polymer between the clay stacks, T_{g1} is the glass transition temperature of polymer between the clay stacks, V_h is the volume fraction of polymer forming hydrogen bonding, and T_{gh} is the glass transition temperature of polymer forming hydrogen bonding.

T_{g2} can be expressed as [141]

$$T_g(h) = T_g^{bulk} + \frac{2\xi}{h_2}(T_g^{interface} - T_g^{bulk}) \tag{3.7}$$

Where h_2 is the thickness of the polymer film between the clay stacks, ξ is the thickness of the interface layer and $T_g^{interface}$ is the glass transition of the interface layer. $T_g^{interface}$ is affected by the wetability or compatibility between the polymer and the wall. If the polymer is fully compatible with the wall, $T_g^{interface}$ will equal T_g^{bulk}, while if the polymer forms an enthalpic favorable interaction with the wall, $T_g^{interface}$ may be higher than T_g^{bulk}, if the polymer is not compatible with the wall, $T_g^{interface}$ may be lower than T_g^{bulk}. The glass transition temperature of polymer in

the gallery space can be calculated in a similar manner, but due to the limited gallery space, the whole film may be effecting an interface layer. Also if there polymer and silicates forms an enthalpic favorable interaction, the silicates may become fully exfoliated eliminating the gallery space.

In the case of the Cloisite 15A nanocomposite, the T_{g1} and T_{g2} terms lower the glass transition temperature, while the T_{gh} item increases the glass transition temperature and dominates the first two terms. As a result the measured glass transition temperature increases. Because of the better dispersion of the silicates, the average distance between the silicates platelets in the Cloisite 30B nanocomposites are smaller than in the Cloisite 15A nanocomposites, and the Cloisite 30B nanocomposite has a smaller h_2 value and the V_2T_{g2} item has a larger absolute value and dominates the hydrogen bonding effect. As a result the glass transition temperature decreased. The PMMA grafted sample has improved polymer-wall compatibility than in the Cloisite 30B nanocomposite, and as a result the observed glass transition temperature increased. For the Somasif MAE120 sample, there is no hydrogen bonding, so the glass transition temperature of the MAE120 sample is lower than the glass transition of the pure polymer.

ξ should be affected by the molecular weight or R_g of polymer and the lower the molecular weight, the smaller ξ [143]. As a result the glass transition temperature for the low molecular weight samples is less affected by the different types of silicates.

3.8 Discussion on the Flammability of Nanocomposites

3.8.1 Mechanism of Low Flammability Nanocomposites

The experiments presented here show that nanocomposites can exhibit significantly reduced flammability compared to the pure matrix polymer. Several explanations have been proposed to explain this observation. The first explanation is the formation of a residue layer at the upper surface of the nanocomposite during gasification, which can shield against radiation entering the polymer matrix and slow the degradation products from entering the gaseous phase and acting as fuel [110, 144]. The second explanation is the clay changes the polymer degradation kinetics by scavenging free radicals due to the iron contained in the clay [145]. A third possibility is that acidic sites created by the surfactant decomposition changes the polymer degradation kinetics [82].

The first explanation is relative easy to understand and is observed in this work. The second explanation is less likely. The iron ions are buried inside the alumina layer of the clay which is sandwiched between two layers of silicate and there is little chance for the iron ions to leave the silicate. For the iron atoms to behave as a free radical scavengers, the radicals need to penetrate the silicate layer to react with the iron ions. In addition, montmorillonites from different geological origins can have Mg^{+2} rather than iron replacing the aluminum in the octahedral site. Reports on the flammability of montmorillonite based nanocomposites from different countries do not vary much [109, 139]. The the nanocomposites with well dispersed Somasif MAE120 synthetic mica (*in situ* polymerization and chloroform

casting) also showed lowered flammability while mica contains little or no iron.

The third explanation is that when the surfactant decomposes, a proton is left at the position of the surfactant as an acidic site. The proton can act as a free radical scavenger. If the scenario described in the third explanation occurs, the flammability of the nanocomposites will be correlated with the amount of acidic sites exposed to the polymer matrix and hence correlated with the amount of clay in the nanocomposite and the degree of exfoliation. If this is true then if the amount of clay increases or the degree of exfoliation increases, the number of acidic sites will increase and the flammability would be expected to drop significantly. However, nanocomposites with Cloisite 30B and Cloisite 15A showed little difference in flammability, although there was a difference in degree of exfoliation. Doubling the amount of clay also showed only a small effect on the flammability as shown in figure 4.5. Generally the surfactant degrades at lower temperature than the polymer matrix and when the polymer matrix begins to degrade the clay platelets may have already collapsed and aggregated, leaving only the exterior surface of the residue exposed to the underlying polymer. Also, if the clay has an effect on the polymer degradation reaction kinetics, the ignition time should be affected by the clay, but no such effect has been observed in cone calorimetry or gasification experiments.

The clay can scavenge free radicals and the results are different for polymerization and thermal degradation. In polymerization, it is assumed that most free radicals are generated at the beginning of the reaction, if a free radical is removed later, there is no new free radical formed to resume the reaction. In thermal degradation, free radicals are generated during the full time span of thermal degradation

process and even if a free radical is eliminated during thermal degradation, the former site of the free radical is probably relatively unstable and could form a new free radical.

Based on this discussion, it is clear that the low flammability of polymer/clay nanocomposites largely arises from physical reasons rather than chemical ones.

3.8.1.1 Structure Integrity

Having a polymer melt with a high viscosity and large complex modulus helps to preserve the structural integrity of the polymer components during a fire.

Structural integrity is important in the real fire situations. If the polymer structure collapses during a fire, the fire can spread more rapidly. If the polymer structure does not collapse, it can help to confine the fire leading to increased safety.

The integrity of a polymeric structure is related to properties such as viscosity, modulus, and char forming ability. If the viscosity of the polymeric material is high, the polymer melt does not readily flow or collapse due to gravity.

3.8.2 Effect of Heat Conductivity on the Fire Safety

The heat conduction process can be expressed by the empirical equation

$$\frac{Q}{t} = -\lambda A \frac{\partial T}{\partial x} \tag{3.8}$$

where Q is the amount of heat, t is time, λ is the heat conductivity, A is the cross section, T is the temperature, and x is the distance in the conducting direction.

The heat conductivity was expressed by Debye as

$$\lambda = c_p \rho s l \tag{3.9}$$

where c_p is the specific heat capacity, ρ is the density, s is the speed of sound in the polymer, and l is the distance between molecules. In the case of polymer/clay nanocomposites the heat conductivity is also affected by the clay particles, which have a higher heat conductivity than the polymer.

The heat conductivity can have a large impact on fire safety on both burning through and fire spreading. On the burning through aspect the heat conductivity has little impact on the flammability of thin polymer walls, but polymer with high thermal conductivity burns faster[146, 147]. For example, ignition requires the material reach a critical temperature, and if the heat conductivity is high, the heat can be more readily dissipated. If a fire is confined in an enclosed space, such as inside a TV set, a cabinet or a room, the heat conductivity of the enclosure or wall has an effect on the ability to contain the fire. If the heat conductivity of the enclosure material is high, the material outside of the enclosure may be ignited by the conducted heat. If the heat conductivity of enclosure material is low, the environment outside is at less risk.

Ideally a structure can be designed that it has a high heat conduction rate at low heat flux and a low heat conduction rate when exposed to a high heat flux. Such structure can consist of a higher heat conduction layer on the surface and a layer beneath the surface layer that can produce bubbles (termed an intumescent material [148]). When the heat flux is low, the surface layer can distribute heat to a

larger surface area to prevent ignition. When the heat flux is large, the intumescent layer can produce bubbles and break the continuity of the surface layer.

Polymer/layered silicate nanocomposites have a higher thermal conductivity before the ignition. The residue has low heat conductivity because it is mostly loosely packed clay. This type of behavior is consistent with a material with good flame retardant properties, however due to the low silicate concentration in nanocomposites the difference in thermal conductivity between the nanocomposite and the pure polymer is relatively small.

Chapter 4

Phosphorus Containing Nanocomposite

4.1 Introduction

To improve flammability it would be beneficial if nanocomposites enhanced char formation during combustion. Char is less flammable compared to most polymers. During combustion polymers release flammable volatile small molecules from the thermal degradation process which fuels the combustion. In contrast char combusts by oxidizing. The oxidization process is a much slower process than the thermal degradation process.

Char is usually a porous solid which has a low heat conduction rate and relatively high modulus compared to polymer melts.

There are two types of char forming polymers, the first type has side groups that are readily removed during degradation. During the thermal degradation, the side groups are removed from the main chain and leave free radicals. The free radicals then form double bonds on the main chain. The main polymer chain then wraps and forms carbon rings. PVC and polyacrylonitrile (PAN) belong to this group of polymers. The char forming properties of PAN has been used to make carbon fibers. The second type of char forming polymer has carbon rings as part of the backbone and during thermal degradation forms char. Polycarbonate belongs to this group of polymers.

By introducing a char forming agent, polymers that are not usually char forming can be modified to form char during thermal degradation. Common char forming agents include halogen, phosphorus and nitrogen compounds. However, if the char forming agent is a small molecule, it can be leached out during the life cycle of the product and lead to decreased flammability resistance and possible environmental issues.

One idea would be to attach the char forming agent to the surface of the clay. Since the clay has a large surface area, a relatively large amount of char forming agent can be introduced into the polymer matrix. It is also possible that the char forming agent attached to the platelets would cause the platelets to fuse together by char. This would give rise to residue composed of char and silicate which could be considered as a layer of silicate reinforced char, and should be stronger than a loosely packed silicate residue layer and increase the potential shielding effect during combustion.

Synergetic behavior of a polymer/layered silicate nanocomposite combined with a char forming agent has been reported, but the char forming agent is not chemically attached to the surface of silicates [149].

4.2 Char Forming Compound

Diethylphosphatoethyltriethoxysilane, which has an phosphate containing silane, was selected as the char forming agent in this research. The silane can be grafted onto the surface of clay by silane chemistry.

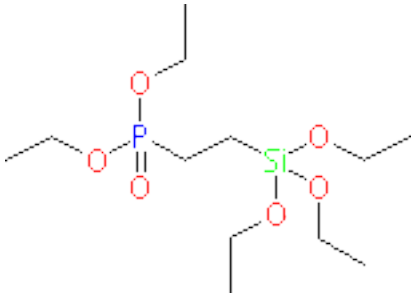

Figure 4.1: Structure of Diethylphosphatoethyltriethoxysilane

Diethylphosphatoethyltriethoxysilane has low toxicity and low environmental impact, it has been used as an anti-piling agent for textile. The structure of diethylphosphatoethyltriethoxysilane is shown in figure 4.1.

4.3 Synthesis

4.3.1 Adding phosphorus to Cloisite 30B Clay

Cloisite 30B clay, diethylphosphatoethyltriethoxysilane, and DMF were mixed at ratio of 2:1:10 with help of sonicating. The mixture was then heated in an oven at 100°C for 3 hours. Then the solution was kept in vacuum at 100°C for 1 hour to remove volatile molecules produced during silanization and to finish the reaction. The clay dispersion in DMF was then mixed with PMMA solution in THF, the nanocomposite is precipitated in water and dried in vacuum at 60°C.

4.4 Structure Characterization with TEM

TEM observation of the nanocomposites with phosphorus modified clay samples are shown in figure 4.2 and 4.3 at low and high magnifications to examine the

dispersion of clay in the PMMA matrix and details of the clay platelets distribution. It can be observed that there are areas with higher mass density around the clay particles, labeled in figure 4.3, which is assumed as to be cross linked diethylphosphatoethyltriethoxysilane.

4.5 Flammability Test

4.5.1 Gasification

The gasification data of nanocomposite samples with phosphorus added clay are shown in figure 4.4. Compared with nanocomposites with 10wt% Cloisite 30B nanocomposite, the nanocomposite containing 10wt% of phosphorus modified clay showed similar ignition time, peak mass loss rate and time to peak mass loss rate. However the total gasification time of phosphorus sample was close to 600 seconds while the total gasification time of sample with Cloisite 30B clay was around 500 seconds. The mean mass loss rate of phosphorus added sample is 7.2 g/sm^2 while the mean mass loss rat of the Cloisite 30B sample is 9.0 g/sm^2 compared to pure PMMA polymer at 19.9 g/sm^2. Compared with the sample without phosphorus, the phosphorus added nanocomposite reduced the mean mass loss rate by about 20%.

4.5.2 Cone Calorimetry

Cone calorimetry data are shown in figure 4.5.

Similar to the gasification experiment, the phosphorus added nanocomposites

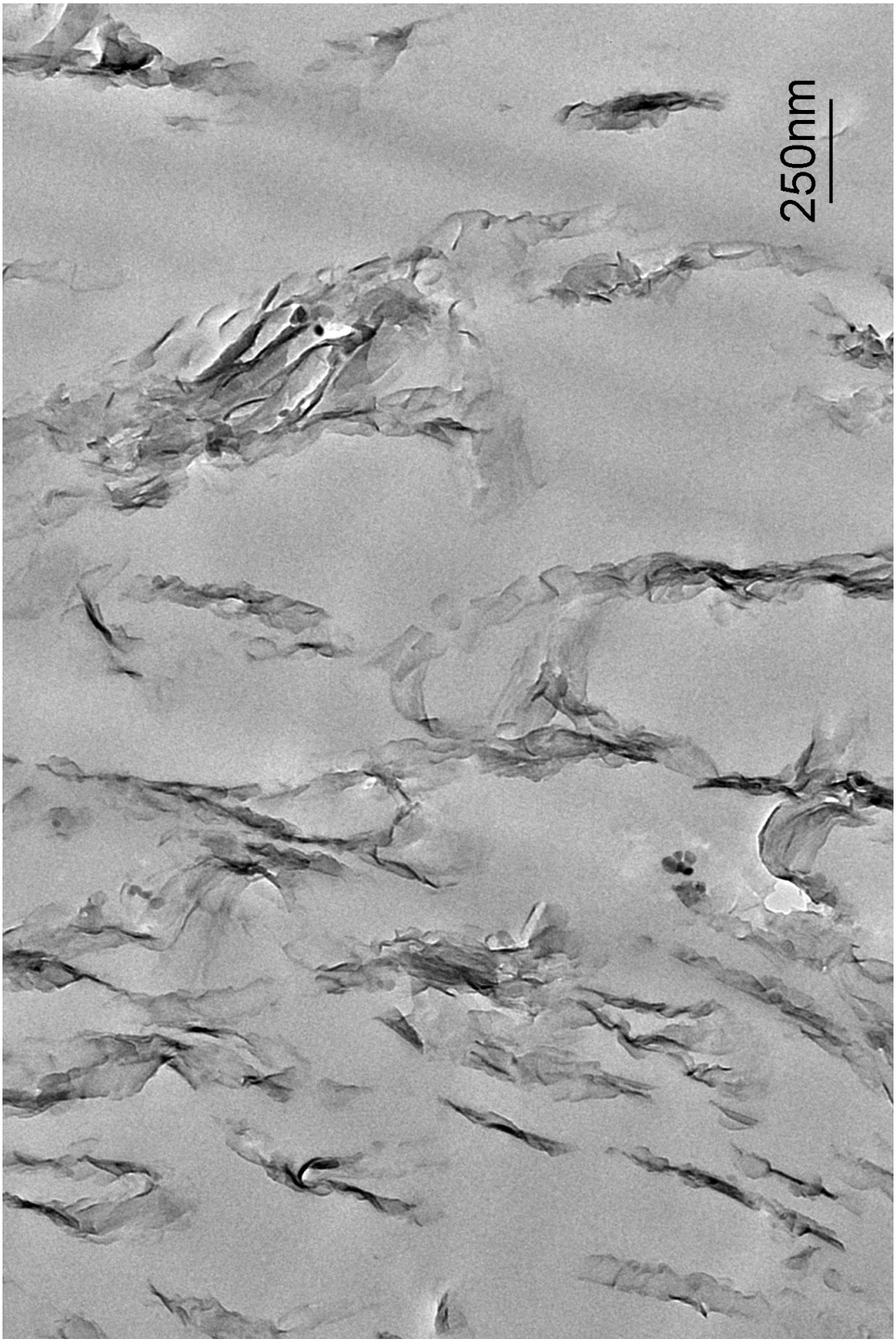

Figure 4.2: TEM of phosphorus Containing Cloisite 30B Clay/PMMA Nanocomposites

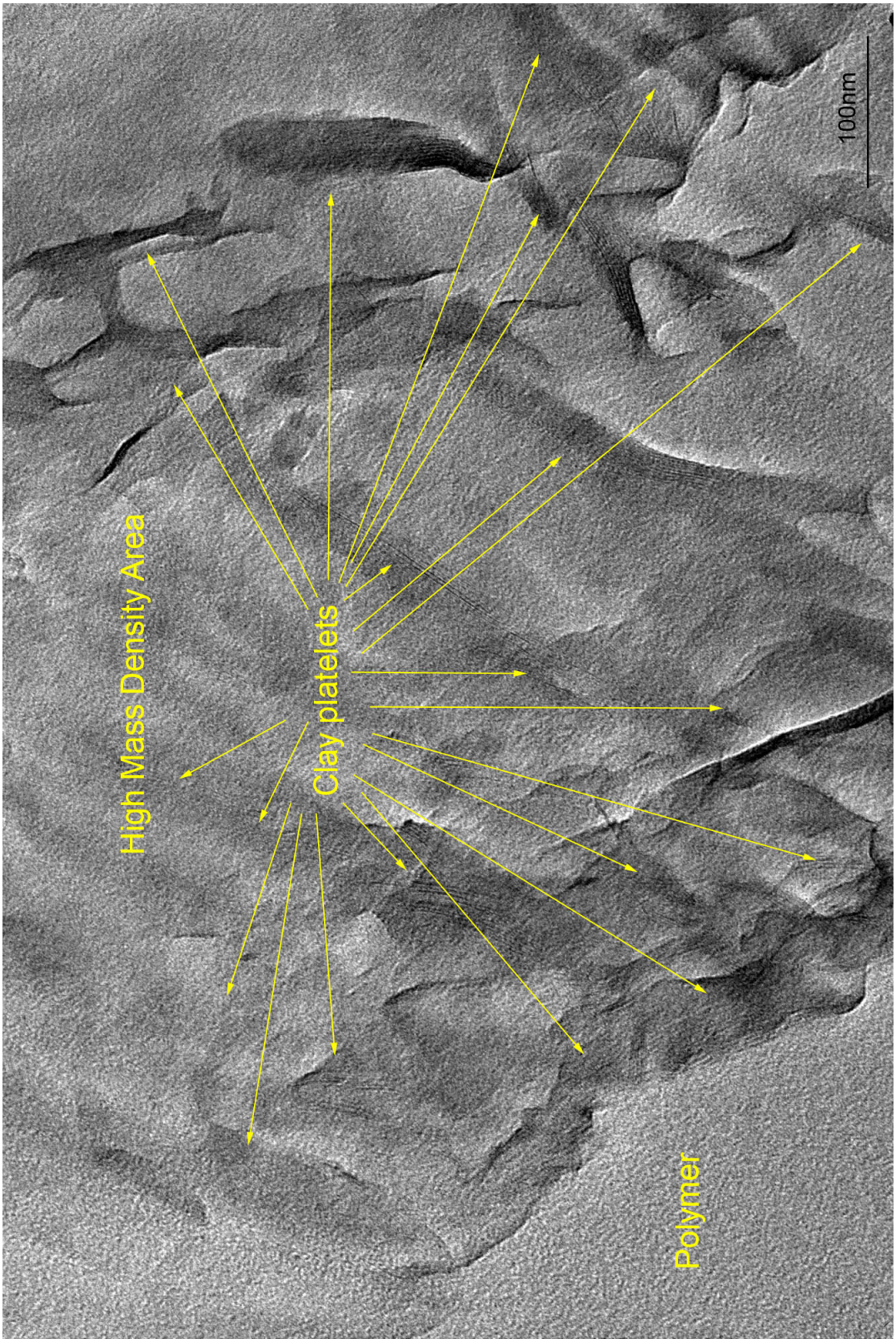

Figure 4.3: TEM of phosphorus Containing Cloisite 30B Clay/PMMA Nanocomposites

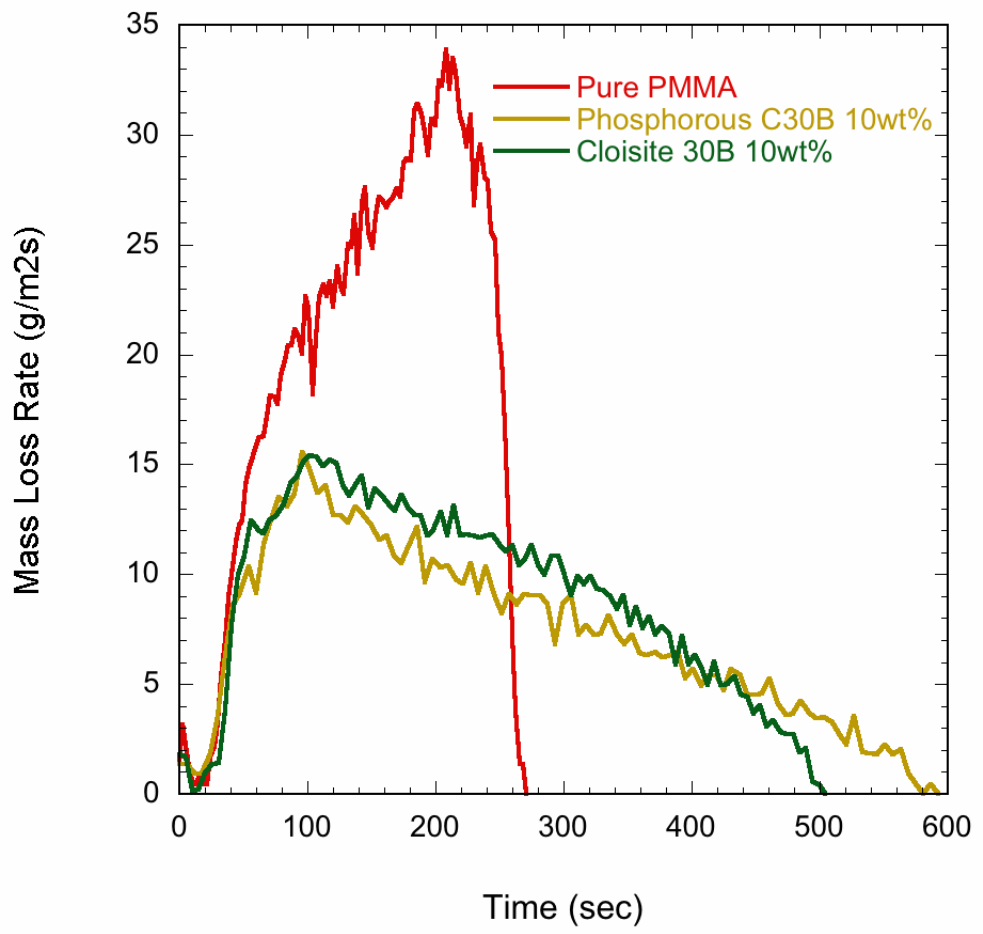

Figure 4.4: Gasification of phosphorus Containing Cloisite 30B Clay/PMMA Nanocomposites

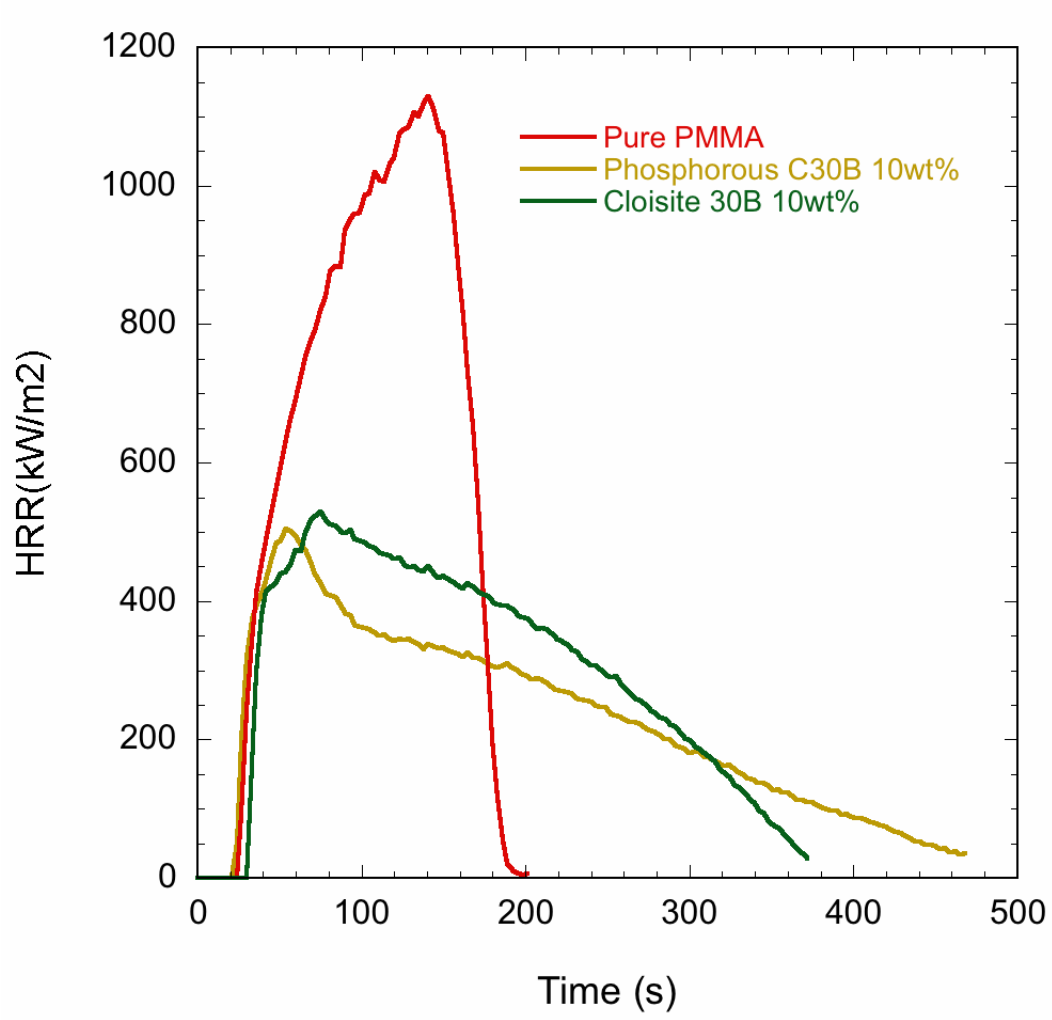

Figure 4.5: Cone Data of phosphorus Containing Clay/PMMA Nanocomposites

showed similar peak heat release rate, but different mean heat release rate. The mean heat release rate of phosphorus added nanocomposite is 224.5 kW/m^2, the mean heat release rate of sample without phosphorus is 298.2 kW/m^2 while the mean heat release rate of the pure polymer is 621.4 kW/m^2. A 25% of reduction in the mean heat release rate was achieved by adding phosphorus to the clay.

The mass evolvement data during the cone calorimetry experiment are shown in figure 4.6. The phosphorus added nanocomposite left 11wt% of residue after cone experiment and the sample with same amount of clay but without phosphorus left 7wt% of residue. The increased 4wt% of residue is assumed to be char formed due to the phosphorus compound.

4.6 Residue Characterization

Residue from the TGA was examined by SEM. The residue from the sample with 10%wt Cloisite 30B and 5%wt phosphorus silane is shown in figures 4.7 and 4.8 at low and high magnification respectively. The original sample was a 0.25 mm thick nanocomposite disk. Figure 4.7 showed bubbles in the residue with diameter as large as 0.8 mm. 4.8 shows the detailed structure of a bubble wall. The wall of the bubble consists of loosely compacted clay stacks. The space between the clay stacks is empty. The additional char formed due to phosphorus is probably attached to the surface or trapped inside the clay stacks.

EDX analysis was also conducted on the residue with results shown in table 4.1. Only a small amount of phosphorus is observed in the residue.

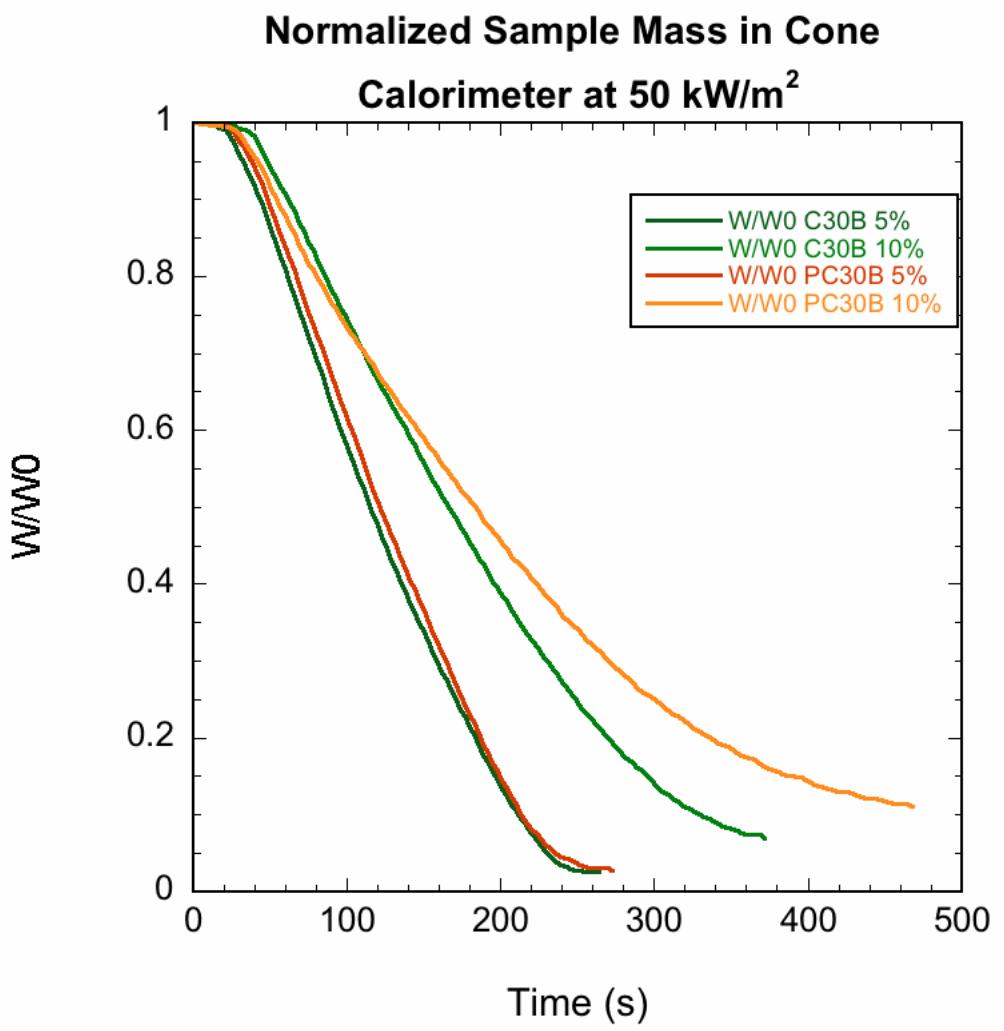

Figure 4.6: Mass Loss During Cone Experiments of phosphorus Containing Clay/PMMA Nanocomposites

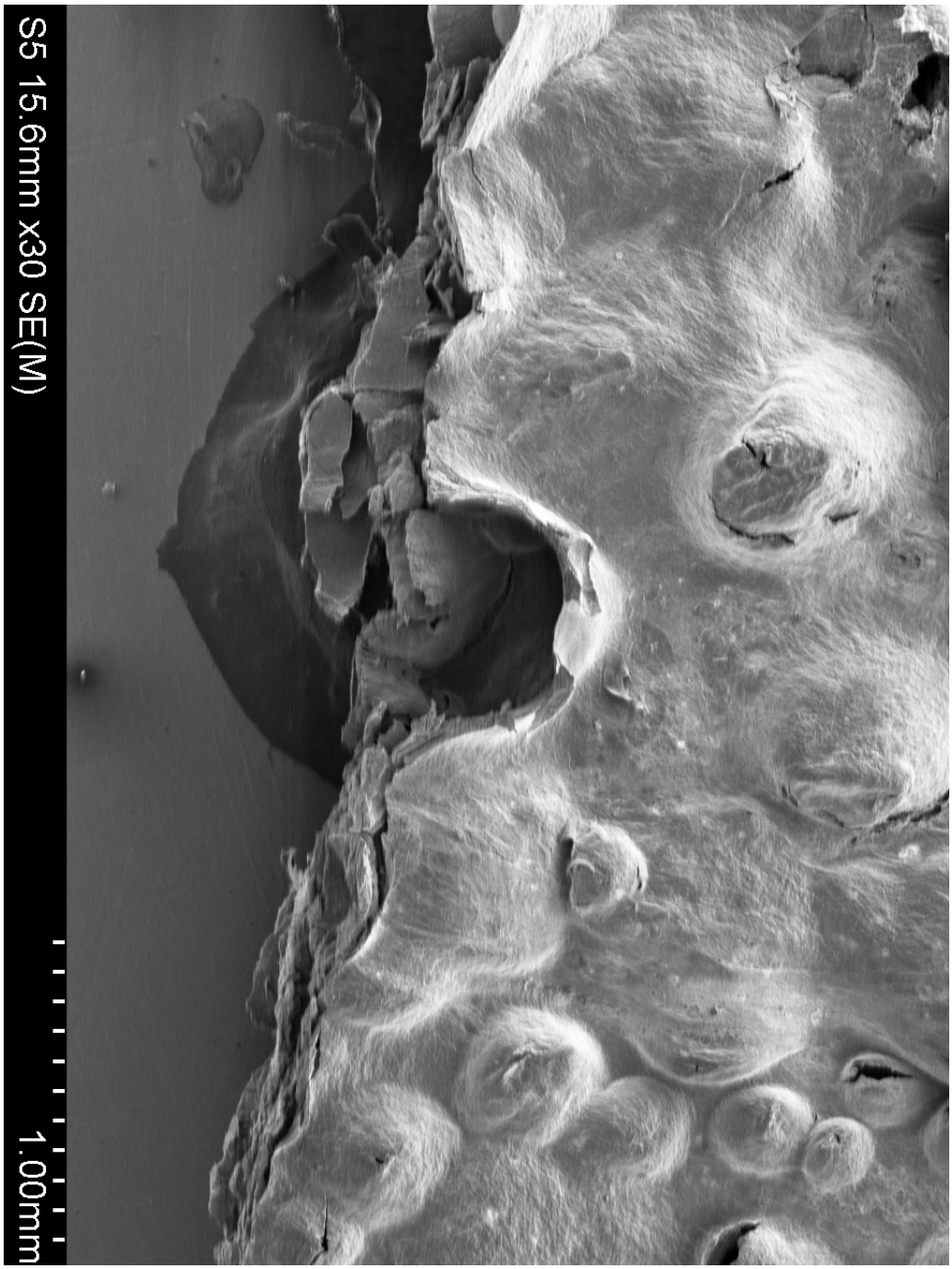

Figure 4.7: Residue from 10wt% of Cloisite 30B/5wt% phosphorus Containing Silane

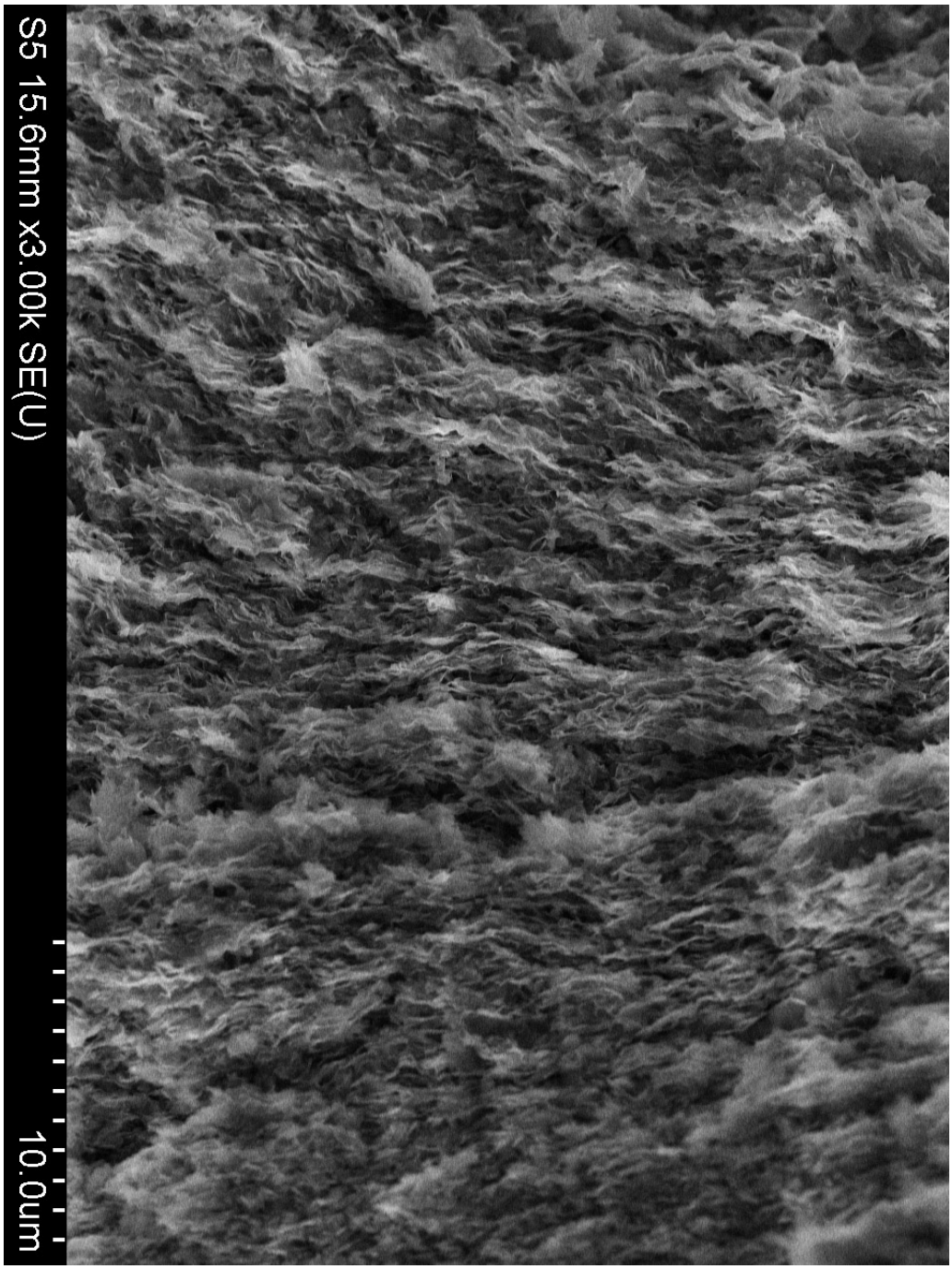

Figure 4.8: Residue from 10wt% of Cloisite 30B/5wt% phosphorus Containing Silane

Table 4.1: EDX Analysis of the Residue from Cloisite 30B Nanocomposites Containing phosphorus Silane

Element	Weight Percentage	Atom Percentage
O	44.48	47.24
C	26.87	38.01
Si	9.01	2.74
Al	3.69	2.32
Mg	0.69	0.48
P	0.61	0.33

4.7 Discussion

4.7.1 Char Formation

The goal of this work was to use phosphorus containing silane to enhance char formation during combustion. The experiments showed some enhanced char formation but the improvement in the char formation was limited.

There are three possible reasons for the relatively small effect of the phosphorus modification on the flammability. First, the char forming ability of the phosphorus (in the form of phosphate) on the selected silane is weak. Second, the ratio of phosphorus to silane is one to one, which may be too small. The sites on the clay for the silane to attach were limited, if there was more phosphorus per silane, more phosphorus could have been attached on the surface of clay. Third, the absolute amount

of phosphorus is relatively small. 4wt% of phosphorus may be added to resins to achieve desired flame retardant ability [150], where there is no more than 0.5wt% of phosphorus added to the PMMA in the phosphorus modification experiment.

4.7.2 Position of the phosphorus Compound During Combustion

The EDX observation examined sample, where the atom ratio of phosphorus is 0.33% and weight percentage is 0.61%. The initial phosphorus content of nanocomposite is about 0.5wt%, and if the phosphorous compound did not leave the condensed phase, the weight percentage of phosphorus in residue should be around 5wt%. It is possible that most of the phosphorus has evaporated during the combustion.

This could explain the difference between the gasification and cone calorimetry experiments. The gasification experiments showed a 20% improvement in the mean mass loss rate and the cone calorimetry experiment showed a 25% improvement in the mean heat release rate. This difference may because the phosphorous atoms in the gaseous phase acted as free radical scavengers and reduced the heat released from the flame. In the gasification experiment, there is no gaseous phase reaction, so such effect was not observed.

Chapter 5

Conclusions

Different layered silicate/PMMA nanocomposites were synthesized by changing the type of the silicate, modification of silicate, polymer molecular weight, and synthesis method to observe the effect of the dispersion of the silicate, the effect of the aspect ratio of silicate, and the molecular weight of the matrix polymer on the flammability of layered silicate/PMMA nanocomposites.

The silicates used included two types of montmorillonite with different organic modifications (Cloisite 15A and Cloisite 30B) and one organically modified synthetic mica (Somasif MAE120).

The structure of the nanocomposites was studied by XRD, SAXS, and TEM. By coupling XRD, SAXS, and TEM together, the dispersion of silicate was determined at different length scales.

Nanocomposites with different degrees of dispersion were produced and confirmed by structural characterization. The flammability of the nanocomposites was characterized by TGA, gasification and cone calorimetry.

An *in-situ* polymerization method was used to produce nanocomposites with a high degree of exfoliation, but the polymer molecular weight reproducibility was relatively poor. A solution mixing method produced nanocomposites with controlled polymer molecular weight but the degree of exfoliation was not as high as the samples

made using the *in-situ* polymerization method. To improve the dispersion for the nanocomposites made by solution mixing, a method to graft short polymer chains onto the silicate surface using a silane coupling agent was developed.

The XRD data showed that the degree of order of the layered silicates in the nanocomposites from high to low is Somasif MAE120, Cloisite 15A, Cloisite 30B and PMMA grafted respectively. Small angle X-ray scattering (SAXS) data confirmed the degree of exfoliation in the nanocomposites from high to low is PMMA grafted, Cloisite 30B, Cloisite 15A and Somasif MAE120. Low magnification TEM confirmed layered silicates are well distributed in the polymer matrix. High magnification TEM confirmed the degree of exfoliation from high to low is consistent with the SAXS data. The structural characterization at different length scales confirmed successful synthesis of nanocomposites with different degrees of exfoliation by changing silicate and that grafting short polymer chains onto the silicates improves the degree of exfoliation. The dispersion in the polymer matrix is further confirmed by glass transition temperature measurements by DSC.

This work confirmed that by forming a well dispersed layered silicate/polymer nanocomposite, the flammability of the nanocomposite can be reduced compared to pure polymer and traditional composite. The peak mass loss rate of nanocomposites can be as low as 53% (low molecular weight) and 48% (high molecular weight) compared to pure PMMA in a gasification experiment. The peak heat release rate of nanocomposites can be as low as 41% (low molecular weight) and 57% (high molecular weight) of pure PMMA in a cone calorimetry experiment. As long as a true nanocomposite is formed, the precise degree of exfoliation has little impact on

the flammability. Nanocomposites with large aspect ratio silicate showed lowered flammability. Nanocomposites with high molecular weight matrix PMMA polymer also showed lowered flammability.

The degradation kinetics of the nanocomposites were also studied, and it was found that nanocomposites showed higher activation energies than the corresponding pure polymers. However the increase in the activation energy is not as important an effect as the stability of the residue layer. Nanocomposites with low molecular weight have an higher activation energy than nanocomposites with high molecular weight, but the nanocomposites with high molecular weight showed lowered flammability. It is also interesting to note that the sample form factor has a significant impact on the nominal reaction order of the nanocomposites as compared to microcomposites or pure polymer. This properties can be used as a quick method to identify the formation of a nanocomposite.

The residues after flammability measurements were examined by SEM and XRD. The residues were loosely packed clay stacks with porous structure. The clay platelets collapsed into stacking structures close to the original unmodified clay structure.

Based on the structural and flammability measurements, it was concluded that the mechanism for lowering the flammability for nanocomposites was from the formation of a shielding layer at the surface of the nanocomposite composed of the collapsed silicate layers. This shielding layer acts to both block heat radiation and to prevent the polymer degradation products from escaping and combusting.

As the improvement in nanocomposite flammability is derived largely from the

physical presence of a residue layer, one method to further lower the flammability is to introduce chemical reagents that can enhance char and residue layer formation during combustion. A phosphorous compound was selected and a method was developed using silane to couple it to the surface of the silicate. The nanocomposites made with phosphorus modified silicate showed enhanced char formation ability and lowered flammability. The nanocomposite with phosphorus modified silicate showed a 20% reduction in mean mass loss rate in a gasification experiment and a 25% reduction in mean heat release rate in a cone calorimetry experiment. This demonstrated a synergy of chemical flame retardants with layered silicate nanocomposites that can further decrease the flammability.

Chapter 6

Future Work

6.1 Introduction

Based on the work presented here and in the literature, it can be concluded that layered silicate nanocomposites do not have low enough flammability to pass industry standards. To increase the flame retardancy, one potential method is to synthesize inorganic phosphate nanocomposites.

Phosphate can potentially enhance the char forming ability of polymer nanocomposites. By enhancing char forming during combustion, the heat release rate and mass loss rate could be lowered and the structural integrity could be enhanced. As a result, the overall flame retardant properties of polymer could be improved.

There are several requirements for the phosphate if it is to be used as a flame retardant. First, the phosphate must have low or no toxicity, which ensures safety in manufacturing, deployment and recycling of the product. Second, the phosphate should be stable at the processing temperature of the polymer, so the phosphate won't prematurely degrade and loose its flame retardancy. Third, the phosphate should have low solubility in water, especially for applications as PCB and IC packaging materials, otherwise it may leach out and cause problems when exposed to a high humidity environment. Phosphates can also lead to environment issues if they leach out into the environment.

It will be an advantage if the phosphate also has a phase transformation (melt, solid state phase transformation, dehydration etc.) at a temperature that is lower than the thermal degradation temperature of the polymer matrix. The phase transformation would absorb energy, lowering the temperature of the polymer matrix. In the case of a small and temporary ignition source (like a candle, match or cigarette), the polymer may not ignite because of the phase transformation. In the case of a large ignition source, the ignition could be postponed.

One of the problems of traditional phosphorous based flame retardants is that the char formation is not uniform, because the phosphorous based flame retardant phase separates into micron sized domains. Only the surface layer of the flame retardant domains can contribute to char formation. If the phosphorous retardant was dispersed as a nanocomposite, it would contribute more effectively as char forming agent during combustion. If the phosphate nanoparticles are well dispersed in the polymer matrix, the char formation should also be more uniform.

Similar to layered silicates, many inorganic phosphates also have a layered structure and many inorganic phosphates also have cation exchange capacity. So it should be possible to organically modify phosphates by cation exchange and produce hydrophobic organically modified phosphates. The organically modified inorganic phosphates should have low water solubility and low chance of leaching out in high humidity environments.

6.2 Proposed Experiment

The proposed experiments can be separated into several steps. The first step is material selection, the second step is synthesis and organic modification of the phosphate nanoparticles, the third step is nanocomposites synthesis, the fourth step is structural characterization and the fifth step is flammability characterization.

6.2.1 Material Selection

There are many inorganic phosphates which are commercially available, some calcium phosphates with their properties are listed in table 6.1 and some others are listed in table 6.2. It can be concluded that the calcium phosphates have the least toxicity [151, 152], the least water solubility and they are potentially the best choice for consideration in synthesizing a nanocomposite.

Octacalcium phosphate can be synthesized by adding phosphate solution to a calcium solution or vice versa [153]. Octacalcium phosphate has a layered structure, and organic modification has been reported [154]. The octacalcium phosphate has been mixed with PEO and some other polyelectrolytes to make composites for bone cement applications [155]. It is possible to make polymer/layered octacalcium phosphate nanocomposites by manner similar to making polymer/layered silicate nanocomposites.

Barium hydrogen phosphate is also a very interesting material with a melting point of $410°C$, which is near the final degradation temperature of PMMA and lower than the degradation temperature of many other polymers. When exposed

to a heat source, barium hydrogen phosphate can absorb energy by melting and shield the surface of polymer by forming a glassy inorganic melt. Barium hydrogen phosphate also has low toxicity. Another potentially interesting inorganic phosphate is zinc phosphate, which has been used as an anticorrosion coating for metals.

Both PMMA and PS would be the logical polymer matrix for this study to examine the effect of flammability on both an unzipping and an unbuttoning type polymer.

6.2.2 Organic Modification of Nanoparticles and Nanocomposite Synthesis

Depending on the phosphate selected, two different organic modification methods could be used. If the phosphate has a layered structure, it could by organically modified by cation exchange. The phosphate would be dispersed in water (or water/ice mixture if the phosphate dissolve in water), then cation surfactant is added to the dispersion. The modified phosphate will become hydrophobic and should phase separate from the water. If the phosphate does not have a layered structure, then the phosphate can be milled into nanoparticles by ball milling or synthesized by a sol-gel method and organically modified by silane or Tyzor ®.

Solution mixing would be the preferred method for making the nanocomposite and the nanocomposite can be retrieved from the solution by either precipitation or evaporating the solvent.

Table 6.1: Commercially Available Calcium Phosphates

Name	CAS No.	Structure	Water Soluble	Toxicity	Tm ($^{\circ}C$)
Tricalcium phosphate	7758-87-4	$Ca_3(PO_4)_2$	no	no, bone and teeth composition [156]	1670 [157]
Hydroxyl-apatite	1306-06-5	$Ca_5(PO4)_3(OH)$	no	no, same as above [158]	800
Octacalcium phosphate	13767-12-9	$Ca_8H_2(PO_4)_6 \cdot 5H_2O$	low	no, bone cement [155, 159]	
Dicalcium phosphate	7757-93-9	$CaHPO_4$	no	no, dietary supplement [160, 161]	
Monocalcium phosphate	7758-23-8	$Ca(H_2PO_4)_2$	no	no, tooth-pastes [162]	1230

Table 6.2: Commercially Available Inorganic Phosphates

Name	CAS No.	Structure	Water Soluble	Toxicity	Tm ($^{\circ}C$)
Aluminum dihydrogen phosphate	13530-50-2	$Al(H_2PO_4)_3$	yes	TSCA listed	?
Aluminum phosphate	7784-30-7	$AlPO_4$	no	TSCA listed	1500
Ammonium hydrogen phosphate	7783-28-0	$(NH_4)_2HPO_4$	yes	TSCA listed	155
Barium hydrogen phosphate	10048-98-3	$BaHPO_4$	yes	Harmful by inhalation and swallow	410
Barium metaphos-phate	13762-83-9	$Ba(PO_3)_2$	no		1560

6.2.3 Structure Characterization

Optical microscopy would be used to examine the existence of large particles. Transmission electron microscopy can be used to study the dispersion of nanoparticles.

SAXS would be used to study the dispersion of nanoparticles. If the selected phosphate has a layered structure, XRD should be used to examine the intercalation and exfoliation of the layered phosphate.

6.2.4 Flammability Characterization

Due to the expected char forming properties, TGA and cone calorimetry would be the major methods used to study the flammability of the polymer/phosphate nanocomposites. Oxygen index flammability can also be used to examine the effect of the phosphate on the flammability. Because the flame retardancy of phosphate is chemical in nature, gasification experiments can only provide supporting data.

Bibliography

[1] H. Murai, Y. Takeda, N. Takano, and K. Ikeda, "Halogen-free materials for PWB and advanced package substrate," in *2000 International Symposium on Advanced Packaging Materials*, 2000.

[2] C. Wong and R. Tummala, *Applied Polymer Science 21st Century*, ch. Polymers for Electronic Packaging in the 12st Century, pp. 659–676. Elsvier, 2000.

[3] J. C. Huang, C. B. He, Y. Xiao, K. Y. Mya, J. Dai, and Y. P. Siow, "Polyimide/poss nanocomposites: interfacial interaction, thermal properties and mechanical properties," *Polymer*, vol. 44, no. 16, pp. 4491–4499, 2003.

[4] S. H. Philips, T. S. Haddad, and S. J. Tomczak, "Developments in nanoscience: polyhedral oligomeric silsesquioxane (POSS)- polymers," *Current Opinion in Solid State and Materials Science*, vol. 8, no. 1, pp. 21–29, 2004.

[5] J. Choi, A. F. Yee, and R. M. Laine, "Toughening of cubic silsesquioxane epoxy nanocomposites using core-shell rubber particles: A three-component hybrid system," *Macromolecules*, vol. 37, no. 9, pp. 3267–3276, 2004.

[6] Z. Tang and N. A. Kotov, "One-dimensional assemblies of nanoparticles: Preparation, properties, and promise," *Advanced Materials*, vol. 17, no. 8, pp. 951–962, 2005.

[7] E. Tang, G. Cheng, X. Pang, X. Ma, and F. Xing, "Synthesis of nano-ZnO/poly(methyl methacrylate) composite microsphere through emulsion polymerization and its UV-shielding property," *Colloid and Polymer Science*, vol. 284, no. 4, pp. 422 – 428, 2006.

[8] S. Pothukuchi, Y. Li, and C. P. Wong, "Development of a novel polymer-metal nanocomposite obtained through the route of in situ reduction for integral capacitor application," *Jounal of Applied Polymer Science*, vol. 93, no. 4, pp. 1531–1538, 2004.

[9] D. H. Cole, K. R. Shull, L. E. Rehn, and P. Baldo, "Metal-polymer interations in a polymer/metal nanocomposite," *Physical Review Letter*, vol. 78, no. 26, pp. 5006–5009, 1997.

[10] N. Seteunou, S. Forster, P. Florian, C. Sanchez, and M. Antonietti, "Synthesis of nanostructured polymer-titanium oxide composites through the assembly of titanium-oxo clusters and amphiphilic block copolymer micelles," *Journal of Materials chemistry*, vol. 12, no. 12, pp. 3426–3430, 2002.

[11] G.-H. Hsiue, J.-K. Chen, and Y.-L. Liu, "Synthesis and characterization of nanocomposite of polyimide-silica hybrid from nanoqueous sol-gel process," *Journal of Applied Polymer Science*, vol. 76, no. 11, pp. 1609–1618, 2000.

[12] S. K. Young and K. A. Mauritz, "Nafion/(organically modified silicate) nanocomposites via polymer in situ sol-gel reactions: Mechanical tensile properties," *Journal of Polymer Scioence: Part B: Polymer Physics*, vol. 40, no. 19, pp. 2237–2247, 2002.

[13] R. Andrews, D. Jacques, D. Qian, and T. Rantell, "Multiwall carbon nanotubes: Synthesis and application," *Accounts of Chemical Research*, vol. 35, no. 12, 2002.

[14] R. H. Baughman, A. A. Zakhidov, and W. A. d. Heer, "Carbon nanotubes - the route toward applications," *Science*, vol. 297, no. 5582, pp. 787–792, 2002.

[15] F. M. Du, R. C. Scogna, W. Zhou, S. Brand, J. E. Fischer, and K. I. Winey, "Nanotube networks in polymer nanocomposites: Rheology and electrical conductivity," *Macromolecules*, vol. 37, no. 24, pp. 9048–9055, 2004.

[16] H. Chung, K. Cho, C. Y. Ryu, and P. M. Ajayan, "Single-step in situ synthesis of polymer-grafted single-wall nanotube composite," *Journal of American Chemical Society*, vol. 125, no. 31, pp. 9258–9259, 2003.

[17] K. W. Putz, C. A. Mitchell, R. Krishnamoorti, and P. F. Green, "Elastic modulus of single-walled carbon nanotube/poly(methyl methacrylate) nanocomposites," *Journal of Polymer Science: Part B: Polymer Physics*, vol. 42, no. 12, pp. 2286–2293, 2004.

[18] B. C. Satishkumar, A. Govindaraj, J. Mofokeng, G. N. Subbanna, and C. N. R. Rao, "Novel experiments with carbon nanotubes: opening, filling closing and functionalizing nanotubes," *Journal of Physics B: Atomic, Molecular and Optical Physics*, vol. 29, no. 21, pp. 4925–4934, 1996.

[19] L. Valentini, J. Biagiotti, J. M. Kenny, and S. Santucci, "Effects of single-walled carbon nanotubes on the crystallization behavior of polypropylene," *Journal of Applied Polymer Science*, vol. 87, no. 4, pp. 708–713, 2003.

[20] L. Valentini, J. Biagiotti, J. M. Kenny, and M. A. L. Manchado, "Physical and mechanical behavior of single-walled carbon nanotube/polypropylene/ethylene-propylene-diene rubber nanocomposites," *Journal of Applied Polymer Science*, vol. 89, no. 10, pp. 2657–2663, 2003.

[21] N. Zhang, J. Xie, and V. K. Varadan, "Functionalization of carbon nanotubes by potassium permanganate assisted with phase transfer catalyst," *Smart Materials and Structure*, vol. 11, no. 6, 2002.

[22] C. Park, Z. Ounaies, K. A. Watson, R. E. Crooks, J. S. Jr., S. E. Lowther, J. W. Connell, E. J. Siochi, J. S. Harrison, and T. L. S. Clair, "Dispersion of single wall carbon nanotubes by in situ polymerization under sonication," *Chemical Physics Letters*, vol. 364, no. 3-4, pp. 303–308, 2002.

[23] D. Gong, C. A. Grimes, O. K. Varghese, W. Hu, R. S. Singh, Z. Chen, and E. C. Dickey, "Titanium oxide nanotube arrays prepared by anodic oxidation," *Journal of Materials Research*, vol. 16, no. 12, 2001.

[24] D. Golberg, Y. Bandoi, L. Bourgeois, K. Kurashima, and T. Sato, "Insights into the structure of BN nanotubes," *Applied Physics Letters*, vol. 77, no. 13, 2001.

[25] G. L. Frey, R. Tenne, M. J. Mathews, M. S. Dresselhaus, and G. Dresselhaus, "Optical properties of MS_2 (M = Mo, W) inorganic fullerene like and nanotube material optical absorption and resonance raman measurements," *Journal of Materials Research*, vol. 13, no. 9, 1998.

[26] "http://webmineral.com/data/halloysite.shtml."

[27] H. L. Frisch and J. E. Mark, "Nanocomposites prepared by threading polymer chains through zeolites, mesoporous silica, or silica nanotubes," *Chemistry of Materials*, vol. 8, no. 8, pp. 1735–1738, 1996.

[28] G.-H. Chen, D.-J. Wu, W.-G. Weng, and W.-L. Yan, "Preparation of polymer/graphite conducting nanocomposite by intercalation polymerization," *Journal of Applied Polymer Science*, vol. 82, no. 10, pp. 2506–2513, 2001.

[29] F. Leroux and J. P. Besse, "Polymer interleaved layered double hydroxide: A new emerging class of nanocomposites," *Chemistry of Materials*, vol. 13, no. 10, pp. 3507–3515, 2001.

[30] F. Leroux and C. Taviot-Gueho, "Fine tuning between organic and inorganic host structure: new trends in layered double hydroxide hybrid assemblies," *Journal of Materials Chemistry*, vol. 15, no. 35-36, pp. 3628–3642, 2005.

[31] S. O'Leary, D. O'Hare, and G. Seeley, "Delamination of layered double hydroxides in polar monomers: new LDH-acrylate nanocomposites," *Chemical Communications*, no. 14, pp. 1506–1507, 2002.

[32] H. B. Hsueh and C. Y. Chen, "Preparation and properties of LDHs/epoxy nanocomposites," *Polymer*, vol. 44, no. 18, pp. 5275–5283, 2003.

[33] H. B. Hsueh and C. Y. Chen, "Preparation and properties of LDHs/polyimide nanocomposites," *Polymer*, vol. 44, no. 4, pp. 1151–1161, 2003.

[34] J. W. Jordan, "Lubricants." United States Patent 2,531,440, 1950.

[35] E. A. Hauser, "Modified gel-forming clay and process of producing same." United States Patent 2531427, 1950.

[36] T. Kurauchi, A. Okada, T. Nomura, T. Nishio, S. Saegusa, and R. Deguchi, "Nylon 6-clay hybrid - synthesis, properties and application to automotive timing belt cover," *International Congress & Exposition, February 1991, Detroit, MI, USA*, 1991.

[37] Y. Kojima, A. Usuki, M. Kawasumi, A. Okada, Y. Kurauchi, and O. Kamigaito, "Synthesis of nylon6-clay hybrid by montmorillonite intercalated with ϵ-caprolactam," *Journal of Polymer Science: Part A: Polymer Chemistry*, vol. 31, no. 4, pp. 983–986, 1993.

[38] Y. Kojima, A. Usuki, M. Kawasumi, A. Okada, T. Kurauchi, O. Kamigaito, and K. Kaji, "Fine structure of nylon-6-clay hybrid," *Journal of Polymer Science: Part B: Polymer Physics*, vol. 32, no. 4, pp. 625–630, 1994.

[39] M. N. Bureau, J. Denault, K. C. Cole, and G. D. Enright, "The role of crystallinity and reinforcement in the mechanical behavior of polyamide-6/clay nanocomposites," *Polymer Engineering and Science*, vol. 42, no. 9, pp. 1897–1906, 2002.

[40] "http://www.americancarfans.com/news.cfm/newsid/ 2041021.012/ page/ 1/ hummer/1.html."

[41] "http://www.specialchem4polymers.com/ resources/ latest/ displaynews.aspx ? id = 1965."

[42] L. M. Sherman, "Chasing nanocomposites, http:// www. plasticstechnology. com /articles/200411fa2.html."

[43] M. Alexandre and P. Dubois, "Polymer-layered silicate nanocomposites: preparation, properties and uses of a new class of materials," *Materials Science & Engineering R-Reports*, vol. 28, no. 1-2, pp. 1–63, 2000.

[44] R. A. Vaia and E. P. Giannelis, "Polymer nanocomposites: Status and opportunities," *MRS Bulletin*, vol. 26, no. 5, pp. 394–401, 2001.

[45] E. P. Giannelis, "Polymer layered silicate nanocomposites," *Advanced Materials*, vol. 8, no. 1, pp. 29–&, 1996.

[46] M. Biswas and S. S. Ray, "Recent progress in synthesis and evaluation of polymer-montmorillonite nanocomposites," in *New Polymerization Techniques and Synthetic Methodologies*, vol. 155 of *Advances in Polymer Science*, pp. 167–221, Springer Berlin / Heidelberg, 2001.

[47] M. Alexandre, P. Dubois, T. Sun, J. M. Garces, and R. Jerome, "Polyethylene-layered silicate nanocomposites prepared by the polymerization-filling technique: synthesis and mechanical properties," *Polymer*, vol. 43, no. 8, pp. 2123–2132, 2002.

[48] M. Arroyo, M. A. Lopez-Manchado, and B. Herrero, "Organo-montmorillonite as substitute of carbon black in natural rubber compounds," *Polymer*, vol. 44, no. 8, pp. 2447–2453, 2003.

[49] S. D. Burnside and E. P. Giannelis, "Synthesis and properties of new poly(dimethylsiloxane) nanocomposites," *Chemistry of Materials*, vol. 7, no. 9, pp. 1597–1600, 1995.

[50] J. M. Brown, D. Curliss, and R. A. Vaia, "Thermoset-layered silicate nanocomposites. quaternary ammonium montmorillonite with primary diamine cured epoxies," *Chemistry of Materials*, vol. 12, no. 11, pp. 3376–3384, 2000.

[51] S. Bourbigot, E. Devaux, and X. Flambard, "Flammability of polyamide-6 /clay hybrid nanocomposite textiles," *Polymer Degradation and Stability*, vol. 75, no. 2, pp. 397–402, 2002.

[52] Y. B. Cai, Q. Li, Q. F. Wei, Y. B. Wu, L. Song, and Y. Hu, "Structures, thermal stability, and crystalline properties of polyamide6/organic-modified fe-montmorillonite composite nanofibers by electrospinning," *Journal of Materials Science*, vol. 43, no. 18, pp. 6132–6138, 2008.

[53] X. Cao, L. J. Lee, T. Widya, and C. Macosko, "Polyurethane/clay nanocomposites foams: processing, structure and properties," *Polymer*, vol. 46, no. 3, pp. 775–783, 2005.

[54] J. H. Chang and Y. U. An, "Nanocomposites of polyurethane with various organoclays: Thermomechanical properties, morphology, and gas permeability," *Journal of Polymer Science Part B-Polymer Physics*, vol. 40, no. 7, pp. 670–677, 2002.

[55] J. H. Chang, Y. U. An, D. H. Cho, and E. P. Giannelis, "Poly(lactic acid) nanocomposites: comparison of their properties with montmorillonite and synthetic mica(ii)," *Polymer*, vol. 44, no. 13, pp. 3715–3720, 2003.

[56] J. H. Chang, S. J. Kim, Y. L. Joo, and S. Im, "Poly(ethylene terephthalate) nanocomposites by in situ interlayer polymerization: the thermo-mechanical properties and morphology of the hybrid fibers," *Polymer*, vol. 45, no. 3, pp. 919–926, 2004.

[57] L. Chen, S. C. Wong, and S. Pisharath, "Fracture properties of nanoclay-filled polypropylene," *Journal of Applied Polymer Science*, vol. 88, no. 14, pp. 3298–3305, 2003.

[58] D. M. Delozier, R. A. Orwoll, J. F. Cahoon, N. J. Johnston, J. G. Smith, and J. W. Connell, "Preparation and characterization of polyimide/organoclay nanocomposites," *Polymer*, vol. 43, no. 3, pp. 813–822, 2002.

[59] X. L. Ji, J. K. Jing, W. Jiang, and B. Z. Jiang, "Tensile modulus of polymer nanocomposites," *Polymer Engineering and Science*, vol. 42, no. 5, pp. 983–993, 2002.

[60] J. Jordan, K. I. Jacob, R. Tannenbaum, M. A. Sharaf, and I. Jasiuk, "Experimental trends in polymer nanocomposites - a review," *Materials Science and Engineering A-Structural Materials Properties Microstructure and Processing*, vol. 393, no. 1-2, pp. 1–11, 2005.

[61] J. Lange and Y. Wyser, "Recent innovations in barrier technologies for plastic packaging - a review," *Packaging Technology and Science*, vol. 16, no. 4, pp. 149–158, 2003.

[62] R. K. Bharadwaj, "Modeling the barrier properties of polymer-layered silicate nanocomposites," *Macromolecules*, vol. 34, no. 26, pp. 9189–9192, 2001.

[63] G. Gorrasi, M. Tortora, V. Vittoria, E. Pollet, B. Lepoittevin, M. Alexandre, and P. Dubois, "Vapor barrier properties of polycaprolactone montmorillonite nanocomposites: effect of clay dispersion," *Polymer*, vol. 44, no. 8, pp. 2271–2279, 2003.

[64] L. Y. Jiang, C. M. Leu, and K. H. Wei, "Layered silicates/fluorinated polyimide nanocomposites for advanced dielectric materials applications," *Advanced Materials*, vol. 14, no. 6, pp. 426–+, 2002.

[65] R. D. D. R. B. Seymour, ed., *History of Polymeric Composites*, ch. A history of Halogenated Flame Retardants, pp. 270–297. VNU Science Press, 1987.

[66] T. G. Gopakumar, J. A. Lee, M. Kontopoulou, and J. S. Parent, "Influence of clay exfoliation on the physical properties of montmorillonite/polyethylene composites," *Polymer*, vol. 43, no. 20, pp. 5483–5491, 2002.

[67] A. S. Zerda and A. J. Lesser, "Intercalated clay nanocomposites: Morphology, mechanics, and fracture behavior," *Journal of Polymer Science Part B-Polymer Physics*, vol. 39, no. 11, pp. 1137–1146, 2001.

[68] R. C. Melenz and M. E. King, "Physical-chemical properties and engineering performance of clays," *Clays and Clay Minerals*, vol. 1, p. 196, 1952.

[69] G. W. Brindley, "Structural mineralogy of clays," *Clays and Clay Minerals*, vol. 1, p. 33, 1952.

[70] A. Meunier, *Clays*. Springer, 2005.

[71] D. M. C. McEwan, "Interlamellar reactions of clays and other substances," *Clays and Clay Minerals*, vol. 9, p. 431, 1961.

[72] E. B. Kinter and S. Diamond, "Characterization of montmorillonite saturated with short-chain amine cations: 2. interlayer surface coverage by the amine cations," *Clays and Clay Minerals*, vol. 10, p. 174, 1962.

[73] S. Yariv and H. Cross, eds., *Organo-Clay Complexes and Interactions*. Marcel Dekker, Inc., 2002.

[74] J. James L. McAtee, "Random interstratification in organophilic bentonites," *Clays and Clay Minerals*, vol. 1, p. 308, 1957.

[75] S. Diamond and E. B. Kinter, "Characterization of montmorillonite saturated with short-chain amine cations: 1. interpretation of basal spacing measurements," *Clays and Clay Minerals*, vol. 10, p. 163, 1962.

[76] R. Tettenhorst, C. W. Beck, and G. Brunton, "Montmorillonite-polyalcohol complexes," *Clays and Clay Minerals*, vol. 9, p. 500, 1961.

[77] D. R. Lewis, "Ion exchange reactions of clays," *Clays and Clay Minerals*, vol. 1, p. 54, 1952.

[78] M. S. Stul and W. J. Mortier, "The heterogeneity of the charge density in montmorillonites," *Clays and Clay Minerals*, vol. 22, no. 5, p. 391, 1974.

[79] C. A. Cody and E. D. Magauran, "Method of treating waste water for organic contaminants with water dispersible organically modified smectite clay compositions." United States Patent: 5130028, July 1992.

[80] M. I. Cohn, "Rubber composition reinforced with a clay which contains olefinically un- saturated cations." United States Patent: 2697699, 1954.

[81] A. R. Swoboda and G. W. Kunze, "Infrared study of pyridine adsorbed on montmorillonite surfaces," *Clays and Clay Minerals*, vol. 13, p. 277, 1965.

[82] M. Zanetti, G. Camino, P. Reichert, and R. Mulhaupt, "Thermal behaviour of poly(propylene) layered silicate nanocomposites," *Macromolecular Rapid Communications*, vol. 22, no. 3, pp. 176–180, 2001.

[83] E. P. Plueddemann, *Silane coupling agents*. Plenum press, 1982.

[84] K. Song and G. Sand, "Characterization of montmorillonite surfaces after modification by organosilane," *Clays and Clay Minerals*, vol. 49, no. 2, pp. 119–125, 2001.

[85] J. G. Zhang, E. Manias, and C. A. Wilkie, "Polymerically modified layered silicates: An effective route to nanocomposites," *Journal of Nanoscience and Nanotechnology*, vol. 8, no. 4, pp. 1597–1615, 2008.

[86] J. Ma, H. Xu, J. H. Ren, Z. Z. Yu, and Y. W. Mai, "A new approach to polymer/montmorillonite nanocomposites," *Polymer*, vol. 44, no. 16, pp. 4619–4624, 2003.

[87] T. Kashiwagi, "Polymer combustion and flammability - role of the condensed phase," in *Twenty-Fifth Symposium (International) on the Combustion/ The Combustion Institute*, pp. 1423–1437, 1999.

[88] C. D. craver and J. Charles E. Carraher, eds., *Applied Polymer Science 21st Century*. Elsevier, 2000.

[89] "federal trade commision complaint on the flammability of plastic products file no. 732-3040," May 1973.

[90] A. F. Grand and C. A. Wilkie, eds., *Fire Retardancy of Polymeric Materials*. CRC Press, 2000.

[91] "How flame retardants prevent fire, http://www.firesafetyinfo.org/ flameretardants/ flameretardants.htm."

[92] L. W. Jacobs, S. F. Chou, and J. M. Tiedje, "Fate of polybrominated biphenyls (PBBS) in soils - persistence and plant uptake," *Journal of Agricultural and Food Chemistry*, vol. 24, no. 6, pp. 1198–1201, 1976.

[93] A. Blum and B. N. Ames, "Flame-retardant additives as possible cancer hazards," *Science*, vol. 195, no. 4273, pp. 17–23, 1977.

[94] A. Kierkegaard, L. Balk, U. Tjarnlund, C. A. De Wit, and B. Jansson, "Dietary uptake and biological effects of decabromodiphenyl ether in rainbow trout (oncorhynchus mykiss)," *Environmental Science & Technology*, vol. 33, no. 10, pp. 1612–1617, 1999.

[95] K. Hooper and T. A. McDonald, "The PBDEs: An emerging environmental challenge and another reason for breast-milk monitoring programs," *Environmental Health Perspectives*, vol. 108, no. 5, pp. 387–392, 2000.

[96] A. Sjodin, L. Hagmar, E. Klasson-Wehler, J. Bjork, and A. Bergman, "Influence of the consumption of fatty baltic sea fish on plasma levels of halogenated environmental contaminants in Latvian and Swedish men," *Environmental Health Perspectives*, vol. 108, no. 11, pp. 1035–1041, 2000.

[97] P. O. Darnerud, G. S. Eriksen, T. Johannesson, P. B. Larsen, and M. Viluksela, "Polybrominated diphenyl ethers: Occurrence, dietary exposure, and toxicology," *Environmental Health Perspectives*, vol. 109, no. Suppl. 1, pp. 49–68, 2001.

[98] K. Booij, B. N. Zegers, and J. P. Boon, "Levels of some polybrominated diphenyl ether (PBDE) flame retardants along the dutch coast as derived from their accumulation in spmds and blue mussels (mytilus edulis)," *Chemosphere*, vol. 46, no. 5, pp. 683–688, 2002.

[99] Y. L. Liu, G. H. Hsiue, C. W. Lan, and Y. S. Chiu, "Flame-retardant polyurethanes from phosphorus-containing isocyanates," *Journal of Polymer Science: Part A: Polymer Chemistry*, vol. 35, no. 9, pp. 1769–1780, 1997.

[100] Y. L. Liu, G. H. Hsiue, C. W. Lan, J. K. Kuo, R. J. Jeng, and Y. S. Chiu, "Synthesis, thermal properties, and flame retardancy of phosphorus containing polyimides," *Journal of Applied Polymer Science*, vol. 63, no. 7, pp. 875–882, 1997.

[101] Y. L. Liu, G. H. Hsiue, and Y. S. Chiu, "Synthesis, characterization, thermal, and flame retardant properties of phosphate-based epoxy resins," *Journal of Polymer Science: Part A: Polymer Chemistry*, vol. 35, no. 3, pp. 565–574, 1997.

[102] "Survey of alternatives to tin-lead solder and brominated flame retardants, http://ieeexplore.ieee.org/iel5/7364/19985/00924545.pdf."

[103] M. Pecht and Y. Deng, "Electronic device encapsulation using red phosphorus flame retardants," *Microelectronics Reliability*, vol. 46, no. 1, pp. 53–62, 2006.

[104] J. W. Gilman, G. L. Jackson, A. B. Morgan, and R. H. Jr., "Flammability properties of polymer-layered-silicate nanocomposites. polypropylene and polystyrene nanocomposites," *Chemistry of Materials*, vol. 12, no. 7, pp. 1866–1873, 2000.

[105] T. Kashiwagi, J. W. Gilman, K. M. Butler, R. H. Harris, H. r. Shields, and A. Asano, "Flame retardant mechanism of silica gel/silica," *Fire and Materials*, vol. 24, no. 6, pp. 277–289, 2000.

[106] T. Kashiwagi, J. R. Shields, R. H. H. Jr., and R. D. Davis, "Flame - retardant mechanism of silica: Effect of resin molecular weight," *Journal of Applied Polymer Science*, vol. 87, no. 9, pp. 1541–1553, 2003.

[107] T. Kashiwagi, E. Grulke, J. Hilding, R. Harris, W. Awad, and J. Douglas, "Thermal degradation and flammability properties of poly(propylene)/carbon nanotube composites," *Macromolecular rapid communication*, vol. 23, no. 13, pp. 761–765, 2002.

[108] T. Kashiwagi, R. H. H. Jr., X. Zhang, R. M. Briber, B. H. Cipriano, S. R. Raghawan, W. H. Awad, and J. R. Shields, "Flame retardant mechanism of polyamide 6 - clay nanocomposite," *Polymer*, vol. 45, no. 3, pp. 881–891, 2003.

[109] A. B. Morgan, J. W. Gilman, T. Kashiwagi, and C. L. Jackson, "Flammability of polymer-clay nanocomposites," in *Fire Safety developments Emerging Needs, Product Developments, Nonhalogen FR's, Standards and Regulations. Proceedings. Fire Retardant Chemicals Association.*, pp. 25–39, 2000.

[110] J. W. Gilman, "Flammability and thermal stability studies of polymer layered-silicate (clay) nanocomposites," *Applied Clay Science*, vol. 15, no. 1-2, pp. 31–49, 1999.

[111] G. Jimenez, N. Ogata, H. Kawai, and T. Ogihara, "Structure and thermal/mechanical properties of poly(epsilon-caprolactone)-clay blend," *Journal of Applied Polymer Science*, vol. 64, no. 11, pp. 2211–2220, 1997.

[112] D. Y. Wang, J. Zhu, Q. Yao, and C. A. Wilkie, "A comparison of various methods for the preparation of polystyrene and poly(methyl methacrylate)

clay nanocomposites," *Chemistry of Materials*, vol. 14, no. 9, pp. 3837–3843, 2002.

[113] M. Zanetti, T. Kashiwagi, L. Falqui, and G. Camino, "Cone calorimeter combustion and gasification studies of polymer layered silicate nanocomposites," *Chemistry of Materials*, vol. 14, no. 2, pp. 881–887, 2002.

[114] D. L. Ho, R. M. Briber, and C. J. Glinka, "Characterization of organically modified clays using scattering and microscopy techniques," *Chemistry of Materials*, vol. 13, no. 5, pp. 1923–1931, 2001.

[115] *Cloisite® 30B Typical Physical Properties Bulletin, published by Southern Clay Products.*

[116] *Cloisite® 15A Typical Physical Properties Bulletin, published by Southern Clay Products.*

[117] "http://www.jade.dti.ne.jp/ coopchem/newmica.html."

[118] H. E. Hermes, H. Frielinghaus, W. Pyckhout-Hintzen, and D. Richter, "Quantitative analysis of small angle neutron scattering data from montmorillonite dispersions," *Polymer*, vol. 47, no. 6, pp. 2147–2155, 2006.

[119] Z. P. Luo and J. H. Koo, "Quantification of the layer dispersion degree in polymer layered silicate nanocomposites by transmission electron microscopy," *Polymer*, vol. 49, no. 7, pp. 1841–1852, 2008.

[120] P. Jash and C. A. Wilkie, "Effects of surfactants on the thermal and fire properties of poly(methyl methacrylate)/clay nanocomposites," *Polymer Degradation and Stability*, vol. 88, no. 3, pp. 401–406, 2005.

[121] K. Steckler, T. Ohlemiller, and T. Kashiwagi, "Condensed phase phenomena in commodity polymers undergoing degradation/gasification," in *Annual Conference on Fire Research*, pp. 51–52, NIST, November 1998.

[122] E. C. Jonas and R. M. Oliver, "Size and shape of montmorillonite crystallites," *Clays and Clay Minerals*, vol. 15, p. 27, 1967.

[123] C. Shang and J. A. Rice, "Interpretation of small-angle x-ray scattering data from dilute montmorillonite suspensions using a modified guinier approximation," *Physical Review E*, vol. 64, no. 2, 2001.

[124] K. Malekani, J. A. Rice, and J. S. Lin, "Comparison of techniques for determining the fractal dimensions of clay minerals," *Clays and Clay Minerals*, vol. 44, no. 5, pp. 677–685, 1996.

[125] M. Morvan, D. Espinat, J. Lambard, and T. Zemb, "Ultrasmall-angle and small-angle X-ray-scattering of smectite clay suspensions," *Colloids and Surfaces A-Physicochemical and Engineering Aspects*, vol. 82, no. 2, pp. 193–203, 1994.

[126] T. Hirata, T. Kashiwagi, and J. E. Brown, "Thermal and oxidative-degradation of poly(methyl methacrylate) - weight-loss," *Macromolecules*, vol. 18, no. 7, pp. 1410–1418, 1985.

[127] T. Kashiwagi, T. Hirata, and J. E. Brown, "Thermal and oxidative-degradation of poly(methyl methacrylate) - molecular-weight," *Macromolecules*, vol. 18, no. 2, pp. 131–138, 1985.

[128] T. Kashiwagi, A. Inaba, J. E. Brown, K. Hatada, T. Kitayama, and E. Masuda, "Effects of weak linkages on the thermal and oxidative-degradation of poly(methyl methacrylates)," *Macromolecules*, vol. 19, no. 8, pp. 2160–2168, 1986.

[129] A. Inaba and T. Kashiwagi, "A calculation of thermal-degradation initiated by random scission .1. steady-state radical concentration," *Macromolecules*, vol. 19, no. 9, pp. 2412–2419, 1986.

[130] L. E. Manring, "Thermal degradation of poly(methy1 methacrylate). 2. vinyl-terminated polymer)," *Macromolecules*, vol. 22, no. 6, pp. 2673–2677, 1989.

[131] L. E. Manring, "Thermal degradation of saturated poly(methyl methacrylate)," *Macromolecules*, vol. 21, no. 2, pp. 528–530, 1988.

[132] L. E. Manring, D. Y. Sogah, and G. M. Cohen, "Thermal-degradation of poly(methyl methacrylate). 3. polymer with head-to-head linkages," *Macromolecules*, vol. 22, no. 12, pp. 4652–4654, 1989.

[133] L. E. Manring, "Thermal-degradation of poly(methyl methacrylate) .4. random side-group scission," *Macromolecules*, vol. 24, no. 11, pp. 3304–3309, 1991.

[134] P. J. Yoon, D. L. Hunter, and D. R. Paul, "Polycarbonate nanocomposites: Part 2. degradation and color formation," *Polymer*, vol. 44, no. 18, pp. 5341–5354, 2003.

[135] L. Z. Qiu, W. Chen, and B. J. Qu, "Morphology and thermal stabilization mechanism of LLDPE/MMT and LLDPE/LDH nanocomposites," *Polymer*, vol. 47, no. 3, pp. 922–930, 2006.

[136] T. D. Fornes, P. J. Yoon, and D. R. Paul, "Polymer matrix degradation and color formation in melt processed nylon 6/clay nanocomposites," *Polymer*, vol. 44, no. 24, pp. 7545–7556, 2003.

[137] S. P. Su and C. A. Wilkie, "The thermal degradation of nanocomposites that contain an oligomeric ammonium cation on the clay," *Polymer Degradation and Stability*, vol. 83, no. 2, pp. 347–362, 2004.

[138] S. Bourbigot, J. W. Gilman, and C. A. Wilkie, "Kinetic analysis of the thermal degradation of polystyrene-montmorillonite nanocomposite," *Polymer Degradation and Stability*, vol. 84, no. 3, pp. 483–492, 2004.

[139] F. Samyn, S. Bourbigot, C. Jama, and S. Bellayer, "Fire retardancy of polymer clay nanocomposites: Is there an influence of the nanomorphology?," *Polymer Degradation and Stability*, vol. 93, no. 11, pp. 2019 – 2024, 2008.

[140] P. Rittigstein, R. D. Priestley, L. J. Broadbelt, and J. M. Torkelson, "Model polymer nanocomposites provide an understanding of confinement effects in real nanocomposites," *Nature Materials*, vol. 6, no. 4, pp. 278–282, 2007.

[141] A. Bansal, H. C. Yang, C. Z. Li, K. W. Cho, B. C. Benicewicz, S. K. Kumar, and L. S. Schadler, "Quantitative equivalence between polymer nanocomposites and thin polymer films," *Nature Materials*, vol. 4, no. 9, pp. 693–698, 2005.

[142] F. D. Blum, E. N. Young, G. Smith, and O. C. Sitton, "Thermal analysis of adsorbed poly(methyl methacrylate) on silica," *Langmuir*, vol. 22, no. 10, pp. 4741–4744, 2006.

[143] C. B. Roth, A. Pound, S. W. Kamp, C. A. Murray, and J. R. Dutcher, "Molecular-weight dependence of the glass transition temperature of freely-standing poly(methyl methacrylate) films," *European Physical Journal E*, vol. 20, no. 4, pp. 441–448, 2006.

[144] J. X. Du, J. Q. Wang, S. P. Su, and C. A. Wilkie, "Additional xps studies on the degradation of poly(methyl methacrylate) and polystyrene nanocomposites," *Polymer Degradation and Stability*, vol. 83, no. 1, pp. 29–34, 2004.

[145] J. Zhu, F. M. Uhl, A. B. Morgan, and C. A. Wilkie, "Studies on the mechanism by which the formation of nanocomposites enhance thermal stability," *Chemistry of Materials*, vol. 13, no. 12, p. 4649, 2001.

[146] X. Liu, "Flammability properties of clay-nylon nanocomposites," Master's thesis, University of Maryland at College Park, College Park, Maryland 20742, August 2004.

[147] M. KIM, "Predicting thermally thin burning of polymer using tga/dsc," Master's thesis, University of Maryland at College Park, College Park, Maryland 20742, December 2006.

[148] S. Bourbigot, M. Le Bras, S. Duquesne, and M. Rochery, "Recent advances for intumescent polymers," *Macromolecular Materials and Engineering*, vol. 289, no. 6, pp. 499–511, 2004.

[149] M. Zanetti, G. Camino, D. Canavese, A. B. Morgan, F. J. Lamelas, and C. A. Wilkie, "Fire retardant halogen-antimony-clay synergism in polypropylene layered silicate nanocomposites," *Chemistry of Materials*, vol. 14, no. 1, pp. 189–193, 2002.

[150] S. Littman and I. Touval, "Novel phosphorus compounds and flame retardant compositions containing same." United States Patent 4097560, June 1978.

[151] L. L. Hench, "Bioceramics," *Journal of the American Ceramic Society*, vol. 81, no. 7, pp. 1705–1728, 1998.

[152] L. L. Hench, "Bioceramics - from concept to clinic," *Journal of the American Ceramic Society*, vol. 74, no. 7, pp. 1487–1510, 1991.

[153] R. Z. Legeros, "Preparation of octacalcium phosphate (OCP) - a direct fast method," *Calcified Tissue International*, vol. 37, no. 2, pp. 194–197, 1985.

[154] S. Aoki, K. Sakamoto, S. Yamaguchi, and A. Nakahira, "Syntheses of octacalcium phosphate containing dicarboxylic acids and effects of the side groups on the crystal growth of octacalcium phosphate," *Journal of the Ceramic Society of Japan*, vol. 108, no. 10, pp. 909–914, 2000.

[155] R. A. Mickiewicz, A. M. Mayes, and D. Knaack, "Polymer-calcium phosphate cement composites for bone substitutes," *Journal of Biomedical Materials Research*, vol. 61, no. 4, pp. 581–592, 2002.

[156] J. S. Bow, S. C. Liou, and S. Y. Chen, "Structural characterization of room-temperature synthesized nano-sized beta-tricalcium phosphate," *Biomaterials*, vol. 25, no. 16, pp. 3155–3161, 2004.

[157] R. Enderle, F. Gotz-Neunhoeffer, M. Gobbels, F. A. Muller, and P. Greil, "Influence of magnesium doping on the phase transformation temperature of beta-tcp ceramics examined by rietveld refinement," *Biomaterials*, vol. 26, no. 17, pp. 3379–3384, 2005.

[158] M. Jarcho, C. H. Bolen, M. B. Thomas, J. Bobick, J. F. Kay, and R. H. Doremus, "Hydroxylapatite synthesis and characterization in dense polycrystalline form," *Journal of Materials Science*, vol. 11, no. 11, pp. 2027–2035, 1976.

[159] L. Chow and E. Eanes, eds., *Octacalcium Phosphate*. Karger, 2002.

[160] C. A. Beevers, "The crystal structure of dicalcium phosphate dihydrate, CaHPO4.2H2O," *Acta Crystallographica*, vol. 11, no. 4, pp. 273–277, 1958.

[161] G. Maclennan and C. A. Beevers, "The crystal structure of dicalcium phosphate, CaHPO4," *Acta Crystallographica*, vol. 8, no. 9, pp. 579–583, 1955.

[162] G. Maclennan and C. A. Beevers, "The crystal structure of monocalcium phosphate monohydrate, Ca(H2PO4)2.H2O," *Acta Crystallographica*, vol. 9, no. 2, pp. 187–190, 1956.